



NAVAL POSTGRADUATE SCHOOL

MONTEREY, CALIFORNIA

THESIS

**TROPICAL CYCLONE RECONNAISSANCE WITH THE
GLOBAL HAWK: OPERATIONAL THRESHOLDS AND
CHARACTERISTICS OF CONVECTIVE SYSTEMS OVER
THE TROPICAL WESTERN NORTH PACIFIC**

by

David W. Damron

December 2013

Thesis Advisor:
Second Reader:

Patrick A. Harr
Barbara Scarnato

Approved for public release; distribution is unlimited

THIS PAGE INTENTIONALLY LEFT BLANK

REPORT DOCUMENTATION PAGE			Form Approved OMB No. 0704-0188	
Public reporting burden for this collection of information is estimated to average 1 hour per response, including the time for reviewing instruction, searching existing data sources, gathering and maintaining the data needed, and completing and reviewing the collection of information. Send comments regarding this burden estimate or any other aspect of this collection of information, including suggestions for reducing this burden, to Washington headquarters Services, Directorate for Information Operations and Reports, 1215 Jefferson Davis Highway, Suite 1204, Arlington, VA 22202-4302, and to the Office of Management and Budget, Paperwork Reduction Project (0704-0188) Washington DC 20503.				
1. AGENCY USE ONLY (Leave blank)		2. REPORT DATE December 2013	3. REPORT TYPE AND DATES COVERED Master's Thesis	
4. TITLE AND SUBTITLE TROPICAL CYCLONE RECONNAISSANCE WITH THE GLOBAL HAWK: OPERATIONAL THRESHOLDS AND CHARACTERISTICS OF CONVECTIVE SYSTEMS OVER THE TROPICAL WESTERN NORTH PACIFIC			5. FUNDING NUMBERS	
6. AUTHOR(S) David W. Damron			8. PERFORMING ORGANIZATION REPORT NUMBER	
7. PERFORMING ORGANIZATION NAME(S) AND ADDRESS(ES) Naval Postgraduate School Monterey, CA 93943-5000			10. SPONSORING/MONITORING AGENCY REPORT NUMBER	
9. SPONSORING /MONITORING AGENCY NAME(S) AND ADDRESS(ES) N/A			11. SUPPLEMENTARY NOTES The views expressed in this thesis are those of the author and do not reflect the official policy or position of the Department of Defense or the U.S. Government. IRB protocol number ____ N/A ____.	
12a. DISTRIBUTION / AVAILABILITY STATEMENT Approved for public release; distribution is unlimited			12b. DISTRIBUTION CODE	
13. ABSTRACT (maximum 200 words) <p>In a tropical cyclone (TC), <i>in situ</i> observations measure storm location, intensity, and structure. These parameters are valuable for initializing numerical models and providing forecasters with current conditions on which to base their forecast. Over the western North Pacific (WPAC), a lack of <i>in situ</i> observations in TCs is hypothesized to be one component that contributes to a recent leveling of forecast skill. In this study, the use of a Global Hawk (GH) unmanned aerial vehicle as an observing platform for TCs over the WPAC is examined. It is hypothesized that the GH can greatly benefit the Department of Defense by reducing the uncertainty in TC track forecasts, which has been mandated by the U.S. Pacific Command as a priority for increasing the area of sea maneuverability</p> <p>A limit to successful GH operations is the ability to operate at altitudes above typical cloud tops of WPAC TCs. A climatology of WPAC TC cloud-top heights and temperatures was examined to relate these parameters to storm characteristics. It is concluded that use of a GH for tropical cyclone reconnaissance in the WPAC is a viable option to provide <i>in situ</i> observations of tropical cyclone characteristics for improved model and operational forecasts.</p>				
14. SUBJECT TERMS Global Hawk, Tropical Cyclone Reconnaissance, Top of Convective Cloud, Top of Cloud, Cloud-Top Temperature, Joint Typhoon Warning Center, Tropical Western North Pacific			15. NUMBER OF PAGES 149	
			16. PRICE CODE	
17. SECURITY CLASSIFICATION OF REPORT Unclassified	18. SECURITY CLASSIFICATION OF THIS PAGE Unclassified	19. SECURITY CLASSIFICATION OF ABSTRACT Unclassified	20. LIMITATION OF ABSTRACT UU	

THIS PAGE INTENTIONALLY LEFT BLANK

Approved for public release; distribution is unlimited

**TROPICAL CYCLONE RECONNAISSANCE WITH THE GLOBAL HAWK:
OPERATIONAL THRESHOLDS AND CHARACTERISTICS OF CONVECTIVE
SYSTEMS OVER THE TROPICAL WESTERN NORTH PACIFIC**

David W. Damron
Lieutenant Commander, United States Navy
B.S., Excelsior College, 2001

Submitted in partial fulfillment of the
requirements for the degree of

**MASTER OF SCIENCE IN METEOROLOGY AND PHYSICAL
OCEANOGRAPHY**

from the

**NAVAL POSTGRADUATE SCHOOL
December 2013**

Author: David W. Damron

Approved by: Patrick A. Harr, PhD
Thesis Advisor

Barbara Scarnato, PhD
Second Reader

Wendell A. Nuss, PhD
Chair, Department of Meteorology

THIS PAGE INTENTIONALLY LEFT BLANK

ABSTRACT

In a tropical cyclone (TC), *in situ* observations measure storm location, intensity, and structure. These parameters are valuable for initializing numerical models and providing forecasters with current conditions on which to base their forecast. Over the western North Pacific (WPAC), a lack of *in situ* observations in TCs is hypothesized to be one component that contributes to a recent leveling of forecast skill. In this study, the use of a Global Hawk (GH) unmanned aerial vehicle as an observing platform for TCs over the WPAC is examined. It is hypothesized that the GH can greatly benefit the Department of Defense by reducing the uncertainty in TC track forecasts, which has been mandated by the U.S. Pacific Command as a priority for increasing the area of sea maneuverability

A limit to successful GH operations is the ability to operate at altitudes above typical cloud tops of WPAC TCs. A climatology of WPAC TC cloud-top heights and temperatures was examined to relate these parameters to storm characteristics. It is concluded that use of a GH for tropical cyclone reconnaissance in the WPAC is a viable option to provide *in situ* observations of tropical cyclone characteristics for improved model and operational forecasts.

THIS PAGE INTENTIONALLY LEFT BLANK

TABLE OF CONTENTS

I.	INTRODUCTION.....	1
A.	MOTIVATION.....	1
II.	BACKGROUND.....	7
A.	REDUCTION IN FORECAST ERRORS AND UNCERTAINTY	7
B.	FUTURE UNCERTAINTY IN REMOTE SENSING CAPABILITY	12
C.	GLOBAL HAWK AND THE HURRICANE AND SEVERE STORMS SENTINAL PROJECT (HS3)	14
D.	EXPERIENCE FROM NASA GLOBAL HAWK FLIGHTS	17
1.	Emily (2005).....	21
2.	Karl (2010)	25
3.	Matthew (2010).....	26
III.	REQUIREMENTS AND RESTRICTIONS.....	33
A.	NASA GLOBAL HAWK PUSH	33
B.	GLOBAL HAWK OPERATIONS CENTER.....	35
C.	CURRENT NASA GLOBAL HAWK INSTRUMENT DESIGN	39
1.	AV1 Payload	39
a.	<i>High-altitude Imaging Wind and Rain Airborne Profiler</i>	39
b.	<i>Hurricane Imaging Radiometer.....</i>	41
c.	<i>High Definition Sounding System</i>	42
2.	AV6 Payload	43
a.	<i>Tropospheric Wind Lidar Technology Experiment..</i>	43
b.	<i>Airborne Vertical Atmospheric Profiling System.....</i>	44
D.	PREVIOUS USE OF THE GH FOR TC RECONNAISSANCE	45
E.	OBSERVANCE OF UPPER-LEVEL TYPHOON FLOW LIFE CYCLE OVER THE WEST PACIFIC (OUTFLOW) MISSION.....	48
1.	OUTFLOW Science Hypotheses.....	48
IV.	WPAC TC CLIMATOLOGY	53
A.	CLOUDSAT DATA IMAGES	53
B.	TC CONVECTIVE ENVIRONMENT IN THE WPAC (2006–2010)	55
1.	2006.....	55
2.	2007.....	61
3.	2008.....	66
4.	2009.....	71
5.	2010.....	76
C.	SUMMARY	83
V.	CASE STUDIES.....	87
A.	TOP OF CONVECTIVE CLOUD (TCC) HEIGHT AND TEMPERATURE	87
1.	19W (Pabuk)	88

2.	22W (Fitow).....	93
3.	23W (Danas)	98
VI.	CONCLUSION	105
A.	SUMMARY	105
1.	BACKGROUND	105
2.	REQUIREMENTS AND RESTRICTIONS	105
3.	WPAC TC CLIMATOLOGY.....	105
4.	CASE STUDIES	106
B.	RECOMMENDATIONS FOR FUTURE STUDY	107
APPENDIX A.	19W (PABUK) HOURLY DATA	109
APPENDIX B.	22W (FITOW) HOURLY DATA	113
APPENDIX C.	23W (DANAS) HOURLY DATA	117
	LIST OF REFERENCES.....	121
	INITIAL DISTRIBUTION LIST	127

LIST OF FIGURES

Figure 1.	An example CloudSat product provided by Colorado State University. This cross-sectional image is of Tropical Cyclone 15W taken on Sept 15, 2009 in the WPAC (from http://www.nrlmry.navy.mil/sat_products.html)	5
Figure 2.	Schematic of current and potential forecast uncertainty in the forecast track of a tropical cyclone over the western North Pacific. Magenta circles define the analyzed radii of tropical-storm-force winds (after slide by M. Angove 2011).....	8
Figure 3.	Average JTWC forecast error of TC track from 1974–2011. Percentages define the rates of improvement for the 72-h forecast (from JTWC Annual Tropical Cyclone Report 2011).....	9
Figure 4.	Average JTWC forecast errors for TC intensity from 1987–2011. Percentages define the rates of improvement for the 48-h forecast (from JTWC Annual Tropical Cyclone Report 2011).....	9
Figure 5.	Average NHC forecast errors for TC track from 1990–2010. Percentages define the overall rate of improvement (from Peter Black, Naval Research Laboratory 2012).....	11
Figure 6.	Average NHC forecast errors for TC intensity from 1990–2010. Percentage defines the overall rate of improvement (from Peter Black, Naval Research Laboratory 2012).....	11
Figure 7.	Summary of passive microwave imager sensors (U.S. and foreign) launched, in operations now, recently failed, or future launches. All future satellites are tentatively listed until actual launch occurs. Launch dates are subject to change at any time and might be delayed multiple years (from J. Hawkins, Naval Research Laboratory, Marine Meteorology Division, Monterey, CA Satellite Meteorology Applications Section 2012)	13
Figure 8.	Structure of a tropical cyclone. The upper-level outflow is depicted by cirrus clouds in the upper part of the schematic	16
Figure 9.	The NASA Global Hawk unmanned aircraft system (UAS) is capable of flight altitudes up to 65,000 feet and flight durations of up to 30 hours. An ideal platforms for investigations of hurricanes, the Hurricane and Severe Storm Sentinel (HS3) mission has utilized two Global Hawks, one with an instrument suite geared toward measurement of the environment and the other with instruments suited to inner-core structure and processes (from National Aeronautics and Space Administration 2011).....	16
Figure 10.	Global Hawk in-flight weather limitations as defined by NASA operating procedures.....	17
Figure 11.	Estimated IR-based cloud top heights from GOES satellite imagery during the period of the ER-2 overflight of Emily on 17 July, 2005. The plotted squares are image pixel heights from all pixels	

	overflown by the ER-2 in the five minutes preceding the image time (colors indicate emissivity of each pixel) as derived from the Automated Cloud Height Algorithm (ACHA). The NASA ER-2 flight level (black line) and 10,000 ft margin (grey shading) are also shown. The strong cell was overflown by the ER-2 at 0753 UTC.....	23
Figure 12.	ACHA cloud top heights (left) and tropical overshooting tops (TOTs) and lightning locations (right) at 0750, three minutes before the ER-2 flew over the strong growing cell (indicated by the arrow) in the western eyewall of Hurricane Emily. Arrow pointing to low clouds.....	24
Figure 13.	As in Figure 10, but for Hurricane Karl (2010).	25
Figure 14.	As in Figure 11, but for Hurricane Karl at 2345 UTC on September 16, 2010. The Global Hawk had just overflown the eastern semicircle of the eyewall at about 59,000 ft. with cloud tops about 53,000 ft. and with a somewhat “bumpy” appearance. However, no TOTs are indicated along the flight path (one TOT, not shown, was detected a few minutes earlier in the south eyewall at 2338 UTC]. While some lightning was noted near the eye between 2000–2200 UTC, and a few TOTs, neither indicator approached the intensity or frequency that characterized the center of Emily during the ER-2 mission.	26
Figure 15.	As in Figures 10 and 12, but for Tropical Storm Matthew (2010).	27
Figure 16.	As in figures 11 and 13, but for Tropical Storm Matthew at 0450 UTC on 24 September 2010.....	28
Figure 17.	NASA <u>revised</u> Global Hawk in-flight weather limitations.....	31
Figure 18.	Photo of the Global Hawk AV-1 in flight (image credit: NASA/DFRC)	34
Figure 19.	Photo of the Global Hawk AV-6 in flight (image credit: NASA/DFRC)	34
Figure 20.	Flight crew and scientists occupy the Global Hawk Operations Center at NASA Dryden during the Genesis and Rapid Intensification Processes hurricane study in the fall of 2010 (from NASA / Tom Tschida; URL: http://www.nasa.gov/centers/dryden/news/FactSheets/FS-098-DFRC.html)	36
Figure 21.	The NASA Global Hawk Mobile Operations Facility is a portable ground control station that can be transported anywhere for remote operations (from NASA/Tony Landis 2010. URL: http://www.nasa.gov/mission_pages/hurricanes/missions/hs3/news/pilot-challenges.html).....	37
Figure 22.	The interior of the NASA Global Hawk Mobile Operations Facility outfitted for operation of the Global Hawks from locations other than NASA’s Dryden Flight Research Center in California. This ground control station also allows for operation of two Global Hawks simultaneously (from NASA/Tony Landis 2010. URL:	

	http://www.nasa.gov/mission_pages/hurricanes/missions/hs3/news/pilot-challenges.html).....	37
Figure 23.	Overview of the Global Hawk communications architecture (from NASA/DFRC 2010. URL: https://directory.eoportal.org/web/eoportal/airborne-sensors/global-hawk).....	38
Figure 24.	Payload Instrument arrangement for AV1	39
Figure 25.	Payload Instrument arrangement for AV6	39
Figure 26.	HIWRAP concept of operations over a tropical cyclone	40
Figure 27.	Schematic of HIRAD observation of hurricane wind speed, and retrievals from Hurricane Earl (2010). White strip in each panel is from piecing together adjacent flight legs	42
Figure 28.	The AVAPS launch tube underneath the tail section of the NASA GH. (c) The GH Mist dropsonde.....	45
Figure 29.	(a) Flight tracks of the NASA Global Hawk utilized during August-September 2010 as part of GRIP. (b) Details of the flight track (green lines) over Hurricane Earl during September 2010. The orange circles and yellow line define the track of Hurricane Earl (from http://grip.jpl.nasa.gov).....	46
Figure 30.	Schematic of the Global Hawk configuration during hurricane overflight missions during NASA GRIP. Instrument definitions are provided in Table 1	47
Figure 31.	Schematic of the impact of a poleward-moving typhoon on the midlatitude circulation across the North Pacific and North America. The typhoon track is defined by the line connecting the two typhoon symbols. Thin black lines and the color shaded region define the 300-hPa stream function and jet stream, respectively. The gray scalloped regions indicate significant cloud systems. The green arrows denote the divergent outflow of the tropical cyclone. The red L defines the location of extratropical cyclogenesis (after Archambault et al. 2013)	51
Figure 32.	A 2006 CloudSat image depicting a vertical cross-section of 02W (Chan-Hom) (from Colorado State University. URL: http://reef.atmos.colostate.edu)	54
Figure 33.	Composite of CloudSat data for the year 2006. Highlighted values mark the maximum for each category	56
Figure 34.	CloudSat satellite pass over 12W at 0436 UTC 14 August 2006. Maximum TCC was 15 km during this satellite pass. Intensity for 12W at time of pass was 40 kt (from Colorado State University. URL: http://reef.atmos.colostate.edu)	57
Figure 35.	CloudSat satellite pass over 16W at 1609 UTC 21 September 2006. Maximum TCC was 16.5 km during this satellite pass. Intensity for 16W at time of pass was 140 kt (from Colorado State University. URL: http://reef.atmos.colostate.edu)	58
Figure 36.	CloudSat satellite pass over 21W at 0407 UTC 14 October 2006. Maximum TCC was 11 km during this satellite pass. Intensity for	

	21W at time of pass was 90 kt (from Colorado State University. URL: http://reef.atmos.colostate.edu)	59
Figure 37.	CloudSat satellite pass over 24W at 0542 UTC 01 December 2006. Maximum TCC was 11 km during this satellite pass. Intensity for 24W at time of pass was 90 kt (from Colorado State University. URL: http://reef.atmos.colostate.edu)	60
Figure 38.	Intensity values (kt) prior to, at, and following the satellite pass over each storm during 2006.....	61
Figure 39.	Composite of CloudSat data for the year 2007. Highlighted values mark the maximum for each category	62
Figure 40.	First CloudSat satellite pass over 02W at 0409 UTC 17 May 2007. Maximum TCC was 12 km during this satellite pass. Intensity for 02W at time of pass was 35 kt (from Colorado State University. URL: http://reef.atmos.colostate.edu)	63
Figure 41.	Second CloudSat satellite pass over 02W at 1653 UTC 20 May 2007. Maximum TCC was 10.5 km during this satellite pass. Intensity for 02W at time of pass was 130 kt (from Colorado State University. URL: http://reef.atmos.colostate.edu)	64
Figure 42.	CloudSat satellite pass over 17W at 0519 UTC 05 October 2007. Maximum TCC was 12 km during this satellite pass. Intensity for 17W at time of pass was 130 kt (from Colorado State University. URL: http://reef.atmos.colostate.edu)	65
Figure 43.	Intensity values (kt) prior to, at, and following the satellite pass over each storm during 2007.....	66
Figure 44.	Composite of CloudSat data for the year 2008. Highlighted values mark the maximum for each category	67
Figure 45.	CloudSat satellite pass over 14W at 0527 UTC 27 August 2008. Maximum TCC was 12.5 km during this satellite pass. Intensity for 14W at time of pass was 50 kt (from Colorado State University. URL: http://reef.atmos.colostate.edu)	68
Figure 46.	CloudSat satellite pass over 15W at 1737 UTC 12 September 2008. Maximum TCC was 13 km during this satellite pass. Intensity for 15W at time of pass was 100 kt (from Colorado State University. URL: http://reef.atmos.colostate.edu)	69
Figure 47.	CloudSat satellite pass over 03W at 0408 UTC 12 May 2008. Maximum TCC was 10.5 km during this satellite pass. Intensity for 03W at time of pass was 75 kt (from Colorado State University. URL: http://reef.atmos.colostate.edu)	70
Figure 48.	Intensity values (kt) prior to, at, and following the satellite pass over each storm during 2008.....	71
Figure 49.	Composite of CloudSat data for the year 2009. Highlighted values mark the maximum for each category	72
Figure 50.	CloudSat satellite pass over 14W at 1817 UTC 09 September 2009. Maximum TCC was 13 km during this satellite pass. Intensity	

	for 14W at time of pass was 30 kt (from Colorado State University. URL: http://reef.atmos.colostate.edu)	73
Figure 51.	CloudSat satellite pass over 15W at 0350 UTC 15 September 2009. Maximum TCC was 15 km during this satellite pass. Intensity for 15W at time of pass was 130 kt (from Colorado State University. URL: http://reef.atmos.colostate.edu)	74
Figure 52.	Second CloudSat satellite pass over 15W at 0422 UTC 18 September 2009. Maximum TCC was 12 km during this satellite pass. Intensity for 15W at time of pass was 110 kt (from Colorado State University. URL: http://reef.atmos.colostate.edu)	75
Figure 53.	Graph depicting intensity values (kt) leading up to and after the satellite made the pass over the storm (2009).....	76
Figure 54.	Composite of CloudSat data for the year 2010. Highlighted values mark the maximum for each category	76
Figure 55.	First CloudSat satellite pass over 02W at 1628 UTC 22 March 2010. Maximum TCC was 17 km during this satellite pass. Intensity for 02W at time of pass was 30 kt (from Colorado State University. URL: http://reef.atmos.colostate.edu)	78
Figure 56.	CloudSat satellite pass over 04W at 0556 UTC 19 July 2010. Maximum TCC was 15.5 km during this satellite pass. Intensity for 04W at time of pass was 30 kt (from Colorado State University. URL: http://reef.atmos.colostate.edu)	79
Figure 57.	CloudSat satellite pass over 17W at 1545 UTC 22 October 2010. Maximum TCC was 15 km during this satellite pass. Intensity for 17W at time of pass was 30 kt (from Colorado State University. URL: http://reef.atmos.colostate.edu)	80
Figure 58.	Second CloudSat satellite pass over 15W at 0455 UTC 17 October 2010. Maximum TCC was 14 km during this satellite pass. Intensity for 15W at time of pass was 140 kt (from Colorado State University. URL: http://reef.atmos.colostate.edu)	81
Figure 59.	Second CloudSat satellite pass over 02W at 0444 UTC 25 March 2010. Maximum TCC was 12.5 km during this satellite pass. Intensity for 02W at time of pass was 45 kt (from Colorado State University. URL: http://reef.atmos.colostate.edu)	82
Figure 60.	Graph depicting intensity values (kt) leading up to and after the satellite made the pass over the storm (2010).....	83
Figure 61.	Scatter plot of TC intensity at the time of the CloudSat pass versus the (a) ToC and (b) TCC. The solid black line defines the linear regression between intensity and each height value.	84
Figure 62.	Scatter plot of TC intensity change versus ToC for (a) change in intensity for -6-h versus ToC; (b) change in intensity for +6-h versus ToC. The solid black line defines the linear regression between intensity change and each height value.....	85

Figure 63.	Scatter plot of TC Tdiff versus (a) ToC and (b) TCC. The solid black line defines the linear regression between Tdiff and each height value.	86
Figure 64.	Cloud-top height (a) and cloud-top temperature (b) for Typhoon Fitow at 1232 UTC 30 October 2013.....	88
Figure 65.	Track of Pabuk during September 2013.....	89
Figure 66.	TCC temperature depiction for 19W on 21 Sept at 0132 UTC	90
Figure 67.	TCC temperature depiction for 19W on 26 Sept at 0132 UTC when Pabuk was near 33N	90
Figure 68.	TCC height depiction for 19W on 21 Sept at 0732 UTC.....	91
Figure 69.	TCC height depiction for 19W on 24 Sept at 0732 UTC.....	92
Figure 70.	TCC height depiction for 19W on 26 Sept at 0132 UTC.....	92
Figure 71.	Cloud-top temperature vs -6-h intensity change for TY Pabuk. This image shows a significant linear relationship between decreasing temperatures and TC intensification. The solid black line defines the linear regression between cloud-top temperature and -6-h intensity change	93
Figure 72.	Track of Fitow during September/October 2013.....	94
Figure 73.	TCC temperature depiction for 22W on 03 Oct at 0432 UTC	95
Figure 74.	TCC temperature depiction for 22W on 06 Oct at 0232 UTC.	96
Figure 75.	TCC height depiction for 22W on 03 Oct at 0632 UTC.....	97
Figure 76.	TCC height depiction for 22W on 06 Oct at 0232 UTC.....	97
Figure 77.	Cloud-top temperature vs -6-h intensity change for TY Fitow. This image shows a significant linear relationship between decreasing temperatures and TC intensification. The solid black line defines the linear regression between cloud-top temperature and -6-h intensity change.	98
Figure 78.	Track of Danas during October 2013.....	99
Figure 79.	TCC temperature depiction for 23W on 05 Oct at 0832 UTC	100
Figure 80.	TCC temperature depiction for 23W on 08 Oct at 0632 UTC	101
Figure 81.	TCC height depiction for 23W on 04 Oct at 2332 UTC.....	102
Figure 82.	TCC height depiction for 23W on 07 Oct at 0732 UTC.....	103
Figure 83.	Cloud-top temperature vs -6-h intensity change for TY Danas. This image shows a non-significant linear relationship between decreasing temperatures and TC intensification. The solid black line defines the linear regression between cloud-top temperature and -6-h intensity change	103
Figure 84.	Cloud-top temperature vs -6-h intensity change for all three TCs (TY Pabuk, TY Fitow, TY Danas). This image shows a significant linear relationship between decreasing temperatures and TC intensification. The solid black line defines the linear regression between cloud-top temperature and -6-h intensity change.....	104

LIST OF TABLES

Table 1.	Listing of NASA airborne overflights of hurricanes and reports, or lack thereof, of turbulence.	19
Table 2.	Instruments aboard NASA Global Hawk on hurricane overflight missions during NASA GRIP in 2010	47

THIS PAGE INTENTIONALLY LEFT BLANK

LIST OF ACRONYMS AND ABBREVIATIONS

ACHA	automated cloud height algorithm
AMPR	advanced microwave precipitation radiometer
AOR	area of responsibility
AV	air vehicle
AVAPS	airborne vertical atmospheric profiling system
CALIPSO	cloud-aerosol lidar and infrared pathfinder satellite observations
CloudSat	cloud satellite
DFRC	Dryden Flight Research Center
DoD	Department of Defense
EAFB	Edwards Air Force Base
EDOP	ER-2 Doppler radar
GH	global hawk
GHMOF	global hawk mobile operations facility
GHOC	global hawk operations center
GloPac	global hawk pacific
GOES	geostationary satellite
GPS	global positioning system
GRIP	genesis and rapid intensification processes
HDSS	high-definition sounding system
HIRAD	hurricane imaging radiometer
HIWRAP	high-altitude imaging wind and rain airborne profiler
HS3	hurricane and severe storm sentinel
JMA	Japanese Meteorological Association
JTWC	Joint Typhoon Warning Center
LIP	lightning instrument package
NASA	National Aeronautics and Space Administration
NCAR	National Center for Atmospheric Research
NGC	Northrop Grumman Corporation
NHC	National Hurricane Center

NOAA	National Oceanic and Atmospheric Administration
NRL	Naval Research Laboratory
NWP	numerical weather prediction
NWS	National Weather Service
ONR	Office of Naval Research
OUTFLOW	observance of upper-level typhoon flow life cycle over the west Pacific
QuickScat	quick scatterometer
Satcom	satellite communications
SFMR	stepped frequency microwave radiometer
SST	sea surface temperature
TC	tropical cyclone
TCC	top of convective cloud
TD	tropical depression
TDO	typhoon duty officer
ToC	top of cloud
TOT	tropical overshooting top
TS	tropical storm
TWiLiTE	tropospheric wind lidar technology experiment
TY	typhoon
UAS	unmanned aerial system
UAV	unmanned aerial vehicle
USAF	United States Air Force
USPACOM	United States Pacific Command
UTC	universal time coordinate
WMO	World Meteorological Organization
WPAC	western North Pacific
XDD	expendable digital dropsondes

ACKNOWLEDGMENTS

I would like to start off by thanking my family back home. They have always shown encouragement throughout my career. Without their love, support, and guidance, this would not have been possible. To my son, Steven, thank you for your support and motivation. His passion for succeeding in life has not only motivated me, but has contributed tremendously to my completion of this significant educational achievement.

I would also like to thank my thesis advisor, Dr. Pat Harr, for his insight, patience, and immense knowledge. His guidance helped me throughout my research and writing of this thesis. I could not have imagined having a better advisor and mentor for this project. I would also like to thank all my other professors here at NPS, as they not only provided essential instruction, but also encouraged the best from me.

I would also like to acknowledge Dr. Barbara Scarnato as the second reader of this thesis and I am gratefully indebted to her for her valuable comments on this thesis.

Finally, I'd like to thank my classmates: LCDR McKeon, LCDR Peixoto de Carvalho, LT Scianna, LT Portell, LT Ziemba, LT Doty, and LT Fritz, for not only being outstanding classmates but also great friends. I wish you the very best of luck in your future naval adventures!

THIS PAGE INTENTIONALLY LEFT BLANK

I. INTRODUCTION

A. MOTIVATION

Tropical cyclones (TCs) in the tropical western North Pacific (WPAC) Ocean present severe forecast challenges to typhoon duty officers (TDOs) at the Joint Typhoon Warning Center (JTWC) located at Pearl Harbor, HI. The JTWC is tasked with providing operational forecasts of TC formation, motion, and intensity in support of all Department of Defense (DoD) installations and activities within the U.S. Pacific Command (USPACOM) area of responsibility. More tropical cyclones form in the WPAC than in any other ocean basins. Over the WPAC, more than 30 storms of at least tropical storm intensity develop each year, and about 18 become typhoons. Typhoons that occur over the WPAC are often among the largest and most intense to occur over all ocean basins. On average, five typhoons a year have maximum winds more than 130 kt (150 mph) (*American Practical Navigator* 1977). Also, circulations covering more than 600 nm in diameter are not uncommon. Most of the storms form east of the Philippines and track across the Pacific toward the Philippines, Japan, and China. A fewer number of storms form in the South China Sea. According to the *American Practical Navigator*, TCs have occurred in all months with the primary TC season over the WPAC extending from April through December. The peak of the season is July through October, when nearly 70% of all typhoons develop (Gray 1979). There is a noticeable seasonal shift in storm tracks in this region. From July through September, storms often track north of the Philippines and recurve into the midlatitudes. Early and late season typhoons typically follow a more westerly track through the Philippines before recurving (*American Practical Navigator* 1977).

A primary operational goal of the JTWC is to maximize accuracy of track and intensity forecasts and minimize the amount of area that must be placed under warning. In April of 2009, JTWC and USPACOM officials held a Tropical Cyclone Conference to discuss the future forecasting parameters and research

activity required to optimize support for U.S. and coalition operations within the USPACOM area of responsibility (AOR) (Uhle 2009). The participants agreed on a number of forecast goals that would reduce uncertainty, provide projections past the current five-day forecast and provide increasing detail of the hydrological impacts of a TC. The USPACOM requested the research and operational METOC communities of the DoD to coordinate and concentrate their efforts toward meeting the following operational objectives over the next 15–20 years:

A. Reduce the size of the area of uncertainty about the forecast position by 50% to increase the operating space for U.S. and coalition forces near a cyclone. Increasingly accurate track forecasts will decrease the number of unnecessary storm evasions and provide for efficient sea and air space management, resulting in substantial savings in operating costs. Suggested specific component metrics of the objective include:

1. Reduce the center position error to less than 75 nm for a 72-h forecast period, 150 nm for a 120-h forecast period and 200 nm for a 168-h forecast period.
2. Predict the radius of 35 kt and 50 kt winds within 20% (by quadrant) through 168-h.
3. Develop and/or improve forecasting products that convey uncertainty in a situation-dependent, storm-following dynamic and probabilistic sense (as opposed to straight historical averages).

B. Improve the forecast of storm effects to enable operational planning for disaster response and force protection. Suggested specific component metrics of this objective include:

1. Forecast the intensity (maximum wind) of the cyclone to within 20% through 168-h.
2. Forecast the cyclone associated storm surge (within 10% of maximum height) to include onset time within six hours, areal coverage within 25%, and duration of inundation within six hours for a 72-h forecast period.
3. Forecast the overland rainfall amount at military installations, population centers, and mudslide risk areas within 25% for amounts over six inches per 24 hours.

Tropical cyclones are observed (measured) using *in situ* and remote platforms. Direct measurements of *in situ* TC conditions and wind speeds are primarily taken by manned reconnaissance aircraft. These measurements are limited due to the extreme conditions associated with a TC. Once a TC is near and/or on land, Automated Surface Observations Systems (ASOS) measure surface conditions, and radiosondes provide vertical profiles of winds, temperature, and moisture. Remote measurements include satellite imagery and Doppler radar. Satellites have greatly improved the ability to monitor and understand TCs. However, the number of operational satellites has been drastically reduced due to satellite life-cycle duration and lack of replacements due to budget constraints.

Numerical weather prediction (NWP) models are a primary source of guidance to TDOs. However, NWP models exhibit sensitivity to initial conditions as TCs occur over relatively data-void regions of the tropical oceans. In an effort to improve numerical forecasts, targeted observations have been used within and near tropical cyclones to help reduce uncertainties in initial conditions used in model integrations (Weissmann, et al. 2011; Reynolds, et al. 2009). The primary means of obtaining these observations are manned aircraft that deploy dropwindsondes from altitudes that range from a few thousand feet to tens of thousands of feet. Organizations such as the National Oceanic and Atmospheric Administration (NOAA) and the National Hurricane Center (NHC) also use WP-3D aircraft and the United States Air Force (USAF) uses the WC-130J aircraft. Unfortunately, these aircraft are only used routinely over the Atlantic Ocean. It is only under special circumstances that aircraft have been available to observe storms over the WPAC, where a considerable amount of DoD assets exist.

Unfortunately, observational resources for *in situ* measurements of TCs are not available in the WPAC. It has been shown that the forecast accuracy of TC movement and intensity are often improved when an increased number of *in situ* observations are obtained by manned aircraft (Weissmann et al. 2011).

When assimilated into the operational NWP models, these data provide a more accurate set of initial conditions for numerical integration.

It can be hypothesized, that the addition, or increase, of *in situ* observations in and around a TC will improve knowledge of the environment in which a TC exists, and improve a TDO's ability to provide accurate forecasts of track, intensity, and structure. Via improving the initial conditions for the NWP models in which TC predictions are based, accuracy of NWP-based forecasts will be improved. The National Aeronautics and Space Administration (NASA) and USAF special aircraft-based observations have been examined for evidence that the *in situ* observations actually do contribute to improved forecast accuracy. Based on these results, an unmanned aircraft, the Global Hawk (GH), is examined as an observing platform for collection of *in situ* observations in the environment of a TC. In this thesis, this strategy is examined in relation to current GH performance capabilities regarding flight altitudes, duration, and observations over the WPAC.

Focus areas of this study include use of satellite observations to define cross-section of TCs in the WPAC from the years 2006–2010. The system of choice for this study is CloudSat (Cloud Satellite) Tropical Cyclone Overpasses (Figure 1) collected from data sets provided by Colorado State University. This will provide an inside look at the vertical extent of average updrafts and downdrafts for TCs in the WPAC. It will also show average size on a horizontal scale as well as intensity levels for different quadrants of each storm.

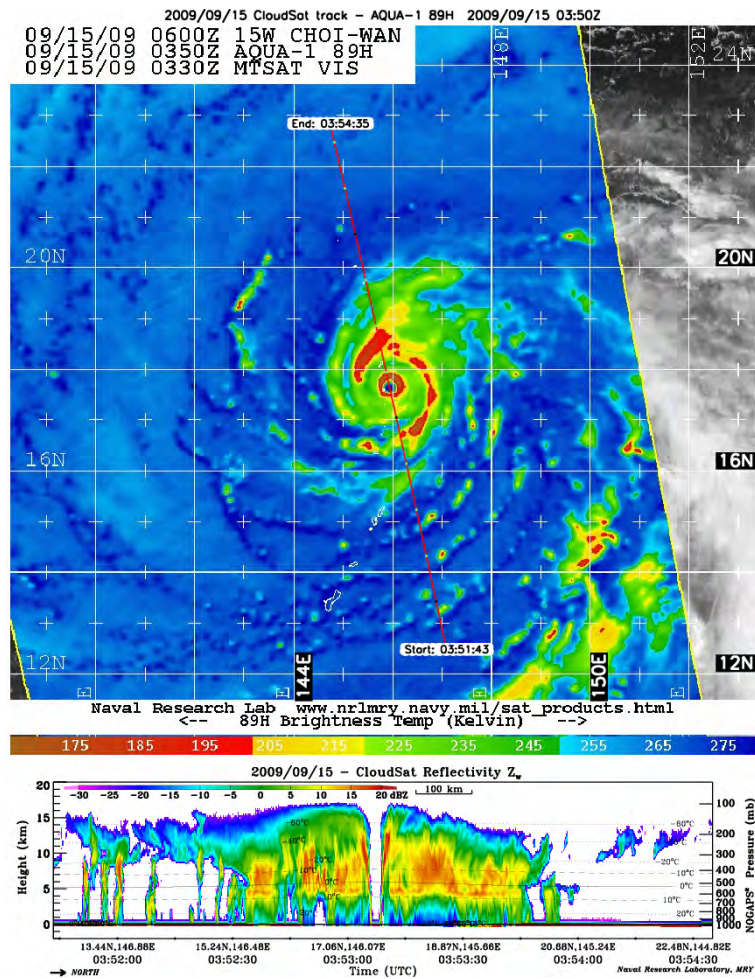


Figure 1. An example CloudSat product provided by Colorado State University. This cross-sectional image is of Tropical Cyclone 15W taken on Sept 15, 2009 in the WPAC (from http://www.nrlmry.navy.mil/sat_products.html)

Another focus will be to examine and study the maximum height of convective cloud tops and associated cloud-top temperatures of three 2013 WPAC TCs. The storms in this study are TC Pabuk (19W), TC Fitow (22W), and TC Danas (23W).

The primary objective of this study is to examine the value of the GH in support of the JWC and DoD assets throughout the WPAC. Operation of the GH in the deep convective environment of the tropical western North Pacific is dependent on the characteristics of the convection and temperatures that impact the GH operations. Therefore, it is necessary to define convective characteristics

such as cloud layer height and temperatures, precipitation intensity, lifetime, and movement. A climatology study of convective parameters will then be analyzed with respect to current restrictions that the USAF and NASA have on the use of their GHs.

II. BACKGROUND

A. REDUCTION IN FORECAST ERRORS AND UNCERTAINTY

Since 1959, the JTWC has been responsible for the issuing tropical cyclone warnings in the WPAC, South Pacific Ocean and Indian Ocean for United States Department of Defense interests, as well as U.S. and Micronesian civilian interests within the command's area of responsibility (AOR). The JTWC provides support to all branches of the U.S. Department of Defense and other U.S. government agencies. Their products are intended for the protection of primarily military ships and aircraft as well as military installations jointly operated with other countries around the world.

A primary operational goal of the JTWC is to minimize the amount of area that must be placed under warning and maximize accuracy of forecast conditions. As a result of the 2009 DoD Tropical Cyclone Conference, Brigadier General William Uhle, USPACOM Deputy Director of Operations, set forth a mandate to reduce the size of uncertainty about the forecast position of a TC by 50% to increase the maneuverability of U.S. and coalition forces near a cyclone (Figure 2). General Uhle stated that increasingly accurate forecasts will decrease the number of unnecessary storm evasions and provide for efficient sea- and air-space management, resulting in substantial savings in operating costs (Uhle 2009).

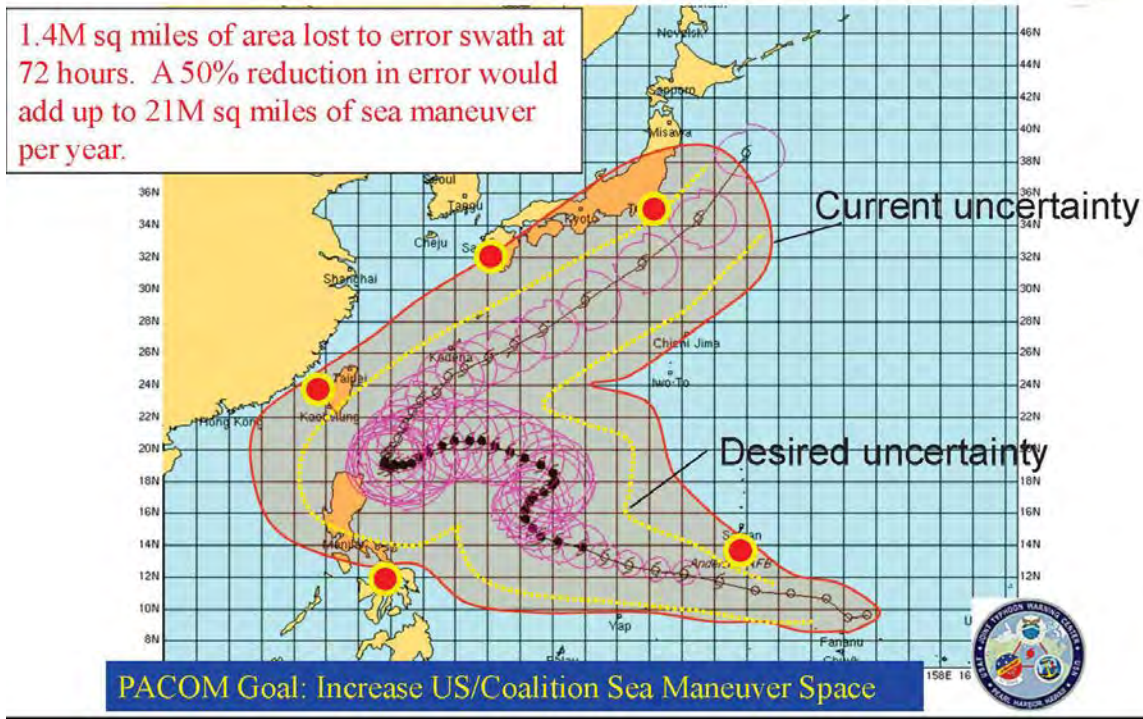


Figure 2. Schematic of current and potential forecast uncertainty in the forecast track of a tropical cyclone over the western North Pacific. Magenta circles define the analyzed radii of tropical-storm-force winds (after slide by M. Angove 2011).

Tropical cyclone forecasts have two main elements: the storm track and the intensity. In this case, intensity is defined as the maximum sustained one minute average wind speed. Over the last few decades, the JTWCF track forecast errors (Figure 3) have declined steadily from 1970 to 2012. The greatest improvement has been made from 1995 to 2004. Possible explanations for this improvement include a better understanding of the TC environment, better numerical models, and the increased use of remote-sensing products. However, after 2005 there has been a dramatic decrease in the rate of improvement in forecast track accuracy. In contrast to forecast track skill, forecast errors of TC intensity have not improved (Figure 4) from 1987 to 2011. From 2004 to 2011, the errors have actually increased slightly compared to 1996 to 2004.

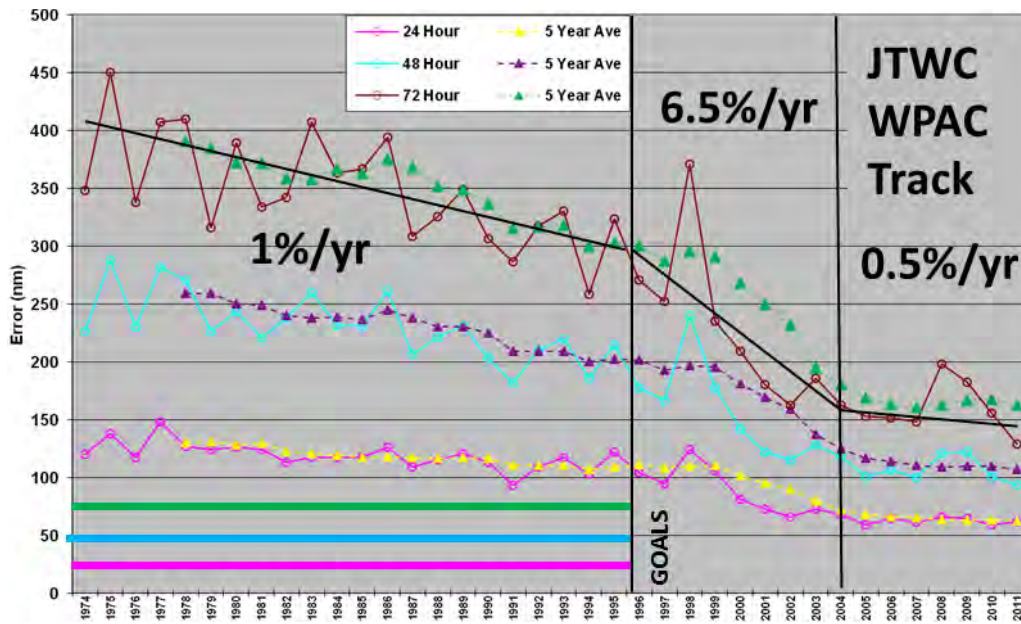


Figure 3. Average JTWC forecast error of TC track from 1974–2011.
Percentages define the rates of improvement for the 72-h forecast
(from JTWC Annual Tropical Cyclone Report 2011)

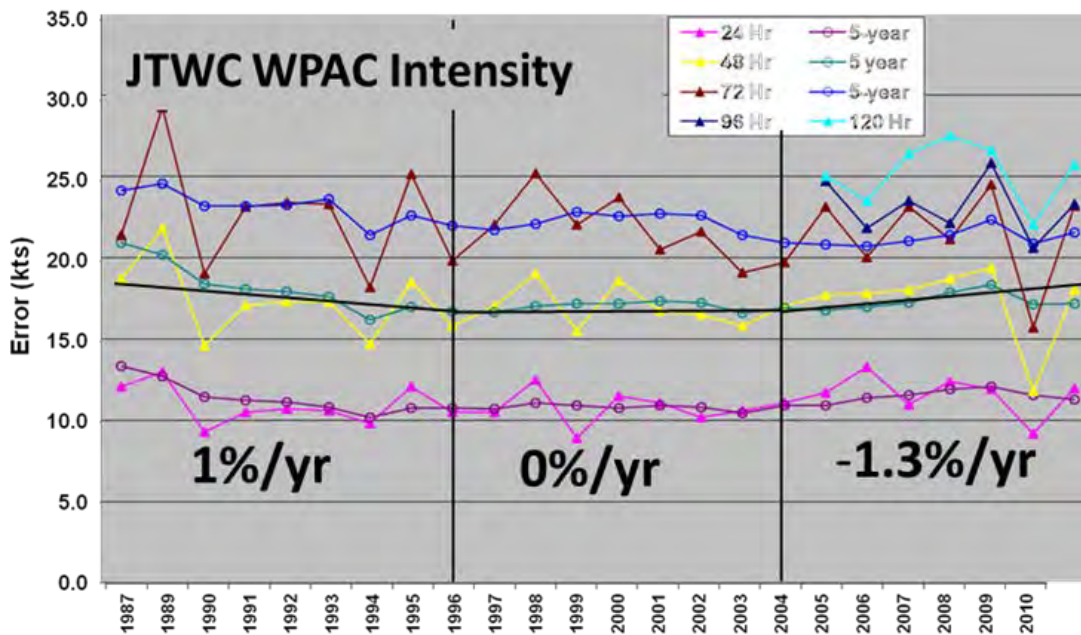


Figure 4. Average JTWC forecast errors for TC intensity from 1987–2011.
Percentages define the rates of improvement for the 48-h forecast
(from JTWC Annual Tropical Cyclone Report 2011)

Based on figures 3 and 4, neither track nor intensity forecast has improved over the most recent five years. Because there is no operational aircraft reconnaissance over the WPAC, storm position and intensity unfortunately is derived from satellite data. These estimates form a basis for the forecast process that incorporates NWP guidance. Because remote sensing capabilities with satellite data may have recently reached a peak in satellite coverage it may not be expected that improvement in future forecast accuracy will be realized. Another factor related to a decrease in the rate of forecast improvement could be that NWP advances have also slowed. From the mid-1990s to the mid-2000s, the improvement in the rate of NWP forecast accuracy of numerical models was significant. Since then the rate of improvement has declined, which could have led to the corresponding decline in the rate of improved forecast accuracy. One last, but very important, contributing factor could be the lack *in situ* data in and around TCs over the WPAC.

The National Hurricane Center (NHC) provides hurricane track and intensity forecasts over the Atlantic Ocean. During the last 20 years, the improvement rate for TC track forecasting (over the Atlantic) has steadily improved (Figure 5). One probable reason for the continued improvement in forecasts over the Atlantic is the timely *in situ* observations obtained by routine aircraft reconnaissance. These aircraft help identify storm location, structure, and intensity. Although the improvement is evident for TC track forecasting accuracy in the Atlantic, the intensity forecasts have not improved (Figure 6). The reason could be related to a lack of understanding of the physical processes that impact TC intensity. These processes include air-sea interaction, precipitation, and environmental interactions.

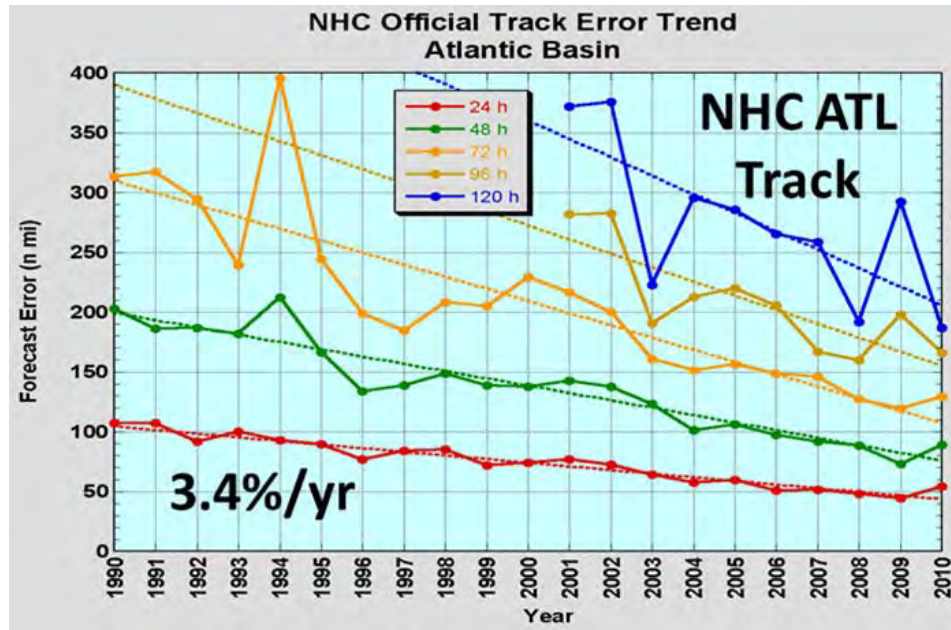


Figure 5. Average NHC forecast errors for TC track from 1990–2010. Percentages define the overall rate of improvement (from Peter Black, Naval Research Laboratory 2012)

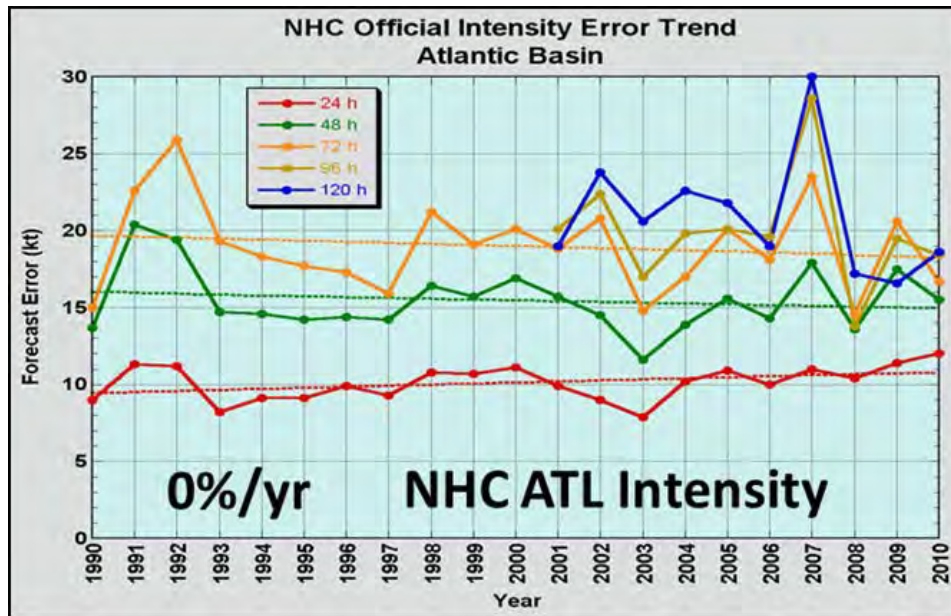


Figure 6. Average NHC forecast errors for TC intensity from 1990–2010. Percentage defines the overall rate of improvement (from Peter Black, Naval Research Laboratory 2012)

Many of the important physical processes that affect storm intensity occur at the lowest levels of the TC. In this boundary layer region, energy is transferred from the warm ocean to the atmosphere. Gathering *in situ* data in this area is important but not usually possible due to the extreme conditions. Because of this limitation, manned aircraft fly through the storm at a typical altitude of 10,000 ft and sample the lower TC region by deploying dropwindsondes. There have been attempts made to operate small unmanned aerial vehicles (UAVs) in this rugged environment (Lin, 2006, Lin and Lee 2008). In these and other experiments, the low-flying UAV has been successfully flown into tropical storms and hurricanes at an altitude of 300 feet (Darack, 2012).

Many studies have documented the importance of the interaction between the TC outflow aloft and the storm intensity (Emanuel, 2007). Storm outflow usually occurs between 50,000 ft and 65,000 ft. Because of these high altitudes, aircraft reconnaissance is not practical and important information on overall storm structure is unavailable to the forecast process.

It is clear that accurate forecasts of TC characteristics depend on a variety of factors. It can be hypothesized that the addition of increased WPAC *in situ* meteorological information in and around a TC would provide improved knowledge of storm characteristics and initial conditions for NWP. Using an Unmanned Aerial Vehicle (UAV) with capabilities of high altitude flights and long duration to possibly capture these missing pieces of information within the structure of a TC should be studied.

B. FUTURE UNCERTAINTY IN REMOTE SENSING CAPABILITY

Polar-orbiting weather satellites circle the earth at a typical altitude of 850 km (530 miles). While a given location on the earth may only be observed once a day, these satellites offer a much higher resolution than geostationary satellites and a variety of products that capitalize on various spectral channels. A significant research effort began to utilize new microwave imaging capabilities based on polar orbiting satellites to provide measurements of TC storm structure

and location (Goerss 2009). A major limitation of these polar-orbiting satellites is that these valuable images are only available when the satellite passes close to the TC. While providing invaluable imagery of storm structure, many of these polar-orbiting satellites have exceeded their life expectancy (Figure 7). Additionally, there are currently no existing programs aimed at replacing existing satellite systems.

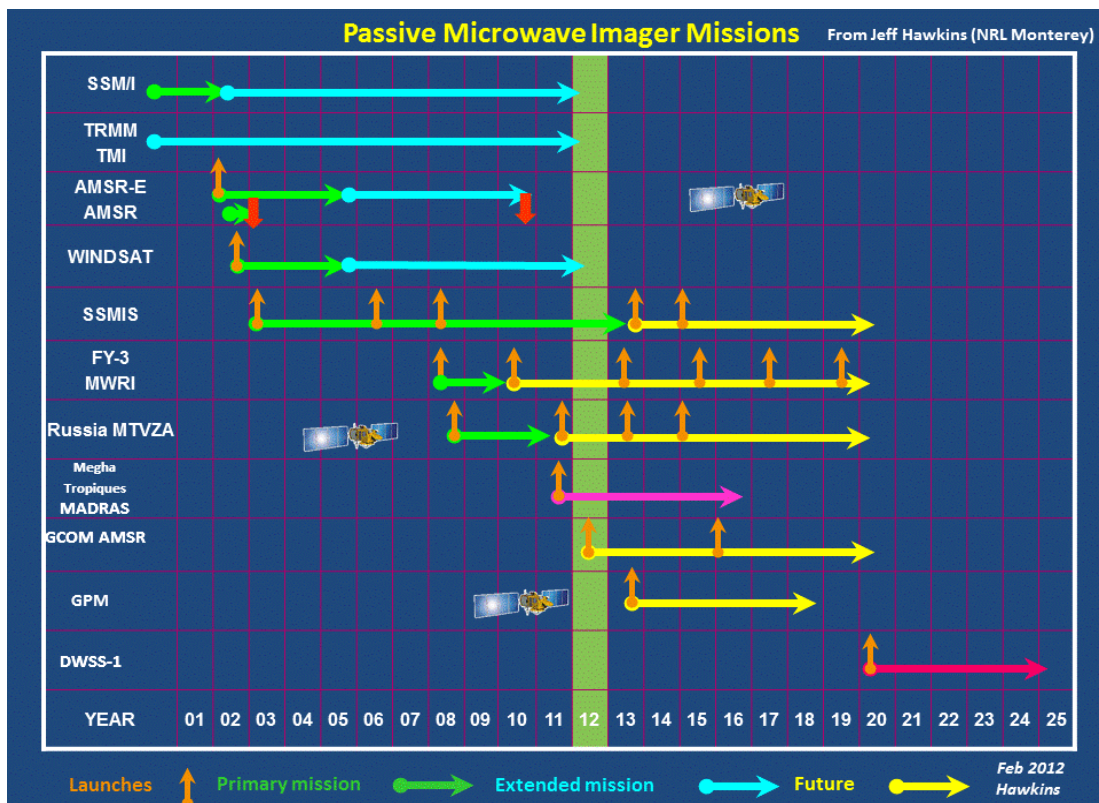


Figure 7. Summary of passive microwave imager sensors (U.S. and foreign) launched, in operations now, recently failed, or future launches. All future satellites are tentatively listed until actual launch occurs. Launch dates are subject to change at any time and might be delayed multiple years (from J. Hawkins, Naval Research Laboratory, Marine Meteorology Division, Monterey, CA Satellite Meteorology Applications Section 2012)

C. GLOBAL HAWK AND THE HURRICANE AND SEVERE STORMS SENTINAL PROJECT (HS3)

Recently, the GH Unmanned Aerial Vehicle (UAV) has been used as a platform for deployment of dropwindsondes in and around tropical cyclones in the NASA Hurricane and Severe Storm Sentinel (HS3) airborne mission. An objective of HS3 is to better define environmental and storm conditions during formation, intensification, and motion. The HS3 mission consists of flying two GHs in and around tropical cyclones to collect environmental data. The observations are used to examine key physical processes associated with TC formation and intensification. These data can then be assimilated into numerical models to define initial conditions. Additionally, sensitivity tests can be conducted to examine how the GH data impacted initial conditions and subsequent forecasts. These impacts are then studied and compared to the actual intensity, structure, and path of the TC.

The HS3 program will consist of one GH focused on measuring the environmental conditions and is equipped with onboard remote sensors developed and deployed by NASA scientists to measure temperature and aerosol characteristics. The environmental GH also includes a system to deploy dropwindsondes, which are small tube-shaped devices, equipped with parachutes that gather and transmit data as they gently fall to the ocean surface. Dropwindsondes provide vertical profiles of temperature, wind, barometric pressure and humidity through the upper-level outflow layer and the environmental structures below. A second GH is used to probe the inner-core of the storm using instruments such as a multi-frequency radiometer system to map ocean surface winds and rainfall rate, especially in the TC eyewall where the strongest winds and heaviest rainfall usually occur. In addition, other NASA instruments on the GH include a conically scanning Doppler radar that will observe the hurricane's wind and rainfall structure along with another radiometer system that will map precipitation features and measure the large thermal

anomaly in the hurricane eye (Parry 2012). The full suite of instruments available for use on the GH is discussed in Chapter III.

At the surface of a Northern Hemispheric TC, the air spirals inward (inflow) in a counterclockwise (cyclonic) circulation. The circulation becomes weaker with height, eventually turning into clockwise (anticyclonic) outflow near the top of the storm (Figure 8). The upper-level TC outflow region is a critical aspect of TC structure (Merrill, 1988) and though its influence on intensification is being studied, it is still poorly understood. The evolving outflow structure and location during the TC life cycle may play a key role in the processes that influence TC intensity changes.

Use of the GH during HS3 has provided vertical profiles of clouds, winds, humidity, temperature and pressure for the entire structure of the tropical cyclones in which it has flown. This can be accomplished because the GHs flying altitude can reach 65,000 ft (19.8 km) and be completely above the storm (Figure 9). With the ability to deploy dropwindsondes from such great heights, scientists and forecasters can explore the dynamical processes at low, mid, and upper levels. These type of *in situ* measurements have never been collected in the important TC outflow layer. Historically, the only measurements that have provided data on the upper-level outflow were from geostationary and polar-orbiting satellites. Observations of outflow could examine whether these TC intensity changes and outflow changes are due to the internal processes of the TC convection, the surrounding environmental interactions, or both. Finally, the use of a GH may provide capabilities of full storm data coverage in lieu of reduced operational satellite capabilities.

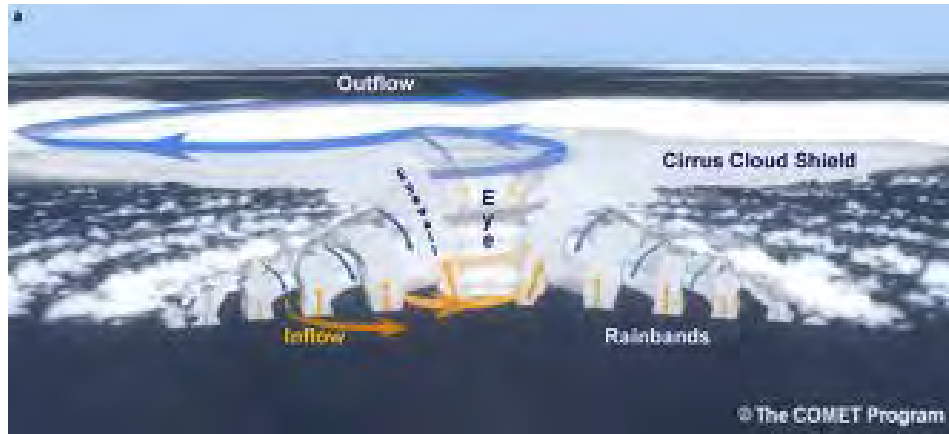


Figure 8. Structure of a tropical cyclone. The upper-level outflow is depicted by cirrus clouds in the upper part of the schematic



Figure 9. The NASA Global Hawk unmanned aircraft system (UAS) is capable of flight altitudes up to 65,000 feet and flight durations of up to 30 hours. An ideal platforms for investigations of hurricanes, the Hurricane and Severe Storm Sentinel (HS3) mission has utilized two Global Hawks, one with an instrument suite geared toward measurement of the environment and the other with instruments suited to inner-core structure and processes (from National Aeronautics and Space Administration 2011)

D. EXPERIENCE FROM NASA GLOBAL HAWK FLIGHTS

When NASA first started utilizing the GH for TC research over the Atlantic Ocean, specific flight operation procedures had to be defined. The in-flight weather restrictions that GH pilots followed were defined based on climatological conditions over the tropics and experience gained in previous GH operations (Figure 10).

Initial In-Flight Weather Limitations for the NASA GH:

- Do not approach thunderstorms within 25 nm during flight at FL500 or below
- When flying above FL500: Do not approach reported lightning within 25NM in areas where cloud tops are reported at FL500 or higher. Aircraft should maintain at least 10000 ft vertical separation from reported lightning if cloud tops are below FL500
- No over-flight of cumulus tops higher than FL500
- No flight into forecast or reported icing conditions
- No flight into forecast or reported moderate or severe turbulence

Figure 10. Global Hawk in-flight weather limitations as defined by NASA operating procedures.

Significant turbulence is by far the most probable hazard to be encountered when flying the GH above TCs. For this reason the flight rules prohibit overflying any storm with cloud tops above FL500 (50,000 ft. pressure altitude) or overflying any storm with lightning regardless of storm top unless the flight level is at least 10,000 ft above cloud top. These flight rules were initially generated partially from flights conducted by the NASA ER-2. The NASA ER-2 has flown over TCs in the late 1990s through the mid-2000s. The latest TC operation was in 2005 when the ER-2 carried instruments that measured the buildup and behavior of tropical storm systems over Mexico, Central America, the eastern North Pacific, Caribbean, and Gulf of Mexico. The aircraft flew over

several hurricanes, including Emily and Dennis that were both intense Category 4–5 storms. The ER-2 collected data measuring the storm vertical structure. Data were collected to map the temperature, humidity, precipitation, and wind structures related to tropical cyclones and other related phenomena that often lead to development of more powerful storms at sea.

Over several decades, NASA has conducted many overflights (Table 1) of tropical cyclones with the ER-2 or GH. In Table 1, three flights by the ER-2 over Cyclone Oliver in the Coral Sea (February 1993) are omitted, as are the 5 GH flights during HS3 (2012) that were over Nadine. No turbulence was encountered during the HS3 flights because the missions were largely focused on the environment and deviated around the only intense convection to occur during the second Nadine flight. The ER-2 or GH, therefore, have made about 35 flights over TCs, mostly without incident. However, there have been some turbulence encounters that caused concern. On 17 July, 2005, the NASA ER-2 experienced significant turbulence overflying the eyewall of Hurricane Emily. There was also significant turbulence experienced by the ER-2 over Hurricane Georges on 25 September, 1998, and Tropical Storm Chantal on 20 August 2001. In all of these events, considerable lightning was observed.

Table 1. Listing of NASA airborne overflights of hurricanes and reports, or lack thereof, of turbulence.

Date	Campaign	Plane	Storm	Field Notes
8/23/98	CAMEX-3	ER-2	Hurricane Bonnie	
8/24/98	CAMEX-3	ER-2	Hurricane Bonnie	
8/26/98	CAMEX-3	ER-2	Hurricane Bonnie	
9/2/98	CAMEX-3	ER-2	Hurricane Earl	A little turbulent at altitude (Heymsfield notes)
9/21/98	CAMEX-3	ER-2	Hurricane Georges	
9/22/98	CAMEX-3	ER-2	Hurricane Georges	
9/25/98	CAMEX-3	ER-2	Hurricane Georges	The pilot Dee Porter experienced considerable turbulence at 63 kft. He reported that the turbulence smoothed out once he increased his altitude to 65 kft. He described the clouds surrounding the eye as a "bubbling caldron."
9/27/98	CAMEX-3	ER-2	Hurricane Georges	No turbulence experienced. Near U. S. Gulf of Mex coast.
8/20/01	CAMEX-4	ER-2	T.S. Chantal	Light turbulence 62–64 kft on second pass
9/10/01	CAMEX-4	ER-2	Hurricane Erin	Small bump over eye reported
9/19/01	CAMEX-4	ER-2	T.S. Gabrielle	Some bumps reported; towers up to 55 kft.
9/23/01	CAMEX-4	ER-2	T.S. Humberto	
9/23/01	CAMEX-4	ER-2	Hurricane Humberto	Two towers came up closer to plane on NW to SE track
9/24/01	CAMEX-4	ER-2	Hurricane Humberto	
7/5/05	TCSP	ER-2	T.D. #4	
7/6/05	TCSP	ER-2	T.S. Dennis	
7/9/05	TCSP	ER-2	Hurricane Dennis	The pilot reported a 38 kt wind out of the east at the ER-2 altitude. He also reported very bad turbulence and some overshooting tops (doming) on the last leg across Dennis.

Table 1 (Cont'd). Listing of NASA airborne overflights of hurricanes and reports, or lack thereof, of turbulence.

Date	Campaign	Plane	Storm	Field Notes
7/15/05	TCSP	ER-2	Pre- T.S. Eugene	
7/16/05	TCSP	ER-2	Pre- T.S. Eugene	
7/17/05	TCSP	ER-2	Hurricane Emily	Severe turbulence
7/24/05	TCSP	ER-2	T.D. #7	
7/25/05	TCSP	ER-2	T.S. Gert	
8/28/10	GRIP	GH	T.S. Frank	
9/2/10	GRIP	GH	Pre-T.S. Karl	
9/12/10	GRIP	GH	Hurricane Earl	
9/16/10	GRIP	GH	Hurricane Karl	
9/24/10	GRIP	GH	T.S. Matthew	

Research conducted by NASA has shown that that the most important cause of significant turbulence above cloud tops is *a very strong updraft reaching the storm top* and penetrating the stable layer usually found there or just above (usually identified as the tropopause, typically at flight level 500–540). Like a rock dropping into a pond, the updraft penetrating this stable layer generates gravity waves that travel upward and outward from the overshooting top. The hazard to the aircraft is clear; short-term, strong accelerations in the x, y, and z directions, and marked changes in indicated air speed that can cause control problems. NASA recently selected 3 storms (Emily, Karl, and Mathew) to identify why or why not turbulence was or was not encountered during the research flights. The findings are summarized below.

1. Emily (2005)

Several publications (e.g., Cecil et al., 2010) have documented in the ER-2 overflight of Emily and the rather harrowing experience of the pilot, Dave Wright, who deserves great credit for obtaining excellent data on this storm and on returning safely to the base of operations in Costa Rica. The main conclusion is that the ER-2 experienced such strong turbulence because it had the misfortune to fly directly over an extremely strong convective cell almost at exactly the time that the cell reached its highest altitude. The ER-2 Doppler (EDOP) radar measured an updraft velocity of greater than 20 m s^{-1} not far below the aircraft, although the cloud top was still about 10,000 ft below the aircraft. All proxies for convective intensity, in addition to the direct measurement of the updraft, were the strongest convective signatures seen by the ER-2 in over 20 tropical cyclone missions that involved approximately 100 passes across storm centers.

Cecil et al. (2010) further concluded that cloud-top height or temperature alone were not good predictors of turbulence, because the ER-2 spent a great deal of time over colder cloud-top temperatures than the cell that caused the problems, without apparent difficulties. It should also be noted that the on-board electric field measurements recorded 28 flashes (Figure 11) during the pass over the strong cell, greater than any cell in all previous ER-2 tropical cyclone flights.

Using the Applied and Computational Harmonic Analysis (ACHA) (Bedka et. al., 2010), Monette et al. (2012) produced products of cloud-top height and temperature for the case of Hurricane Emily (Figure 12) and other cases in which the ER-2 and GH have flown.

When the ER-2 encountered severe turbulence, the ACHA indicated tops near 52,000 ft. As Cecil et al. show, the EDOP radar top at 0753 UTC was about 56,000 ft and still growing. Therefore, the ER-2 at 65,000 ft probably was slightly less than 10,000 ft above the top, not slightly more as indicated by the IR-derived

cloud-top shown here. All other ACHA-derived cells were overflowed by at least 10,000 ft. by the ER-2.

The second eyewall pass that caused concern was at 0844 UTC, but no ACHA height determination could be made at that time. Additionally, a large amount of lightning was detected (Figure 12) during the time of the ER-2 observations. Note that there is uncertainty in the lightning locations from the ground networks and most of the lightning shown to the northwest of the aircraft symbol is likely associated with the small convective cell in the western eyewall. The tropical overshooting tops (TOTs) are also analyzed from GOES imagery but separately from ACHA, and indicate overshoots of the existing cirrus anvil tops and the locations of likely strong active updrafts.

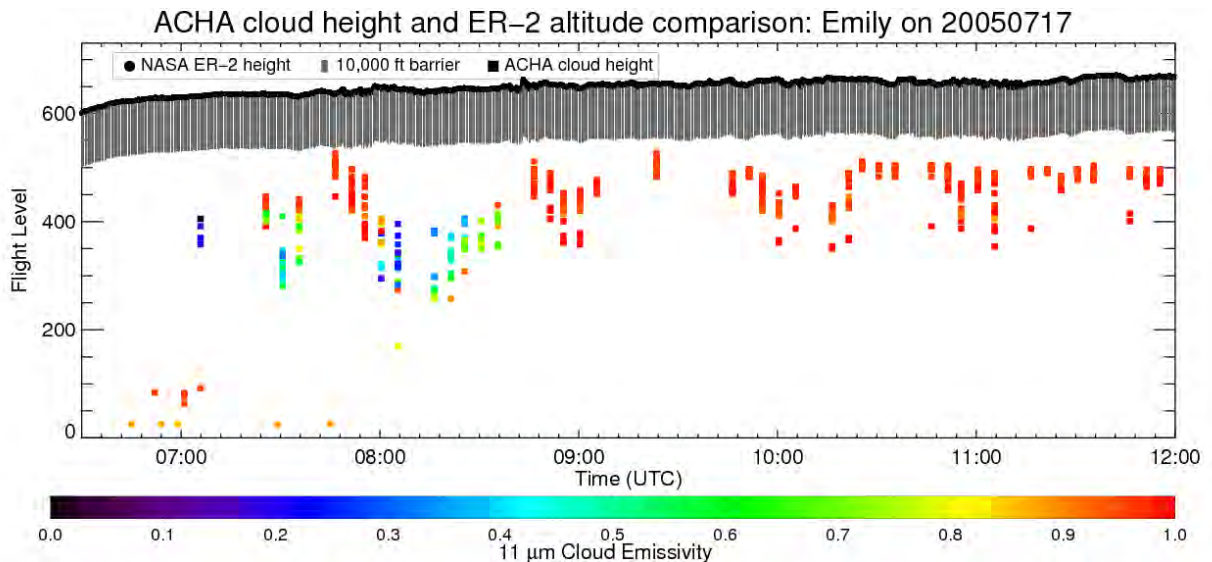
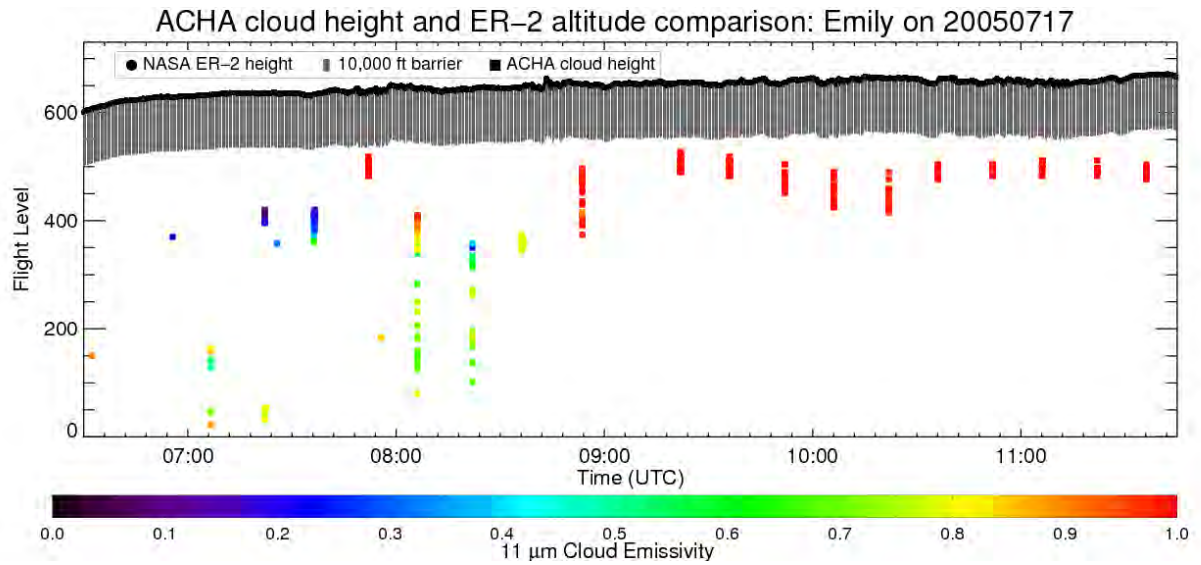


Figure 11. Estimated IR-based cloud top heights from GOES satellite imagery during the period of the ER-2 overflight of Emily on 17 July, 2005. The plotted squares are image pixel heights from all pixels overflowed by the ER-2 in the five minutes preceding the image time (colors indicate emissivity of each pixel) as derived from the Automated Cloud Height Algorithm (ACHA). The NASA ER-2 flight level (black line) and 10,000 ft margin (grey shading) are also shown. The strong cell was overflowed by the ER-2 at 0753 UTC.

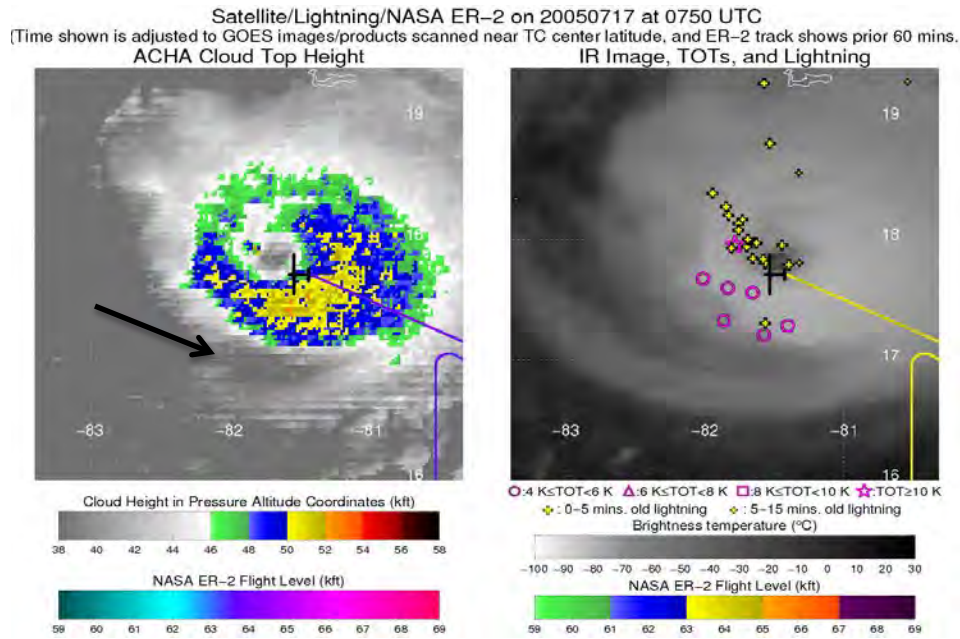


Figure 12. ACHA cloud top heights (left) and tropical overshooting tops (TOTs) and lightning locations (right) at 0750, three minutes before the ER-2 flew over the strong growing cell (indicated by the arrow) in the western eyewall of Hurricane Emily. Arrow pointing to low clouds.

In addition to the direct *in situ* vertical velocity measurements from EDOP, several other factors also indicate that this specific cell at this specific time was unusually strong. The EDOP-measured 40 dBZ reflectivity extended above 14 km (46 kft), the lightning flash rate was unusually great as measured from the Lightning Instrument Package (LIP) instrument and from the long-range lightning detection networks. Also, the passive microwave data from the Advanced Microwave Precipitation Radiometer (AMPR) showed brightness temperatures of about 100 K (well below typical values of >150–225 K for convection). These indicators of convective intensity seem to be more indicative of severe conditions than the cloud-top height or temperature because the ER-2 had previously overflown a large region of higher and colder cloud tops without incident.

2. Karl (2010)

In a landmark achievement during GRIP, the GH made about 20 consecutive overflights of the eye of Hurricane Karl during a 14-h period on 16–17 September 2010. No particular difficulty was experienced with turbulence during these overflights, in spite of overflying within about 5,000 ft. of some very cold cloud tops in the eyewall (Figure 13).

Between 2000–2200 UTC 16 September (Figure 13 and 14), there were periodic indications of lightning and TOTs in the eyewall of Karl. However, starting at 2200 UTC all lightning close to the center ceased for about 6 hours. The TOTs were sporadic and generally weaker near the center of Karl than during Emily.

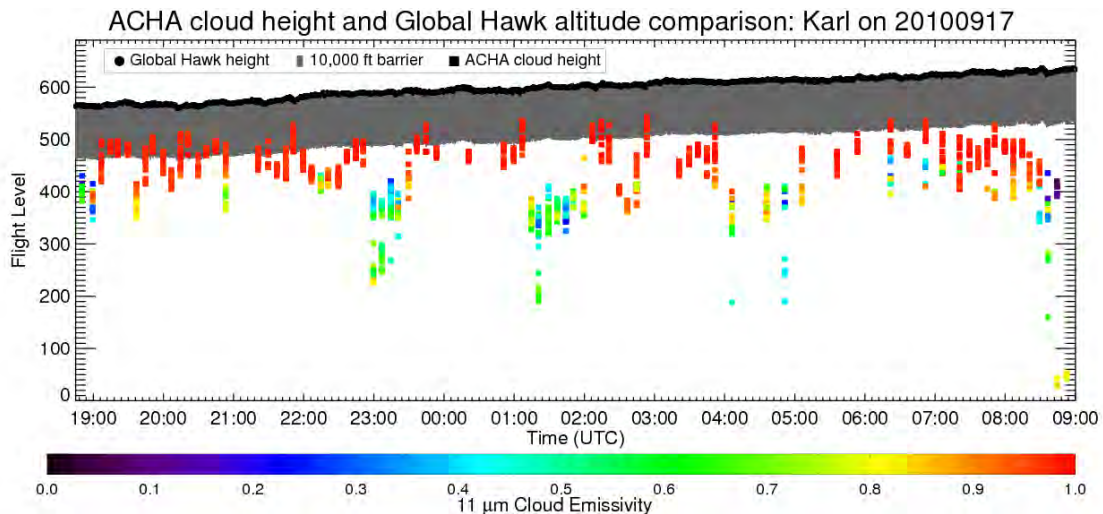


Figure 13. As in Figure 10, but for Hurricane Karl (2010).

Satellite/Lightning/Global Hawk on 20100916 at 2350 UTC
(Time shown is adjusted to GOES images/products scanned near TC center latitude, and GH track shows prior 60 mins.)
ACHA Cloud Top Height Visible Image and Tropical Overshooting Tops

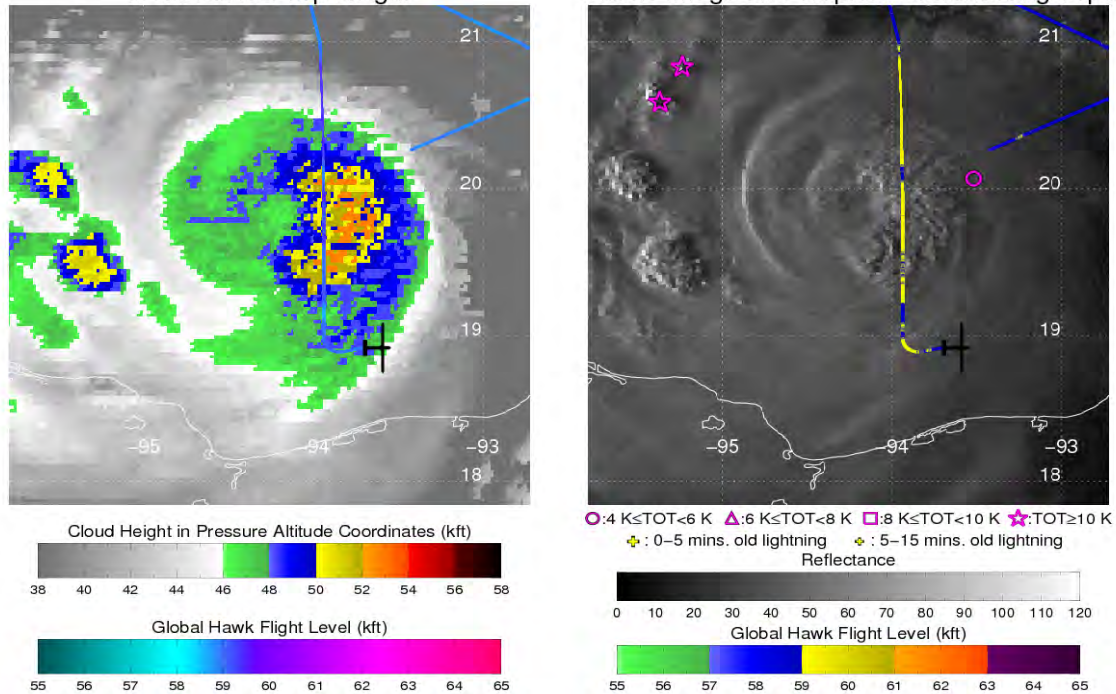


Figure 14. As in Figure 11, but for Hurricane Karl at 2345 UTC on September 16, 2010. The Global Hawk had just overflown the eastern semicircle of the eyewall at about 59,000 ft. with cloud tops about 53,000 ft. and with a somewhat “bumpy” appearance. However, no TOTs are indicated along the flight path (one TOT, not shown. was detected a few minutes earlier in the south eyewall at 2338 UTC). While some lightning was noted near the eye between 2000–2200 UTC, and a few TOTs, neither indicator approached the intensity or frequency that characterized the center of Emily during the ER-2 mission.

3. Matthew (2010)

During the period of GH overflights of Matthew (Figure 15), the convective cells appeared to have had an intensity somewhat greater than those during the Karl overflight, but not as strong as those during the ER-2 investigation of Emily. This characterization of the convection occurred in spite of the fact that the ACHA-derived cloud-top heights (Figures 15 and 16) for Matthew were generally the coldest and highest of the three examples. Note the large number of cloud heights that reached 55–58 kft, coming within about 5000 ft of the GH flight altitude periodically throughout the flight (Figures 15 and 16). Inspection of the

detailed links for Matthew demonstrates that there were occasional bursts of lightning and TOTs for some limited regions. However, only rarely did these (independent) indicators of intense convection persist in the same region for more than about 30 minutes. In contrast, a region of cold, high cloud tops persisted northeast of the center for many hours. In the example shown in Figure 16, a single TOT was detected with a high cold top at 0450 UTC where the GH passed at about 0443 UTC. A group of lightning flashes were also detected in that same location at 0507 and 0537 UTC (not shown), but neither of these convective-intensity indicators reached the magnitude that they did for the Emily event.

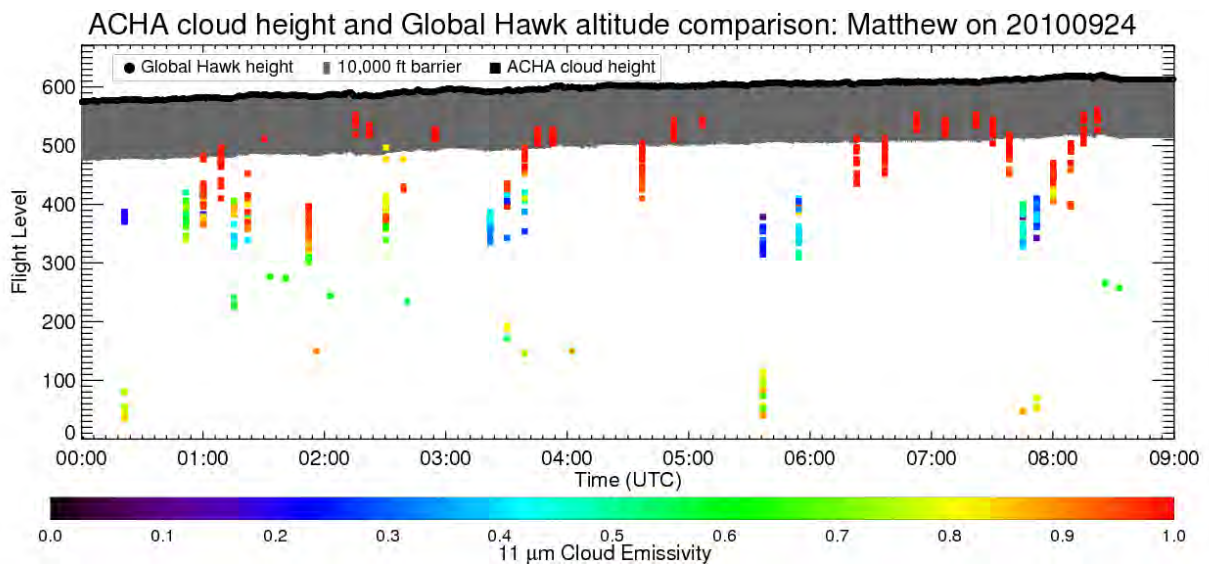


Figure 15. As in Figures 10 and 12, but for Tropical Storm Matthew (2010).

Satellite/Lightning/Global Hawk on 20100924 at 0450 UTC
(Time shown is adjusted to GOES images/products scanned near TC center latitude, and GH track shows prior 60 mins.)
ACHA Cloud Top Height IR Image, TOTs, and Lightning

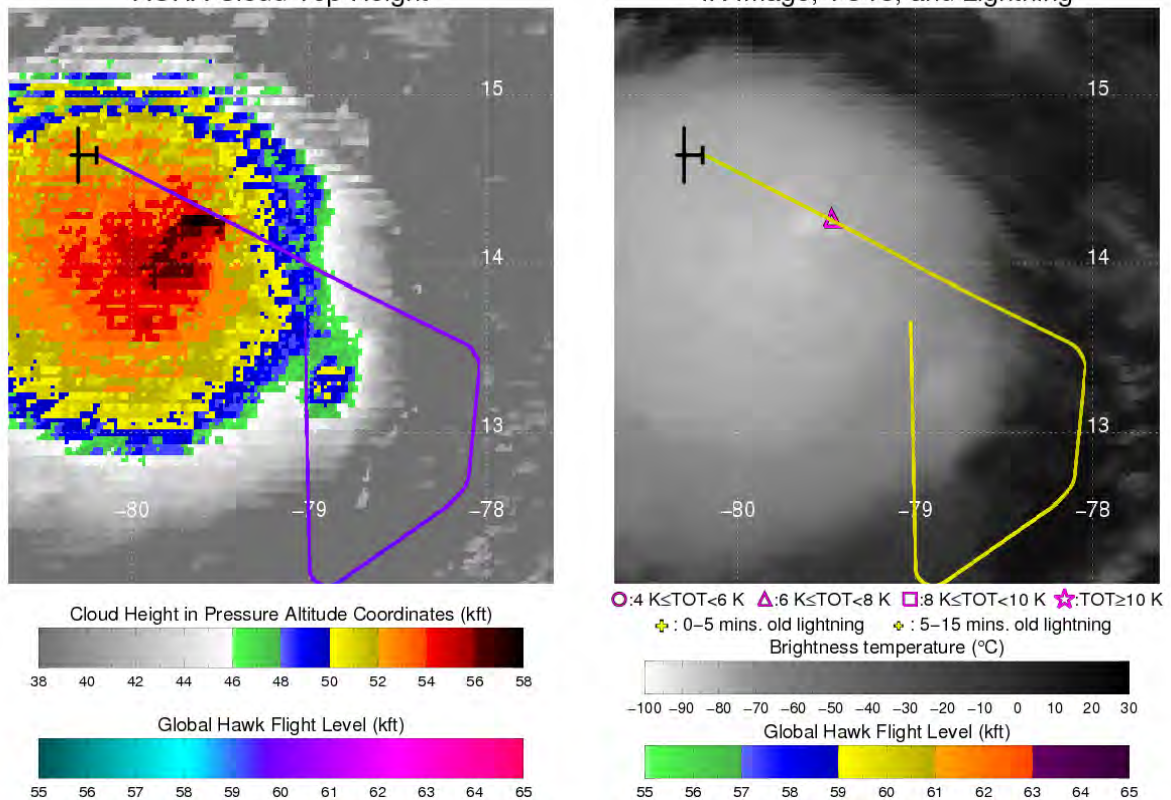


Figure 16. As in figures 11 and 13, but for Tropical Storm Matthew at 0450 UTC on 24 September 2010.

4. Preliminary conclusions on Global Hawk capabilities

The convective cell that caused serious concern about the safety of the ER-2 in Emily was especially strong for a tropical cyclone environment. In fact, the cell was probably as strong or stronger than any that had been overflowed by the ER-2 in 20 previous flights over tropical cyclones. Specifically, what made that cell a safety concern was the magnitude of the vertical velocity of the updraft, at least 20 m s^{-1} at the time the ER-2 overflew it. Such a strong updraft can generate strong gravity waves at and above the tropopause, posing a potential danger to aircraft far above the maximum altitude of the updraft itself or its associated cloud top. Indeed, the ER-2 was probably at least 9000 ft above that cloud top.

Cloud-top height, *by itself*, is not an especially good indicator of the intensity of convection and the likelihood of turbulence. Additionally, overflying high cloud tops (i.e., > 50,000 ft) should be of no particular concern unless there is other evidence of very strong convective updrafts beneath those tops in the path of the aircraft.

Lightning, especially lightning with a high flash rate, is well correlated with convective intensity (Zipser et al. 2013). Lightning with a minimal flash rate (say 1–3 flashes per minute) is indicative of updraft speeds of about 10 m s^{-1} in the mixed phase region where charge is being separated, generally at altitudes about 20–25 kft in a hurricane. That is still stronger than typical updrafts (more like 5 m s^{-1}). An unresolved issue is whether there is a high and instantaneous correlation between vertical velocity in the middle troposphere (necessary for lightning generation) and near cloud top (more direct concern for overflights).

Tropical overshooting tops indicate significant vertical velocity at the cloud-top canopy that penetrate the stable layer at which surrounding cloud tops have spread out (anvil tops). An indirect measure of vertical velocity at cloud top is the magnitude of the brightness temperature difference between the coldest overshooting pixel (TOT) and the immediate surrounding anvil top (Monette et al. 2012). One should be especially cautious about overflying TOTs with deficits of 8–10 K or more for newer cells and smaller values when embedded in existing cold cloud tops. Such tops may indicate updraft speeds greater than $10\text{--}15 \text{ m s}^{-1}$. However, more research is needed on the use of this convective indicator, because it is suggested that the time scale of an individual TOT (if it is more like a small bubble rather than a deep jet) is normally less than 5–10 minutes. This is significant because the TOT that was a problem for the Emily flight was only detected in available GOES imagery as a potential hazard 3 minutes before the encounter.

5. NASA Summary

The current GH flight rules would probably not have been effective in the single event of greatest concern (the Emily encounter). The cloud top had not reached 50,000 ft until about three minutes before the encounter. The TOT and lightning data would not have been available until near the overflight time since this was a rapidly growing cell. Avoiding such a cell probably requires continual monitoring of the forward camera and storm scope, whether or not cloud tops have been exceeding specific limits. However, the current overflight rules as strictly interpreted would have prohibited significant fractions of the successful GH overpasses of Karl and Matthew that proved not to be hazardous.

Through this study, NASA decided that revisions to the weather in-flight limitations (Figure 17) were warranted and validated these with the following three points:

(1) Newly-developed tools to diagnose potential hazardous conditions are now available. However, these must be used carefully and collectively. The focus should not solely be on cloud-top height, but also should incorporate indicators of the presence of intense convection, especially if they have persisted in a region of the TC for the past 30–60 minutes. Notably, these indicators include lightning with flash rates greater than 1–2 flashes per minute as indicated by current long-range networks, and TOTs, in which the critical magnitude may vary with the extent or temperature of the background cloud canopy. Any regions with both of these indicators of intense convection are “red flags” that could trigger the recommendation for avoidance unless they can be overflown by at least 10,000 ft.

(2) To have a better chance of avoiding overflight of truly intense “surprise” cells such as the Emily example, knowing that they are not necessarily related to particularly high cloud tops, any region exhibiting a sudden increase in lightning flash rate should be monitored using a combination of the storm scope and the forward video camera. If there is evidence of a rapidly growing cell

directly ahead of the GH, the pilots should consider a diversion to avoid it by at least 10–20 nm. The message here is that the satellite and ground-based remote sensing tools may not refresh in time for such cases.

(3) Regions of cold cloud tops that have not exhibited indicators of intense convection as in (1) above should be considered acceptable for overflights within 5000 ft of cloud tops. The occasional TOT or lightning flash should be cause to monitor the region carefully, as in (2) above, but not necessarily cause for complete avoidance.

Revised In-Flight Weather Limitations for the NASA GH:

- Do not approach thunderstorms within 25 nm during flight at FL500 or below.
- Aircraft should maintain at least 5000 ft vertical separation from significant convective cloud tops except:
 - a) When cloud tops above FL500: Do not approach reported significant lightning activity or indicators of significant overshooting tops within 25 nm.
 - b) When cloud tops are below FL500, maintain 10000 ft separation from reported significant lightning or indicators of significant overshooting tops.
- No flight into forecasted or reported icing conditions
- No flight into forecasted or reported moderate or severe turbulence

Figure 17. NASA revised Global Hawk in-flight weather limitations.

THIS PAGE INTENTIONALLY LEFT BLANK

III. REQUIREMENTS AND RESTRICTIONS

A. NASA GLOBAL HAWK PUSH

Northrop Grumman Corporation (NGC) originally manufactured the GH UAV for the USAF. The USAF transferred two GHs to NASA in the fall of 2007. In May 2008, NASA (Dryden Flight Research Center/DFRC) at Edwards Air Force Base (EAFB), CA and the NGC of Rancho Bernardo, CA signed a Space Act Agreement to re-fit and maintain the two GHs transferred from the USAF for use in high-altitude, long-duration Earth science missions.

Each GH UAV vehicle has demonstrated the capability to carry more than 1500 lb of payload to altitudes up to 65,000 ft, and can surpass 30 hours and 11,000 nm in a single flight. Since 2009, the two NASA GH UAV units have been referred to as AV-1 (Air Vehicle-1) (Figure 18) and AV-6 (Figure 19).

The GH is a revolutionary aircraft for science because of its extended range and endurance, which are about twice those of commercial aircraft. Operators pre-program a flight path, then the plane flies under remote control for as long as 30-h, staying in contact through satellite and line-of-site communications links to a ground control station at NASA's DFRC in California's Mojave Desert.

Global Hawks are well established as military aircraft: The USAF has deployed them since 2001; 30 have been built and 26 remain operational. But April 2010 marked the first time a GH had been used for earth science. As scientists and NASA officials gathered inside a Dryden hangar to admire Air Vehicle-1, the first GH made, its sister airplane, AV-6, was heading up the Pacific Northwest coast on a 24-hour flight, which was the first of five flights planned as part of the GH Pacific (GloPac) mission. The GloPac mission was a joint effort between NASA and the National Oceanic and Atmospheric Administration (NOAA) to demonstrate the aircraft's scientific utility.



Figure 18. Photo of the Global Hawk AV-1 in flight (image credit: NASA/DFRC)



Figure 19. Photo of the Global Hawk AV-6 in flight (image credit: NASA/DFRC)

B. GLOBAL HAWK OPERATIONS CENTER

Global Hawk pilots operate the aircraft remotely from a new ground station at Dryden dubbed the Global Hawk Operations Center (GHOC) (Figure 20). The GHOC is divided into three compartments: a lobby where air conditioners cool the giant stacks of computer hardware that keep the airplane flying, and two glass-encased rooms that both face an enormous screen displaying a live camera feed from the aircraft. To qualify to work in the operations center, GH pilots must have 150 flight hours and sensor operators must have 250 flight hours of experience.

The pilots work out of the front room. In the back room, sit more than a dozen payload operators, keeping their eyes on computer monitors as their instruments stream real-time data to them. Pilots control the aircraft using four computer monitors, a keyboard, and a mouse. There is no yoke nor joystick. Although they have a moving map that lets them track the aircraft's progress over remote locations, there is no feeling of motion. The GH track is pre-planned; the aircraft flies on a scheduled airspeed and its bank angles are pre-set, although pilots can make mid-flight adjustments. All GH pilots are rated to fly manned aircraft. The pilots commented that it is possible to become so engaged during a GH flight that it seems like flying a manned aircraft. They add that much of the sensory information available to pilots of manned aircraft is missing for the unmanned aircraft pilots. It is not possible to smell the fuel, see the weather and terrain, hear the engine starting, or feel the movement from a ground control center. An unmanned aircraft pilot is dependent upon computers and their displays for updates on the health of the vehicle.



Figure 20. Flight crew and scientists occupy the Global Hawk Operations Center at NASA Dryden during the Genesis and Rapid Intensification Processes hurricane study in the fall of 2010
(from NASA / Tom Tschida; URL: <http://www.nasa.gov/centers/dryden/news/FactSheets/FS-098-DFRC.html>)

During take-off and landing of the GH, the aircraft must be in line-of-sight communications with the pilot. During the HS3 operation, the pilots deployed to Wallops to manage flight activity from the Global Hawk Mobile Operations Facility (GHMOF) (Figures 21 and 22). Operation of the aircraft is transferred to Dryden after reaching an altitude of approximately 30,000 feet. Additional pilots sitting in the Dryden's GHOC will receive the verbal hand-off via telephone, cross check data links with pilots at Wallops, and assume responsibility for the aircraft operation until the mission is completed when the landing operation transfers back to Wallops. This close coordination alleviates the necessity to deploy a larger number of pilots.



Figure 21. The NASA Global Hawk Mobile Operations Facility is a portable ground control station that can be transported anywhere for remote operations (from NASA/Tony Landis 2010. URL: http://www.nasa.gov/mission_pages/hurricanes/missions/hs3/news/pilot-challenges.html)



Figure 22. The interior of the NASA Global Hawk Mobile Operations Facility outfitted for operation of the Global Hawks from locations other than NASA's Dryden Flight Research Center in California. This ground control station also allows for operation of two Global Hawks simultaneously (from NASA/Tony Landis 2010. URL: http://www.nasa.gov/mission_pages/hurricanes/missions/hs3/news/pilot-challenges.html)

The NASA GH payload communication links (Figure 23) are fully independent of the communication links used to operate the aircraft. Four dedicated Iridium Satcom communication links are used for continuous narrow band communications between the GHOC and the payloads on the aircraft. This narrow band communications capability allows pilots to send payload commands from dedicated payload workstations in the Payload Operations Room of the GHOC and receive real-time status and low-rate data from their instruments throughout the duration of the mission. The flight crew uses two additional Iridium links to monitor power consumption by individual payloads, and to control features such as lasers and dropsonde dispensing.

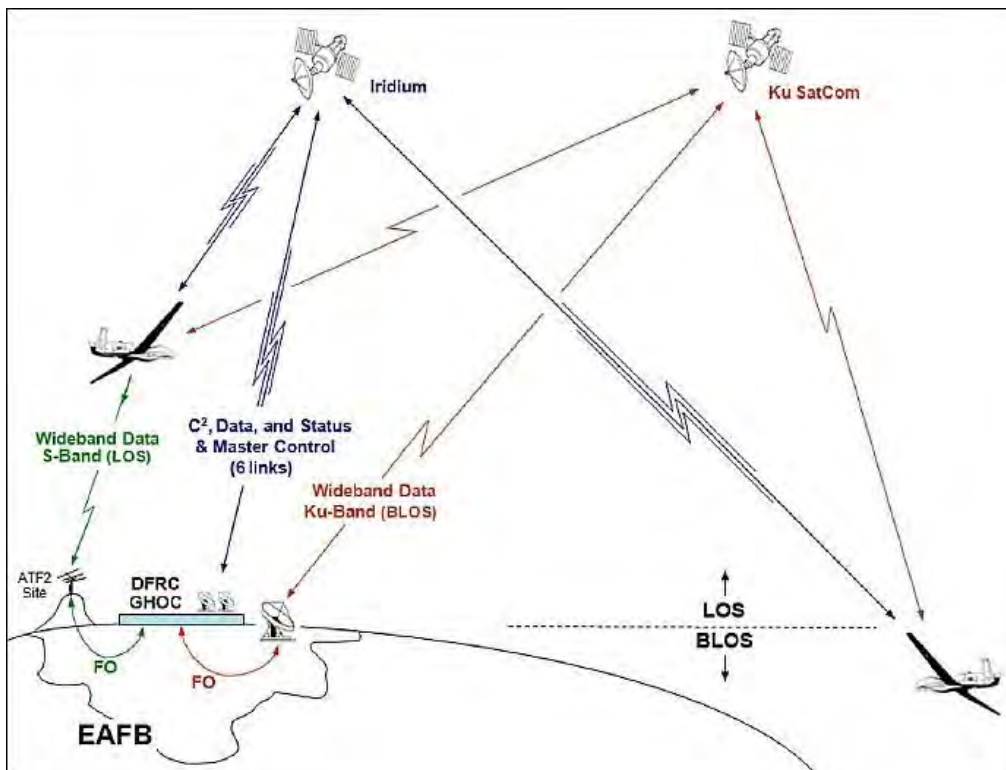


Figure 23. Overview of the Global Hawk communications architecture (from NASA/DFRC 2010. URL: <https://directory.eoportal.org/web/eoportal/airborne-sensors/global-hawk>)

C. CURRENT NASA GLOBAL HAWK INSTRUMENT DESIGN

Currently NASA utilizes two GHs; AV1 and AV6 (Figures 24 and 25). In the current configurations of AV-1 (Figure 24) and AV6 (Figure 25) for the HS3 program, AV1 is designed to observe the inner core of a TC and the AV2 is designed to observe the environment in which the TC is moving.

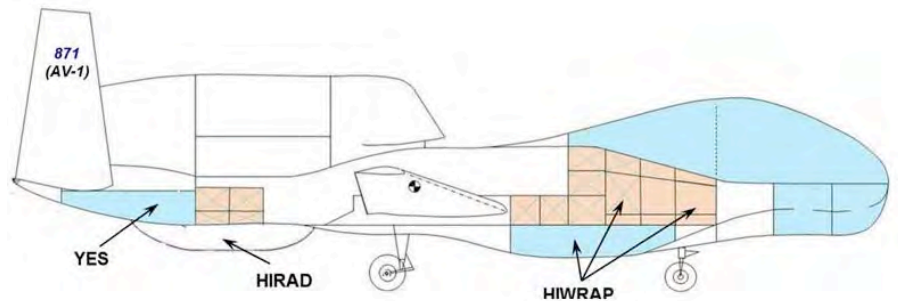


Figure 24. Payload Instrument arrangement for AV1

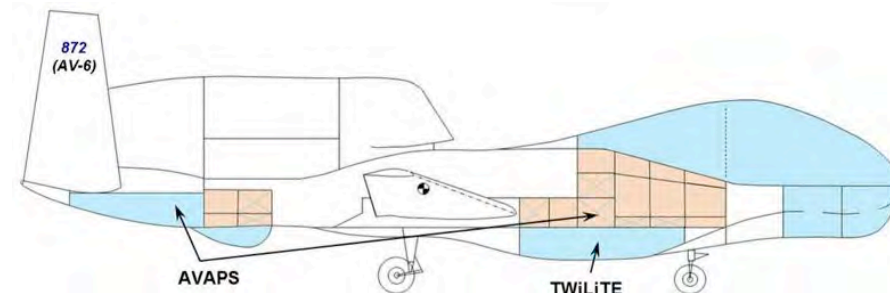


Figure 25. Payload Instrument arrangement for AV6

1. AV1 Payload

a. *High-altitude Imaging Wind and Rain Airborne Profiler*

The high-altitude imaging wind and rain airborne profiler (HIWRAP) (Figure 26) is a dual-frequency (Ku- and Ka-band, or ~14 and 35 GHz), dual-beam (30° and 40° incidence angle), conically scanning radar (Heymsfield et al. 2008). HIWRAP uses solid-state transmitters along with a novel pulse

compression scheme that results in a system that is considerably more compact and requires less power than typical radars used for precipitation and wind measurements (Figure 26). By conically scanning at ~16 rpm, its beams sweep below the GH collecting Doppler velocity/reflectivity profiles to yield the three-dimensional wind field. The unique HIWRAP sampling and phase-correction strategy (frequency diversity Doppler processing technique) is used to de-alias Doppler measurements. The HIWRAP dual-wavelength operation enables it to map full tropospheric winds from cloud and precipitation volume backscatter measurements, derive information about precipitation drop-size distributions, and estimate the ocean surface winds using scatterometry techniques similar to the NASA QuikSCAT. Winds are retrieved using a gridding approach that takes into account the conical scan geometry (Heymsfield et al. 2008). HIWRAP has undergone a number of performance improvements such as reduced pulse compression range side lobes, better isolation between channels, and a boost in sensitivity of about 10 dBZ at Ka-band.

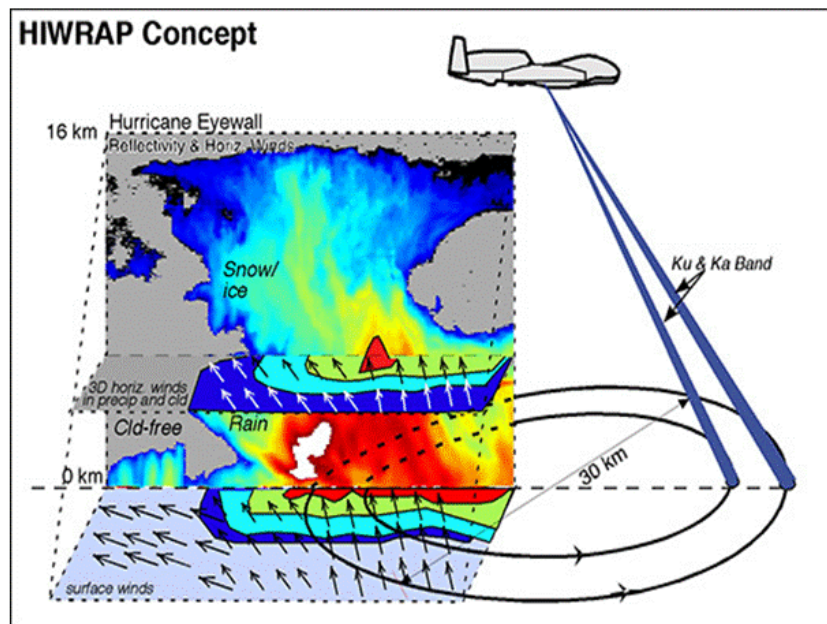


Figure 26. HIWRAP concept of operations over a tropical cyclone

b. Hurricane Imaging Radiometer

The hurricane imaging radiometer (HIRAD) is a C-band radiometer that was developed to retrieve ocean surface wind speed and rain rates up through category-5 hurricane intensity (Jones et al. 2008). It is based upon the Stepped Frequency Microwave Radiometer (SFMR) approach (Uhlhorn and Black 2003) that NOAA and Air Force Reserve reconnaissance aircraft use for operational surface wind and rain estimates. However, HIRAD provides cross-track scanning methodology (Figure 27) to the SFMR nadir-only measurements. It measures upwelling radiation emitted by the ocean surface and intervening rain layer at 4.0, 5.0, 6.0, and 6.6 GHz frequencies. Emissions by the ocean surface increase at these frequencies as the surface becomes disturbed and foam-covered with increasing wind speed. The higher frequencies are more sensitive to rain than the lower frequencies, so the combination of frequencies allows simultaneous retrieval of surface wind speed and rain rate. Unlike the narrow (~1.3 km scene) nadir-viewing SFMR, HIRAD maps a ~60 km wide swath.

HIRAD flew on a NASA WB-57 during GRIP (2010) in hurricanes Earl and Karl. Currently, HIRAD is flying on the NASA GH in the HS3 program during 2012 through 2014. The HIRAD provides the primary measurement of storm intensity, defined by the maximum sustained surface wind speed, intensity change, and the horizontal structure of surface wind speeds (Figure 27). These are fundamental measurements for characterizing the response of the TC to upper-level forcing or convective processes. It is unique in its ability to measure the surface wind speed, even through heavy rain that obscures the lowest altitudes for other remote sensors (i.e., HIWRAP).

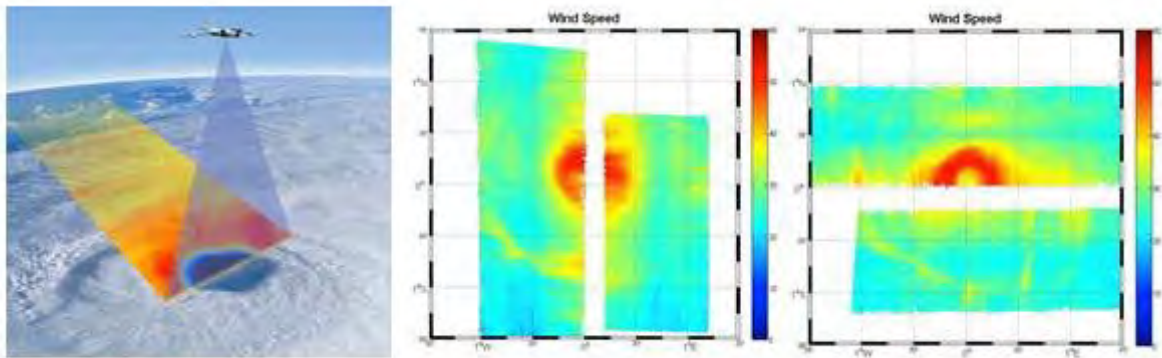


Figure 27. Schematic of HIRAD observation of hurricane wind speed, and retrievals from Hurricane Earl (2010). White strip in each panel is from piecing together adjacent flight legs

c. High Definition Sounding System

The high definition sounding system (HDSS) measures vertical profiles of pressure, temperature, humidity and winds at 4 Hz, and sea surface temperature (SST). The HDSS has 96 expendable Digital Dropsondes (XDD) that can be deployed as quickly as every three seconds. Multiple sondes may be tracked simultaneously in flight. This is particularly well suited for the over-storm aircrafts as it is able to release several sondes over features such as the TC eyewall to capture sharp gradients that often exist in the region. For reliability, dual-redundant automated dropsonde dispensers each have a dedicated receiver and embedded controller. Each XDD contains a battery and a processor running firmware to manage the sensors and UHF telemetry link as well as configuration capability in dual fall rate modes: slow and fast-fall. Optical activation within the automated dropsonde dispenser enables channel and time slice programming prior to release. In addition to measuring SST, the system provides nearly noise-free pressure, temperature, and humidity data that do not require any post processing. This high signal-to-noise ratio enables extraction of parameters such as Richardson number. The data system performs automated quality control and calculates standard parameters such as potential temperature, equivalent potential temperature, and equipotential altitude. Data

are provided instantaneously via a web display, enabling real-time adjustment of flight patterns by the mission scientists to target specific storm features. HDSS is an ONR-funded development that has flown on the NASA P-3 and DC-8 and will fly on the NASA WB-57 in 2013. It will eventually be integrated onto the GH.

2. AV6 Payload

a. Tropospheric Wind Lidar Technology Experiment

The tropospheric wind lidar technology experiment (TWiLiTE) is a scanning direct-detection Doppler Lidar that measures range-resolved profiles of wind speed and direction by transmitting a laser pulse to the atmosphere and detecting the Doppler-shifted frequency of the laser light backscattered by the air molecules (Gentry et al. 2007). Because the primary scattering target is the molecular backscattered signal, TWiLiTE is the first true clear-air airborne Doppler Lidar. Developed under the NASA Instrument Incubator Program, TWiLiTE is designed for autonomous operation on high altitude aircraft (e.g. NASA GH, ER-2 or WB-57) and has previously flown on the ER-2, most recently in October 2012. Integration and flight-testing of TWiLiTE on the GH will be completed in 2013 in preparation for the HS3 2014 deployment. The TWiLiTE Lidar operates at a laser wavelength of 355 nm in the ultraviolet spectrum to maximize the molecular signal return. A novel Holographic Optical Element (HOE) telescope is coaxially aligned to transmit the laser pulse, and collect the atmospheric return, at a 45° nadir angle to produce vertical profiles of radial wind speed versus range. The HOE is rotated in azimuth in a step-stare conical scanning pattern. The radial wind data from multiple azimuth look angles can be combined to derive horizontal vector wind information. In addition to the wind products, TWiLiTE has a total backscatter detector channel (not spectrally resolved) that can be used to derive basic cloud properties. Therefore, TWiLiTE can collect full profiles of the vertical structure of the horizontal wind field in clear-air conditions and optically thin cloud from the lower stratosphere to the surface.

b. Airborne Vertical Atmospheric Profiling System

The airborne vertical atmospheric profiling system (AVAPS) dropsonde has been used for hurricane research (NASA, NOAA, and the USAF hurricane reconnaissance program) for over a decade (Hock and Franklin 1999; Halverson et al. 2006). Dropsondes (Figure 28) provide *in situ*, high-vertical-resolution profiles of temperature, pressure, humidity and winds. The GH dropsonde system is funded by NOAA and built by the National Center for Atmospheric Research (NCAR), which has decades of experience with dropsonde systems. This design is based on a mature and stable technology. Over 500 dropsondes in total have been released from the GH in three flights during the Pacific Winter Storms and Pacific Atmospheric Rivers (WISPAR) campaign, during two 2011 HS3 science test flights and in six science flights during the 2012 HS3 deployment between February 2011 and September 2013. During HS3, the raw sonde data were successfully transmitted from the GH to a ground server, and then relayed to NOAA dropsonde scientists for real-time quality control processing, data and image production and dissemination to HS3 scientists, collaborators, and hurricane forecasters. The data products and images were available in near-real time and World Meteorological Organization (WMO) temp drop messages were transmitted to the National Weather Service (NWS) data gateway for possible real-time data assimilation in NWS and other numerical weather models.

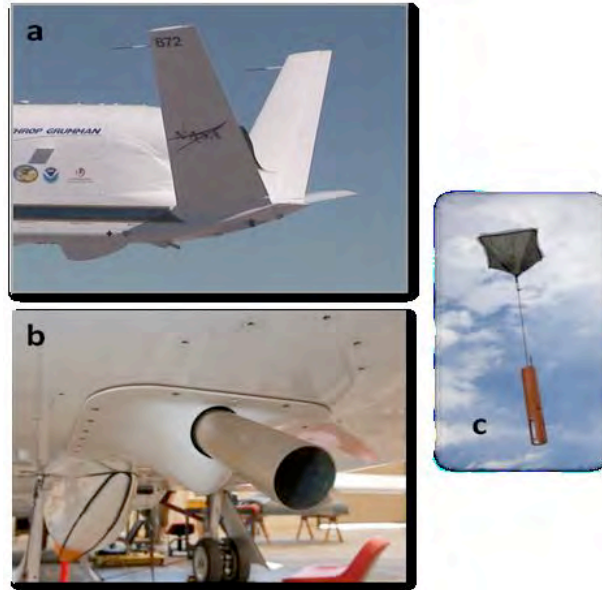


Figure 28. The AVAPS launch tube underneath the tail section of the NASA GH. (c) The GH Mist dropsonde

D. PREVIOUS USE OF THE GH FOR TC RECONNAISSANCE

During the summer of 2010, NASA conducted the tropical cyclone Genesis and Rapid Intensification Project (GRIP) over the tropical North Atlantic. During this program, a NASA GH was utilized to overfly several tropical cyclones (Figures 29A and 29B). In each case, flight operations were conducted from the NASA Dryden Flight Research Center, California. During those operations, the GH was instrumented to define the character of the inner TC structure and the large-scale environment in which the tropical cyclone exists (Figure 30, Table 2).

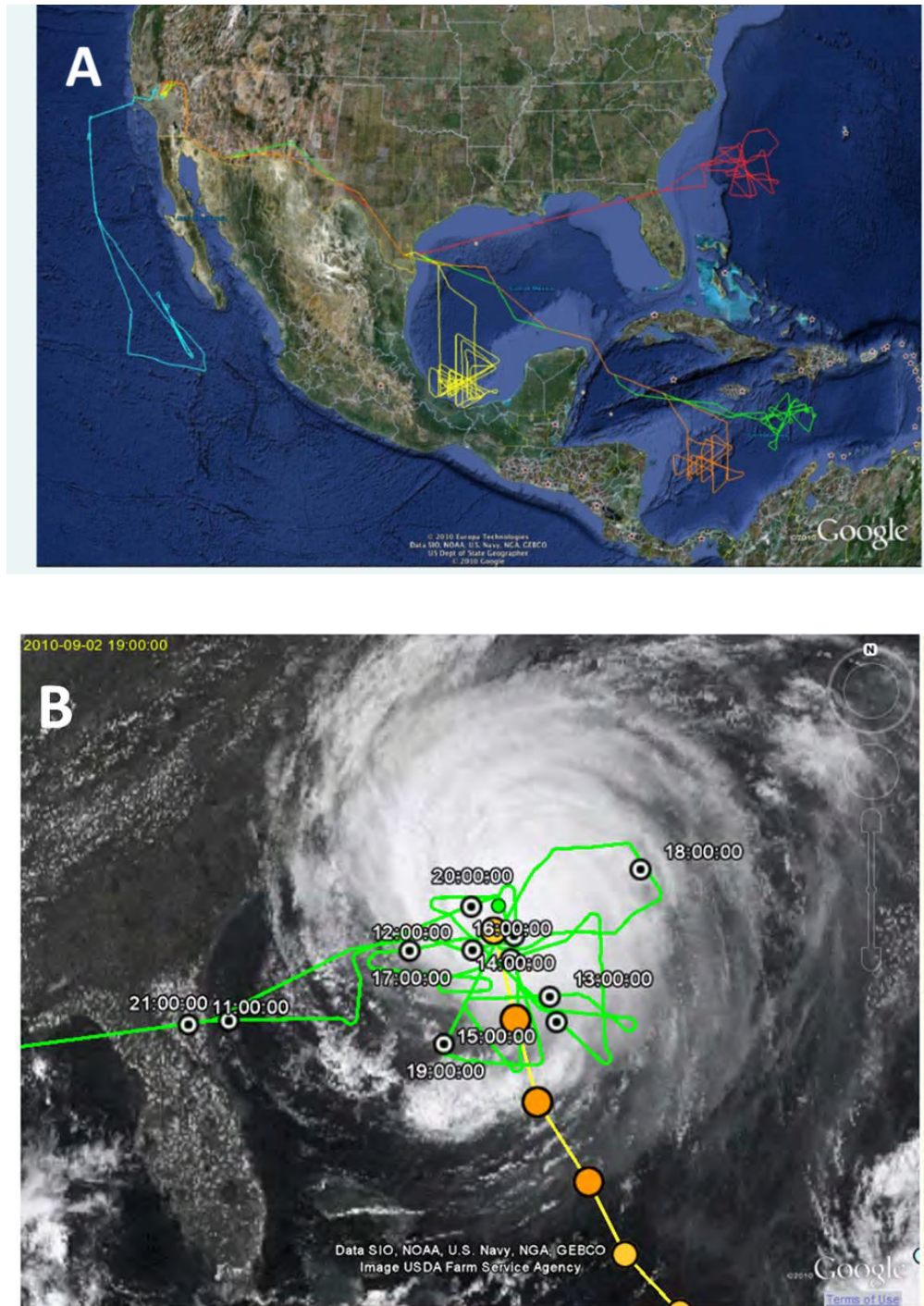


Figure 29. (a) Flight tracks of the NASA Global Hawk utilized during August-September 2010 as part of GRIP. (b) Details of the flight track (green lines) over Hurricane Earl during September 2010. The orange circles and yellow line define the track of Hurricane Earl (from <http://grip.jpl.nasa.gov>)

Table 2. Instruments aboard NASA Global Hawk on hurricane overflight missions during NASA GRIP in 2010

Instrument Name	Measured Parameters
HIRAD: Hurricane Imaging Radiometer	Surface wind speed and rain rate over the ocean
HIWRAP: High Altitude Imaging Wind and Rain Profiler	Three-dimensional profile of winds and rain
HAMSR: High Altitude MMIC Sounding Radiometer	Vertical profiles of temperature, water vapor, and liquid water.

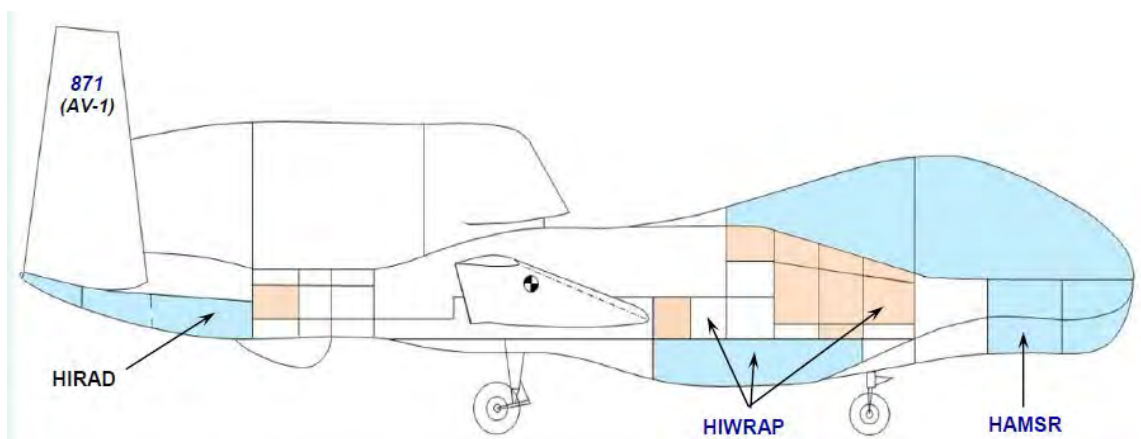


Figure 30. Schematic of the Global Hawk configuration during hurricane overflight missions during NASA GRIP. Instrument definitions are provided in Table 1

The primary objectives of the GH flights in GRIP were to obtain observations of the three-dimensional character of the atmosphere in and around the TC to increase understanding of key physical processes associated with TC formation and intensification. Although a dropwindsonde system was planned to be implemented on the NASA GH prior to GRIP, this was not completed and no dropwindsondes were deployed from the GH during GRIP. While valuable for process studies, the data obtained during GRIP were not utilized to initialize numerical models for hurricane forecasting.

The Hurricane and Severe Storm Sentinel (HS3) is a five-year mission specifically targeted to investigate the processes that underlie hurricane

formation and intensity change in the Atlantic Ocean basin. HS3 is motivated by hypotheses related to the relative roles of the large-scale environment and storm-scale internal processes.

The HS3 is addressing the controversial role of the Saharan Air Layer in tropical storm formation and intensification as well as the role of deep convection in the inner-core region of storms. Addressing these science questions requires sustained measurements over several years due to the limited sampling opportunities in any given hurricane season. Past NASA hurricane field campaigns have all faced the same limitation: a relatively small (three to four) sample of storms forming during the campaigns under a variety of scenarios and undergoing widely varying evolutions. The small sample is not just a function of tropical storm activity in any given year, but also the distance of storms from the base of operations.

E. OBSERVANCE OF UPPER-LEVEL TYPHOON FLOW LIFE CYCLE OVER THE WEST PACIFIC (OUTFLOW) MISSION

The Observance of Upper-level Typhoon Flow Life cycle Over the West Pacific (OUTFLOW) is a proposed five-year mission that will increase understanding of the role of typhoons over the western North Pacific as precursors to extreme weather over North America. Unique capabilities provided by NASA facilities allow for the first-time study of dynamics associated with weather events over one region (the western North Pacific) and their downstream impact on the dynamics and predictability of weather events over another region (the eastern North Pacific and North America).

1. OUTFLOW Science Hypotheses

The two (AV1 and AV6) GH unmanned aircraft systems with complementary payloads optimized to measure the near-storm and large-scale environments are proposed for use in OUTFLOW. Three deployments of five-week duration and an average of ten flight missions will be made from Andersen Air Force Base, Guam during September and October of 2015–2017. The 25–27-

h endurance and 60,000 ft average altitude of these aircraft provides for observations from a variety of sensors of the interaction between typhoon outflow and the subtropical, and extratropical environment that have never before been systematically obtained.

The OUTFLOW project obtains observations critical to understanding how a typhoon interacts with its environment, and the impact of the interaction on typhoon intensity, structure, track, and downstream forcing. Aircraft payloads will measure temperature, relative humidity, and wind profiles from dropsondes (AVAPS/minisonde), continuous sampling of winds from a direct detection Doppler wind Lidar (TWiLiTE), sea-surface temperature from dropsondes (HDSS/XDD), surface winds and rainfall (HIRAD), and three-dimensional wind and precipitation fields from the HIWRAP conically scanning Doppler radar.

An overarching goal of the OUTFLOW project is to improve understanding of how weather over the western North Pacific acts as a key upstream precursor to extreme weather over North America. The North Pacific jet stream defines the medium through which the two remote regions are dynamically linked.

While some programs over the WPAC examined typhoon formation, intensity, and structure changes, OUTFLOW is the first investigation with an innovative approach aimed specifically at interactions between a typhoon and its environment and forcing of extreme weather downstream.

Tropical cyclone convection is considered to be the aggregate latent heat release from convective and stratiform elements within the cyclonic circulation that include individual convective cells, eyewall convection, and rainbands. Additionally, interaction between a TC and its environment refers to either outflow changing the large-scale environment or the large-scale environment changing outflow. Outflow-induced changes to the environment intensify the midlatitude jet stream and/or build a downstream ridge. Environmental-induced changes to outflow organize the outflow into preferred channels that may extend poleward and equatorward from the TC.

Within the framework of the project, outflow from the TC is considered to be either active or passive with respect to TC convection. Active outflow is defined as forcing a convective response, thereby inducing structural and intensity changes in the TC core. In contrast, passive outflow is defined as responding to convective changes in the TC core.

Given the link between the western North Pacific and North America during TC recurvature (Figure 31), the OUTFLOW hypotheses target mechanisms for TC-induced circulation anomalies and how dynamical processes modulate downstream predictability. To test these hypotheses, combined observing and modeling strategies will explore the three-dimensional distribution of mass and momentum in the context of how upper-level outflow from a TC interacts with its environment. For the first time, this interaction will be observed throughout the entire life cycle of TCs over the western North Pacific. Based on this framework, it is hypothesized that:

- H-1. The risk of extreme weather over North America increases following an upstream interaction between typhoon outflow and the jet stream over the western North Pacific.
- H-2. In some circumstances, storm processes drive the interaction between typhoon outflow and the environment. In other circumstances, environmental factors drive the interaction.
- H-3. Observing typhoon-outflow interactions will improve understanding and predictability of the dynamical link between these interactions and extreme weather downstream over North America.

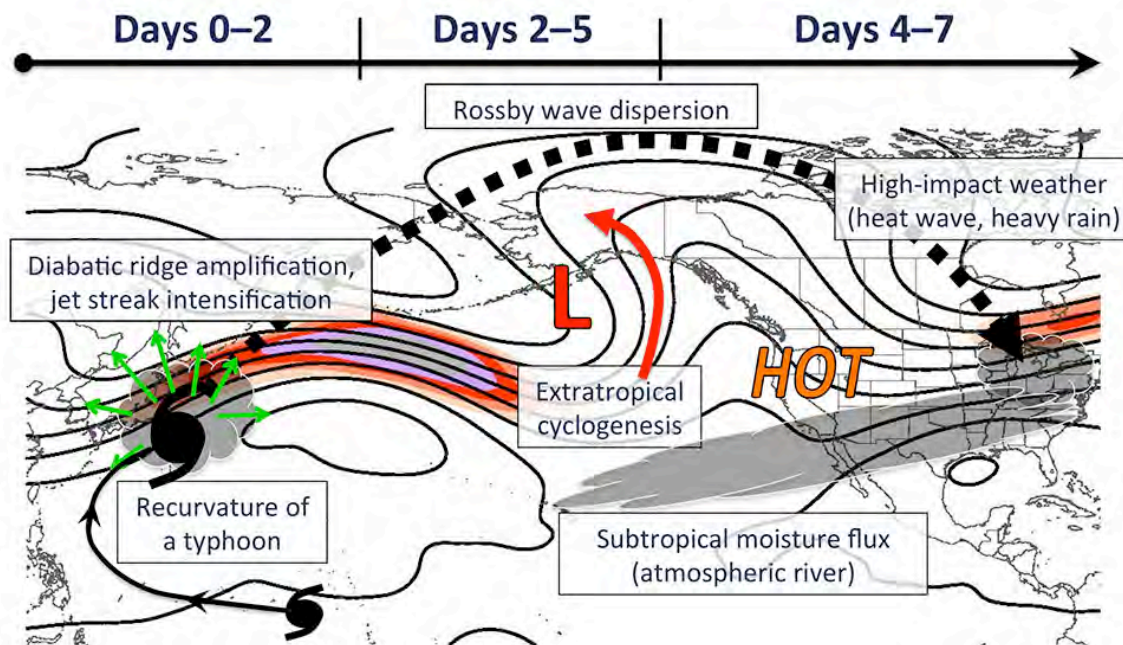


Figure 31. Schematic of the impact of a poleward-moving typhoon on the midlatitude circulation across the North Pacific and North America. The typhoon track is defined by the line connecting the two typhoon symbols. Thin black lines and the color shaded region define the 300-hPa stream function and jet stream, respectively. The gray scalloped regions indicate significant cloud systems. The green arrows denote the divergent outflow of the tropical cyclone. The red L defines the location of extratropical cyclogenesis (after Archambault et al. 2013)

The OUTFLOW hypotheses are formulated to increase understanding of:

- (i) Processes related to outflow, the environment, and downstream impacts; (ii) Processes related to typhoon convection and outflow; and (iii) Predictability of typhoon intensity, structure, and forcing of downstream weather.

The OUTFLOW project employs a set of aircraft and instruments that are ideally suited for testing the above hypotheses. Using two extended duration NASA unmanned airborne systems (UASs), NASA operational satellites, NASA global analyses, and high-resolution simulations, a measurement strategy is proposed to uncover the essential mechanisms of the two-way interaction between a TC and its environment over the western North Pacific. A numerical modeling strategy is proposed to focus the observational aspects, processes,

and predictability. Specific objectives related to TC convection, outflow, and the environment are:

- O-1. To measure and understand how outflow modulates TC convection and how TC convection modulates outflow;
- O-2. To measure key processes that reveal how a TC modifies the large-scale environment over the course of its life cycle;
- O-3. To relate key factors that link TC convection, upper-level outflow, and downstream impacts to processes internal to the TC and processes external to the TC;
- O-4. To understand how key factors related to convection–outflow and TC–environment interactions influence the predictability of storm intensity, structure, track, and downstream impacts.

In summary, the OUTFLOW project obtains observations critical to increasing understanding of how a TC interacts with its environment, and the impact of the interaction on TC intensity, structure, and downstream forcing. The OUTFLOW project befits the unique role of NASA to advance Earth system science and extend the study, understanding, and predictability of extreme weather events on a near-global scale.

IV. WPAC TC CLIMATOLOGY

While safe operations of the GH in and around TCs are a necessity, it is desirable to utilize the GH for maximum data collection. Current flight rules and restrictions may lead to diverting way from regions that are of primary science interests. To assess this likelihood, the GH restrictions are examined in reference to climatological conditions associated with TCs over the WPAC.

A. CLOUDSAT DATA IMAGES

To examine possible limitations associated with utilizing the GH for TC reconnaissance, a limited climatology of cloud-top height distribution for clouds in the WPAC is examined. Tropical cyclones that occurred between 2006 and 2010 are examined to define the maximum cloud height and the maximum convective cloud height. This would then be compared to the operational GH threshold discussed in chapter II. It is assumed that lightning will likely be in the vicinity of the maximum convective cloud height and that the GH can fly at or near a max altitude of 65,000 ft.

Because observations of cloud-top height and temperature must be obtained remotely, a TC CloudSat database (example in Figure 32) is used to define satellite overpasses of TCs over the WPAC. These passes identify the maximum cloud height and also the maximum convective height by utilizing the CloudSat reflectivity values. Based on the collection of passes, a reflectivity of 8 dBZ and higher is used to indicate the vertical extent of active convection. The 8 dBZ value is used to define the level at which strong updrafts are likely to reach.

CloudSat is the first satellite-based millimeter-wavelength cloud radar that is more than 1000 times more sensitive than existing weather radars (Boain 2003). Unlike ground-based weather radars that use centimeter wavelengths to detect raindrop-sized particles, the CloudSat radar allows detection of much smaller particles of liquid water and ice that constitute large cloud masses. To obtain an accurate vertical cross-sectional view of TC structure, the satellite must

pass directly over the TC. Therefore, the narrow swath width of the instrument and sparse locations of TCs limits the number of CloudSat passes directly over TCs.

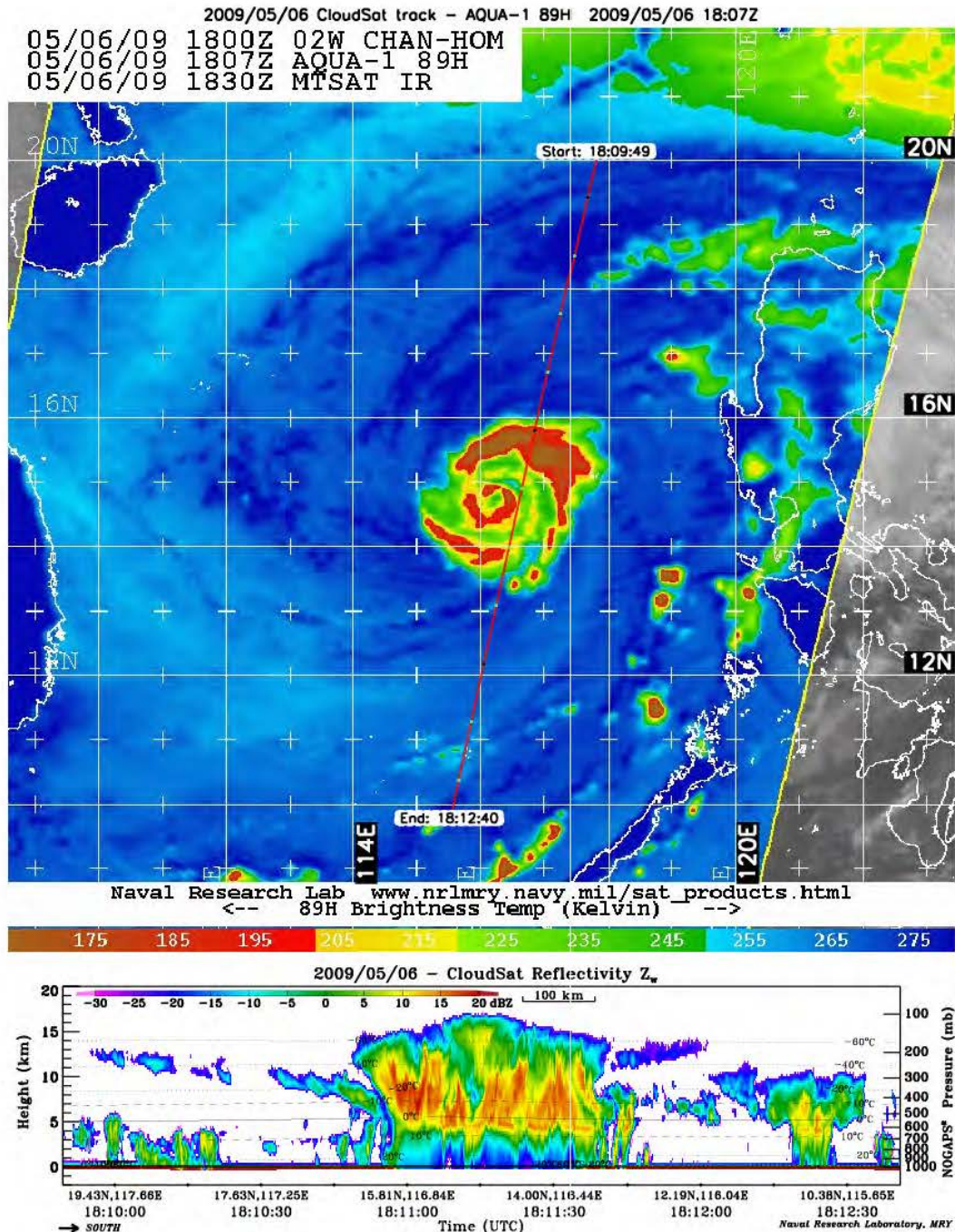


Figure 32. A 2006 CloudSat image depicting a vertical cross-section of 02W (Chan-Hom) (from Colorado State University. URL: <http://reef.atmos.colostate.edu>)

B. TC CONVECTIVE ENVIRONMENT IN THE WPAC (2006–2010)

As defined above, the tracks of TCs between 2006 and 2010 were examined to identify all CloudSat passes that were directly over the TC. As a first order, it is thought that cloud-top height and the convective cloud height should be related to storm intensity. Therefore, in the description of each year, some statistics are presented with regard to the weakest and most intense TC. In the summary, more general statistical analysis is presented.

1. 2006

As mentioned in previous chapters, the JTWC is responsible for the issuing of TC warnings in the WPAC. Each storm upon which a warning is issued is given a numerical value followed by a “W” indicating it’s a WPAC storm. The numerical value given to the TC corresponds to the order of formation for that particular year. In 2006, a total of 26 TCs formed over the WPAC. Of those 26 TCs, vertical cross-sections defined by CloudSat overpasses were available for 14 storms. Since some TCs had multiple passes, a total of 22 cross-sectional images are available for 2006 (Figure 33). For each satellite overpass, the TC intensity (kt), pass coverage, top of cloud (km), and top of convective cloud (km) are defined. The intensity change is indicated by past (i.e., -12-h and -6-h), current, and future (+6-h) intensity. The TC intensity is defined by the JTWC best track. The CloudSat data values were obtained from the CloudSat analysis performed by the Naval Research Laboratory (NRL) in Monterey, CA. The pass coverage value indicates what portion of the TC was observed. A pass value of “1” is a pass directly over the TC center. A pass value of “2” indicates a pass over the second outer band from the TC center and so on. Data that are highlighted in Figure 2 indicate the maximum values for that particular parameter in 2006.

2006							
NAME	INTENSITY (KT) -12 HOURS	INTENSITY (KT) -6 HOURS	INTENSITY (KT)	INTENSITY (KT) +6 HOURS	PASS	TOP OF CLOUD (KM)	TOP OF CONVECTIVE CLOUD (KM)
03W	35	40	45	45	2	17	16.5
04W	100	100	110	120	1	17.5	17
04W	100	90	85	85	2.3	16.5	13.5
06W	55	60	65	70	2	17	16.5
06W	70	70	65	65	2	15.5	13
07W	55	55	65	65	1	16	12.5
10W	45	45	45	50	2	16	15
11W	45	45	50	50	1	17	16.5
11W	45	45	45	45	2	17	15
11W	45	50	55	45	1	16	15
12W	25	30	40	40	2	16	15
14W	115	110	110	100	2	17	13
16W	120	130	140	140	2	17	16.5
16W	115	105	95	90	1	17	12.5
21W	90	90	90	80	2	16	11
22W	90	90	90	90	2	16	14
23W	115	125	125	105	1	17.5	16.5
24W	35	40	45	50	1	17	16.5
24W	100	95	90	80	3	15	11
24W	90	80	80	75	1	17.5	16.5
24W	80	65	50	55	1	15.5	13
25W	80	100	90	65	2	15	12
MEAN					22	16.5	14.5

Figure 33. Composite of CloudSat data for the year 2006. Highlighted values mark the maximum for each category

The intensity values for 2006 range from 40 kt (12W) to 140 kt (16W). During the Cloud-Sat overpass of 12W (Figure 34), the Top of Cloud (ToC) height was 16 km (52.5 kft) and the Top Convective Cloud (TCC) height was 15 km (49.2 kft). The ToC for the most intense storm (16W) (Figure 35) was 17 km (55.8 kft) while the highest TCC was 16.5 km (54.1 kft). The difference in intensity for these 2 storms was 100 kt but the difference in cloud heights was minimal. Furthermore, both CloudSat passes were over an outer band of each storm (e.g., pass coverage of 2).

The minimum TCC height was measured in 21W (Figure 36) and 24W (Figure 37). These minimum values were 11 km (36.1 kft) and they were associated with category 2 storms (90 kt). For each storm over which a CloudSat pass occurred (Figure 38), nine were intensifying, five were steady, and eight were weakening. The mean ToC value was 16.5 km (54.1 kft) and the mean TCC was 14.5 km (47.6 kft).

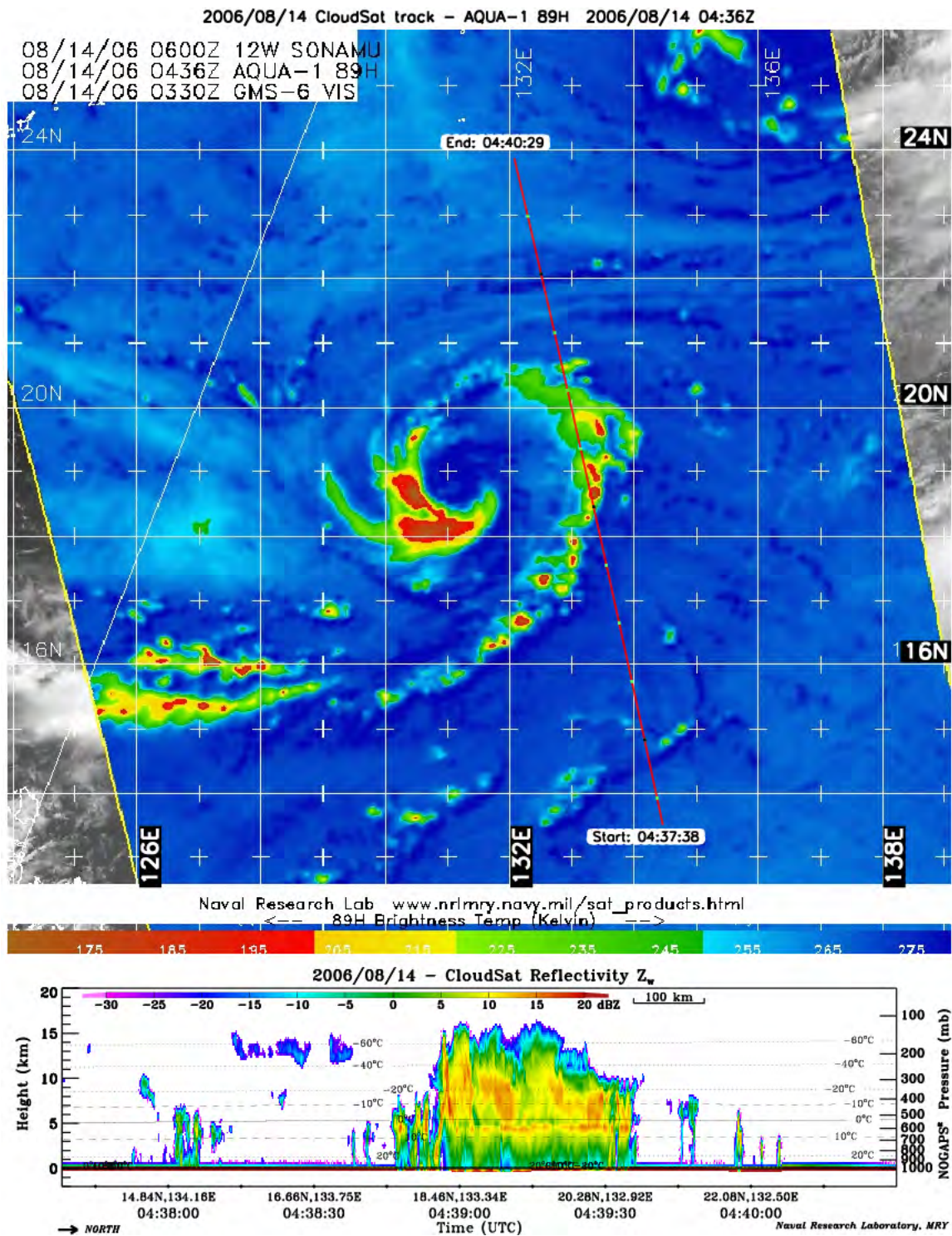


Figure 34. CloudSat satellite pass over 12W at 0436 UTC 14 August 2006.
Maximum TCC was 15 km during this satellite pass. Intensity for 12W at
time of pass was 40 kt (from Colorado State University.
URL: <http://reef.atmos.colostate.edu>)

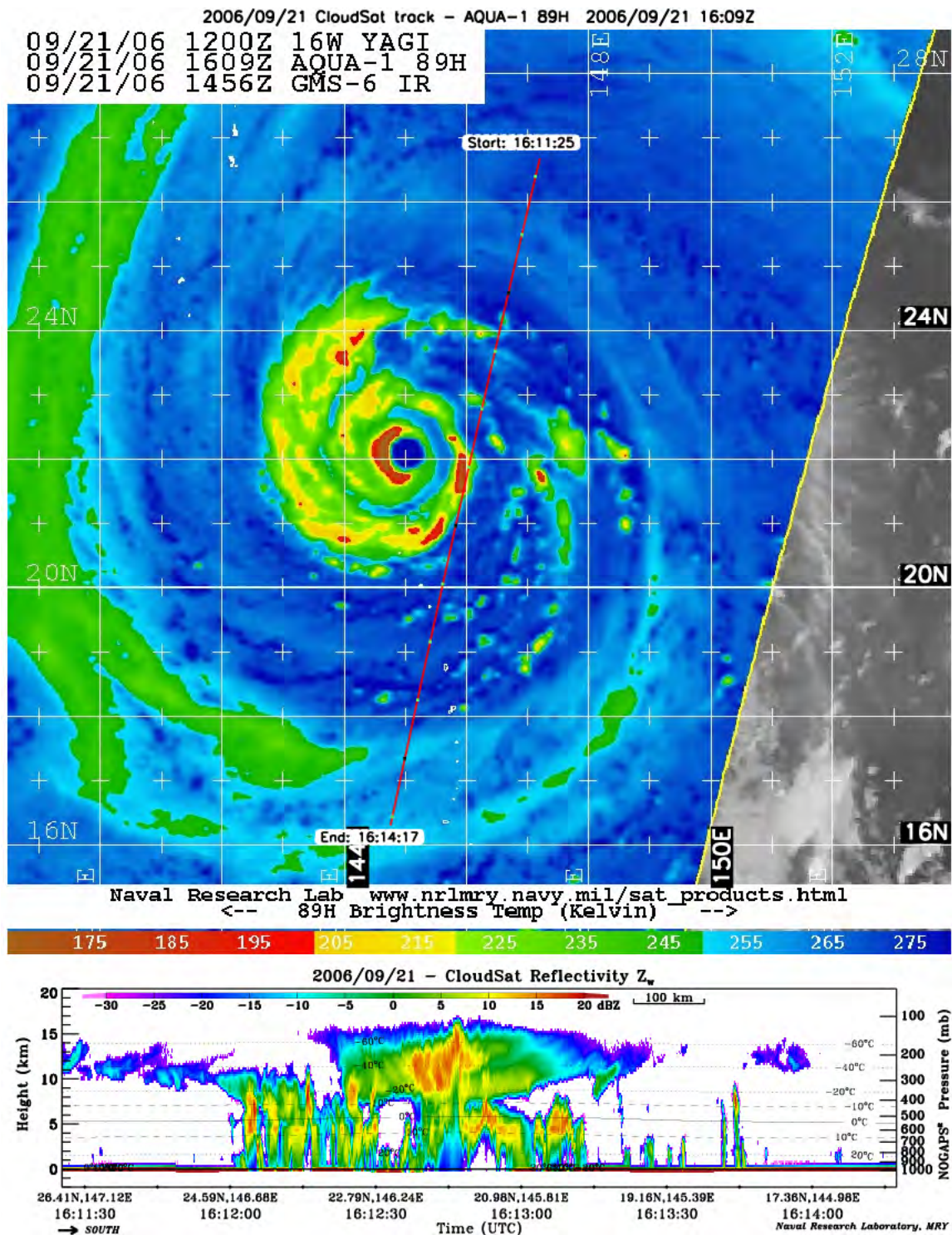


Figure 35. CloudSat satellite pass over 16W at 1609 UTC 21 September 2006. Maximum TCC was 16.5 km during this satellite pass. Intensity for 16W at time of pass was 140 kt (from Colorado State University. URL: <http://reef.atmos.colostate.edu>)

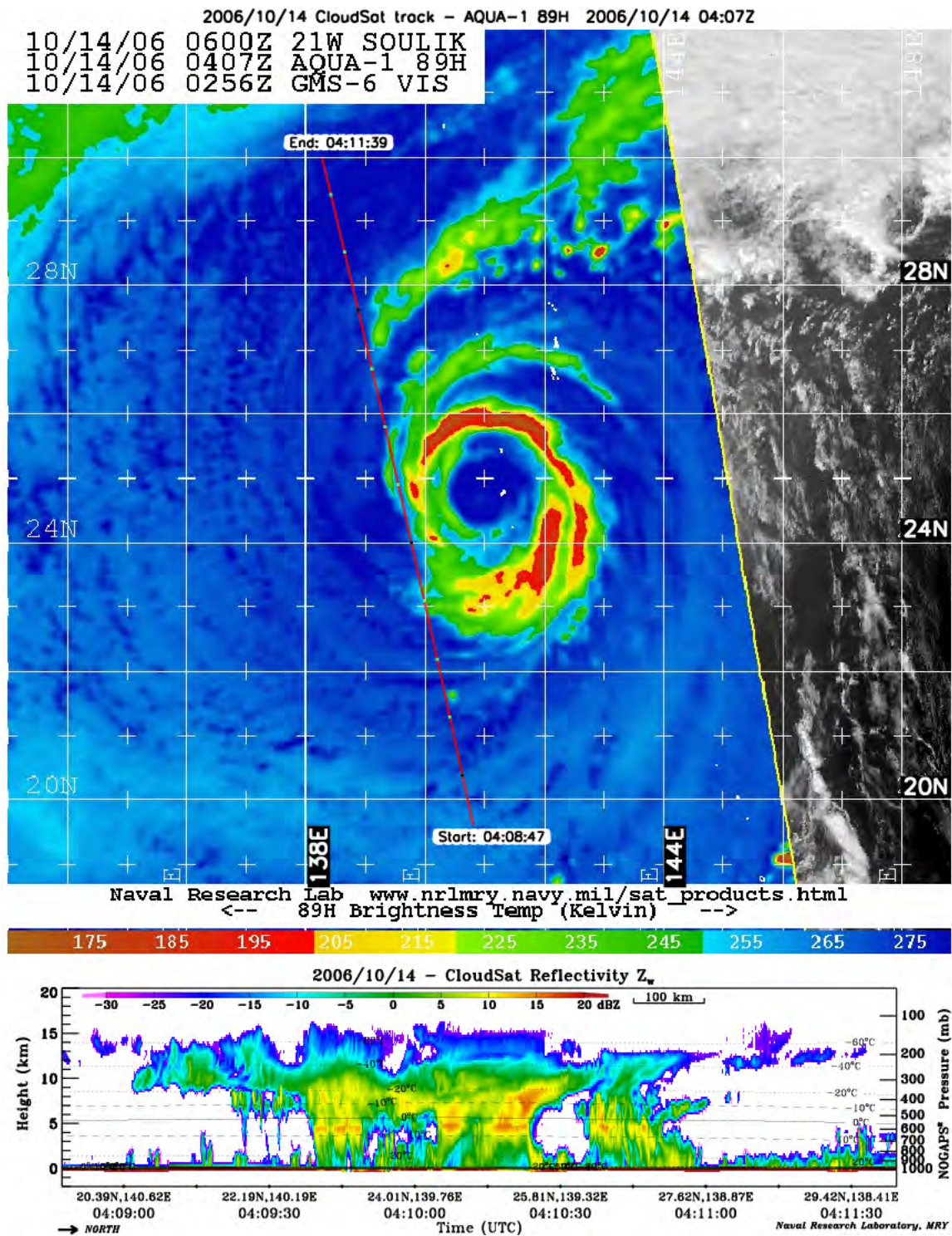


Figure 36. CloudSat satellite pass over 21W at 0407 UTC 14 October 2006.
 Maximum TCC was 11 km during this satellite pass. Intensity for 21W
 at time of pass was 90 kt (from Colorado State University.
 URL: <http://reef.atmos.colostate.edu>)

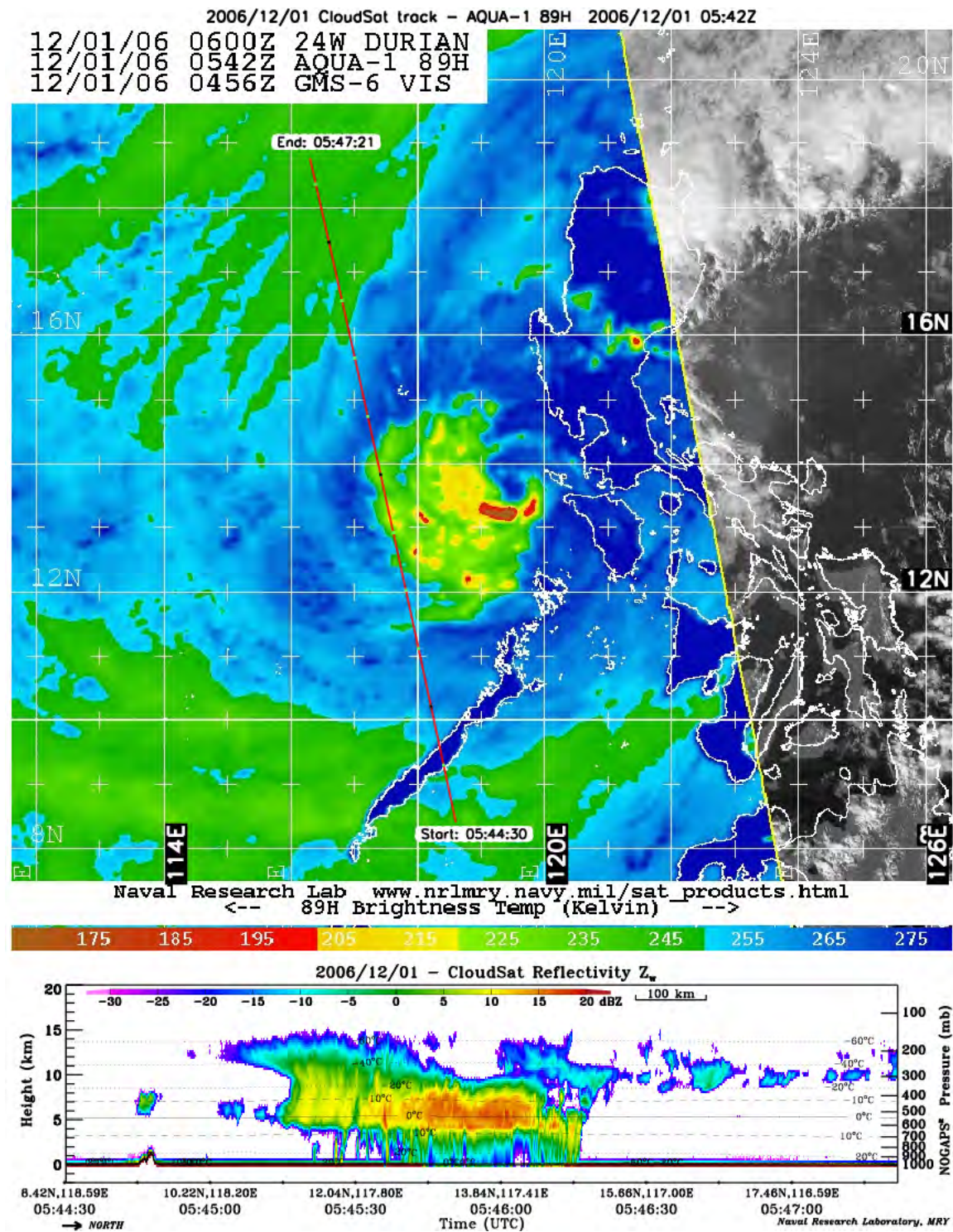


Figure 37. CloudSat satellite pass over 24W at 0542 UTC 01 December 2006.
 Maximum TCC was 11 km during this satellite pass. Intensity for 24W at
 time of pass was 90 kt (from Colorado State University.
 URL: <http://reef.atmos.colostate.edu>)

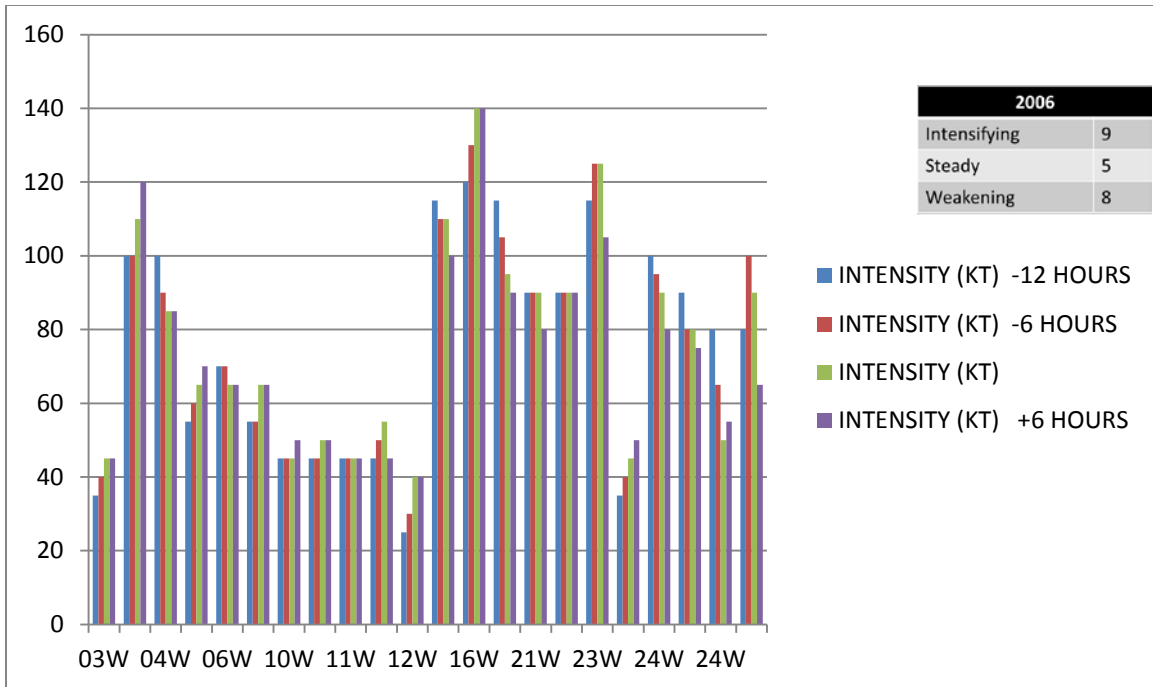


Figure 38. Intensity values (kt) prior to, at, and following the satellite pass over each storm during 2006

2. 2007

In 2007, a total of 27 TCs formed over the WPAC. Of those 27 TCs, CloudSat-based vertical cross-sections were available for 16 TCs. A total of 28 cross-sections are available for 2007 (Figure 39).

2007							
NAME	INTENSITY (KT) -12 HOURS	INTENSITY (KT) -6 HOURS	INTENSITY (KT)	INTENSITY (KT) +6 HOURS	PASS	TOP OF CLOUD (KM)	TOP OF CONVECTIVE CLOUD (KM)
01W	65	65	75	80	2	15.5	13
02W	30	30	35	45	3	15	12
02W	115	130	130	120	2	15	10.5
04W	50	55	55	60	2	16.5	15
04W	115	125	125	125	2	17	13
04W	125	125	125	125	3	15.5	13
05W	35	45	65	65	1.2	17	16
07W	65	70	65	55	2	17	14
10W	80	80	80	80	2	15.5	11.5
10W	75	75	75	75	1.2	15	13
11W	60	65	65	65	1	15	14
12W	90	85	75	60	1	14.5	12
13W	30	35	45	65	2	17	15
13W	95	115	125	135	2	15.5	14
13W	105	75	50	35	2	13.5	11
15W	NEW	20	25	30	2	15.5	13
16W	70	70	70	70	1	17	14
17W	35	40	60	65	1	17	15.5
17W	60	65	75	80	2.3	15.5	13
17W	125	130	130	130	3	15.5	12
17W	130	130	130	125	2	16	14
19W	25	35	50	55	1	16.5	14.5
19W	115	115	115	90	2	15.5	13
21W	60	65	65	55	2	15.5	12
21W	65	55	50	40	1	17	16.5
22W	25	30	30	35	1	15.5	14
24W	80	85	85	90	3	15.5	12.5
24W	95	90	85	85	1	17.5	17
MEAN					2.8	15.9	13.5

Figure 39. Composite of CloudSat data for the year 2007. Highlighted values mark the maximum for each category

The storm intensities at the time of satellite overpass in 2007 range from 35 kt (02W) to 130 kt (02W and 17W). Tropical Cyclone 02W had two passes over the system. The first pass was conducted on 17 May and had an intensity of 35 kt. The second pass was conducted on 20 May and had an intensity of 130 kt. The ToC for the first pass of 02W (Figure 40) was 15 km (49.2 kft) with the TCC maximum at 12 km (39.4 kft). The ToC for the second pass of 02W (Figure 41) was also 15 km (49.2 kft) with the TCC maximum at 10.5 km (34.4 kft). The first pass with a lower intensity actually had a higher TCC than the pass with the much higher intensity. The ToC for 17W (Figure 42) was 15.5 km (50.9 kft) with a TCC of 12 km (39.4 kft). The difference in intensity for these 2 storms was 95 kt but once again the difference in cloud heights was minimal. The minimum TCC values came from the second pass of 02W when it was a category 4 storm (130

kt). For each storm over which a CloudSat pass exists (Figure 43), 12 were intensifying, 11 were steady, and five were weakening. The mean ToC value was 15.9 km (52.2 kft) and the mean TCC was 13.9 km (45.6 kft).

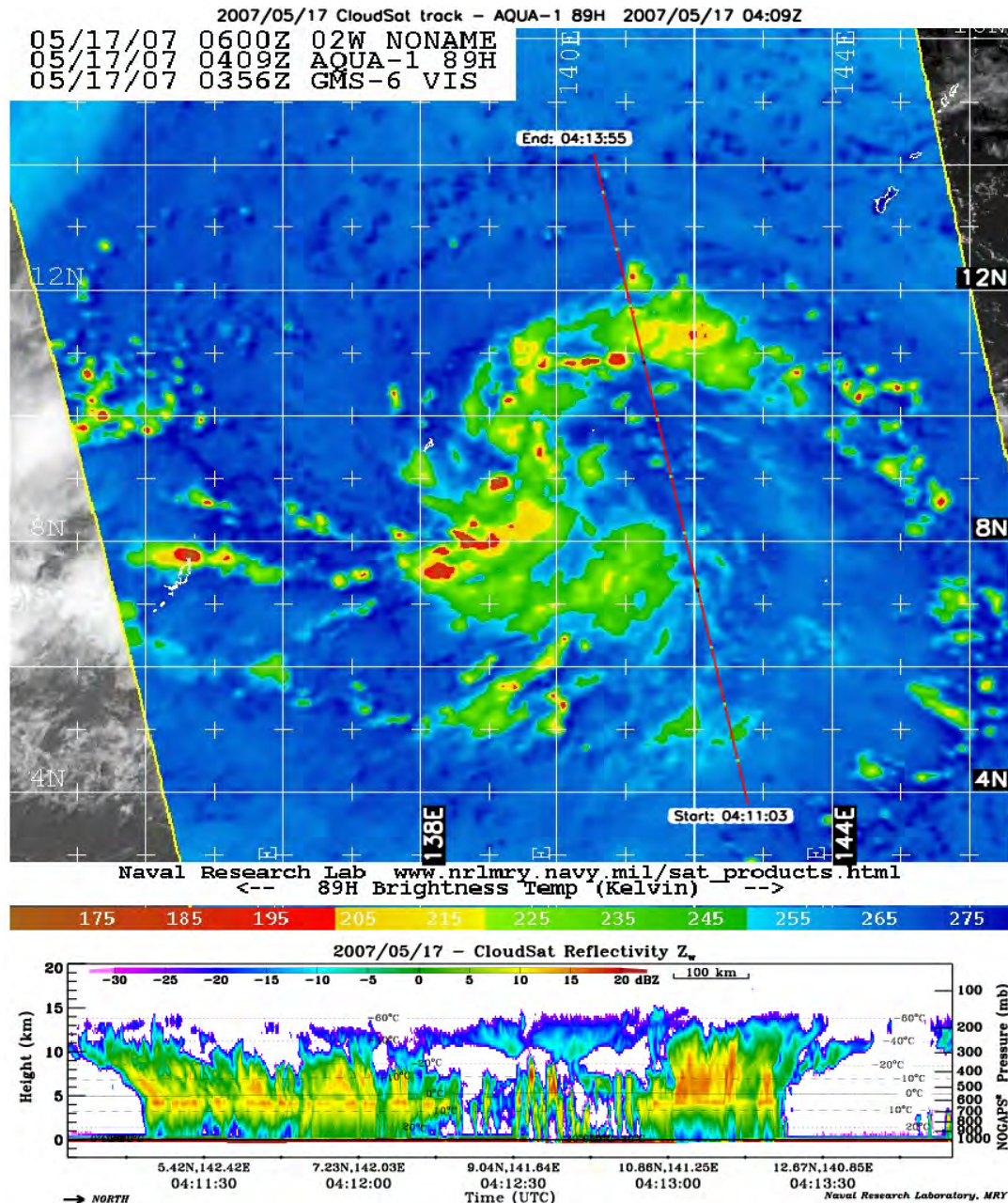


Figure 40. First CloudSat satellite pass over 02W at 0409 UTC 17 May 2007. Maximum TCC was 12 km during this satellite pass. Intensity for 02W at time of pass was 35 kt (from Colorado State University. URL: <http://reef.atmos.colostate.edu>)

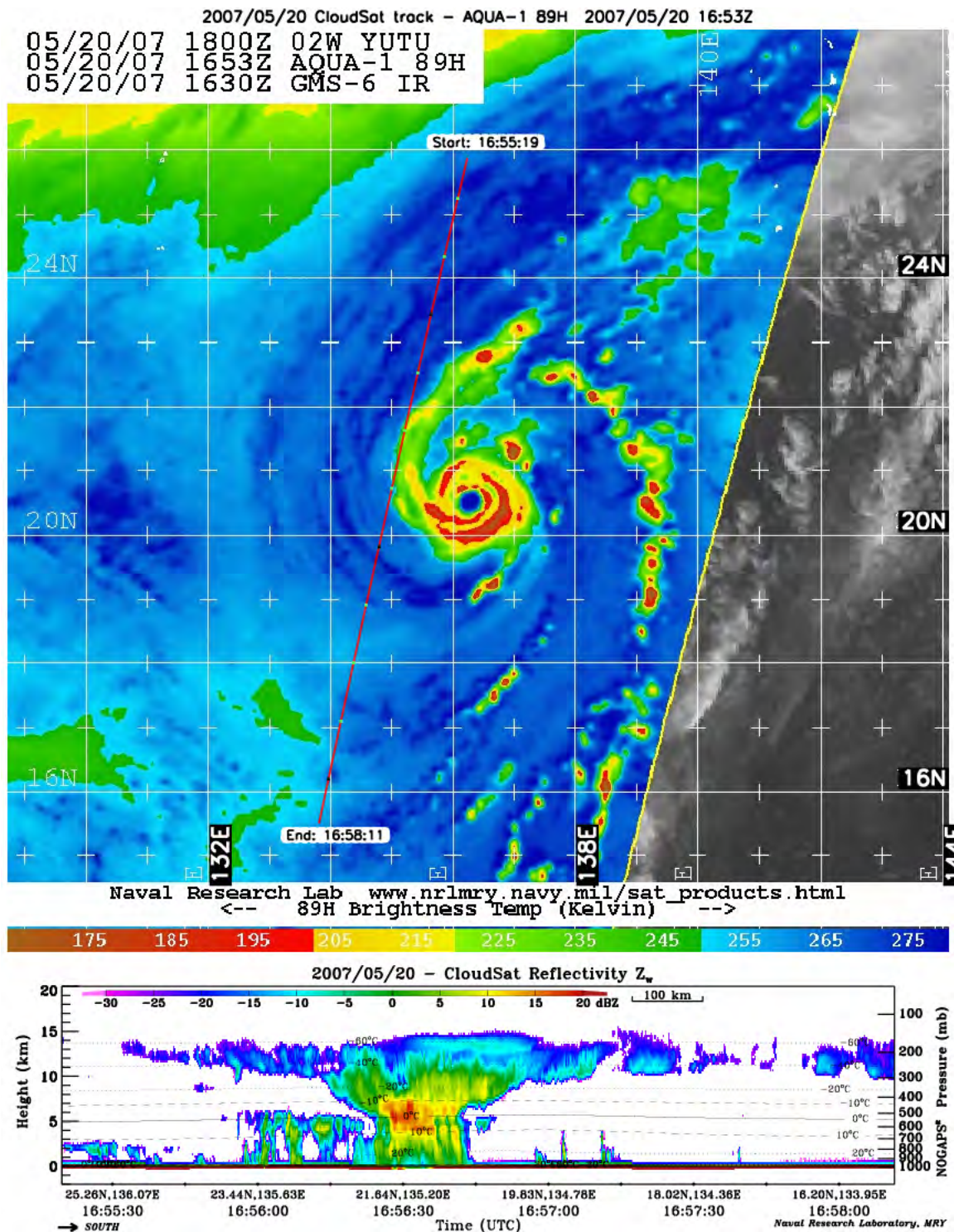


Figure 41. Second CloudSat satellite pass over 02W at 1653 UTC
 20 May 2007. Maximum TCC was 10.5 km during this satellite pass.
 Intensity for 02W at time of pass was 130 kt (from Colorado State
 University. URL: <http://reef.atmos.colostate.edu>)

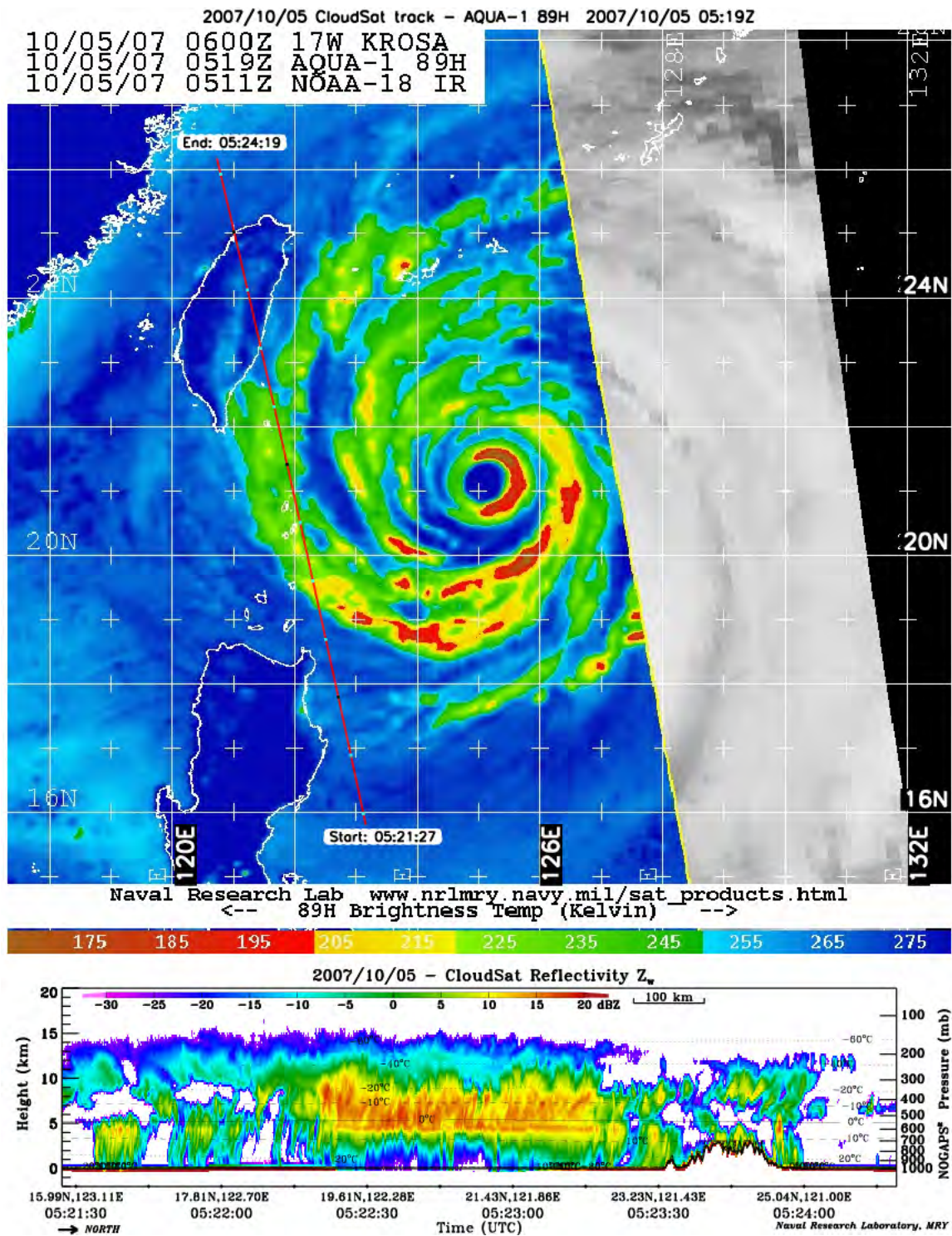


Figure 42. CloudSat satellite pass over 17W at 0519 UTC 05 October 2007.
 Maximum TCC was 12 km during this satellite pass. Intensity for 17W at
 time of pass was 130 kt (from Colorado State University.
 URL: <http://reef.atmos.colostate.edu>)

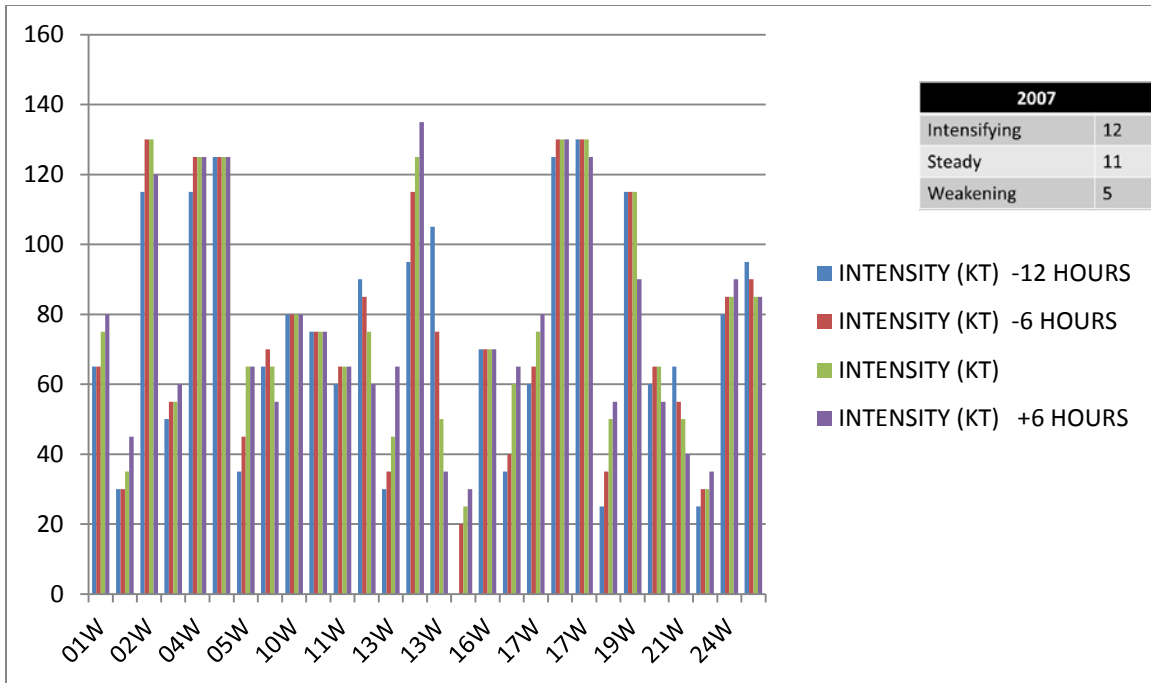


Figure 43. Intensity values (kt) prior to, at, and following the satellite pass over each storm during 2007

3. 2008

In 2008, a total of 27 TCs formed over the WPAC. Of those 27 TCs, CloudSat-based vertical cross-sections were available for 16 TCs. A total of 23 cross-sections are available for 2008 (Figure 44).

2008							
NAME	INTENSITY (KT) -12 HOURS	INTENSITY (KT) -6 HOURS	INTENSITY (KT)	INTENSITY (KT) +6 HOURS	PASS	TOP OF CLOUD (KM)	TOP OF CONVECTIVE CLOUD (KM)
02W	40	45	50	65	2.3	16	14.5
02W	80	85	90	90	3	15.5	13
03W	120	115	95	85	3	14	13
03W	95	85	75	55	3	14.5	10.5
06W	95	95	95	85	1	16	12
07W	45	55	65	70	2	16	14
07W	80	75	60	60	2	17.5	17
09W	30	35	35	45	1	17	15.5
09W	60	65	70	75	2	16.5	16
09W	95	85	70	60	2.3	15	13
10W	40	45	45	45	1.2	17	15
12W	55	55	50	50	2	16	14
13W	70	65	65	55	2	16	14
14W	30	35	30	30	2	15	12.5
15W	45	50	65	70	3	15.5	13
15W	115	115	100	100	2.3	15	13
17W	35	35	35	35	2	14	13.5
18W	60	65	80	85	1	16.5	16
19W	50	55	65	70	2	16	14
19W	65	70	80	90	1	17	16
20W	25	30	40	45	2	17	15
26W	35	35	35	40	1	17	16.5
27W	55	60	60	65	1	16.5	14
MEAN					2.3	15.9	14.1

Figure 44. Composite of CloudSat data for the year 2008. Highlighted values mark the maximum for each category

The intensity values for 2008 range from 30 kt (14W) to 100 kt (15W). The ToC for 14W (Figure 45) was 15 km (49.2 kft) with the TCC maximum at 12.5 km (41.0 kft). The ToC for 15W (Figure 46) was 15 km (49.2 kft) while the TCC maximum was 13 km (42.7 kft). The difference in intensity for these 2 storms was 70 kt but the difference in cloud heights was again quite minimal. The minimum TCC values occurred during 03W (Figure 47). This minimum value was 10.5 km (34.4 kft) and was associated with a category 1 storm (75 kt). For each storm over which a CloudSat pass exists (Figure 48), 11 were intensifying, six were steady, and six were weakening. The mean ToC value was 15.9 km (52.2 kft) and the mean TCC was 14.1 km (45.9 kft).

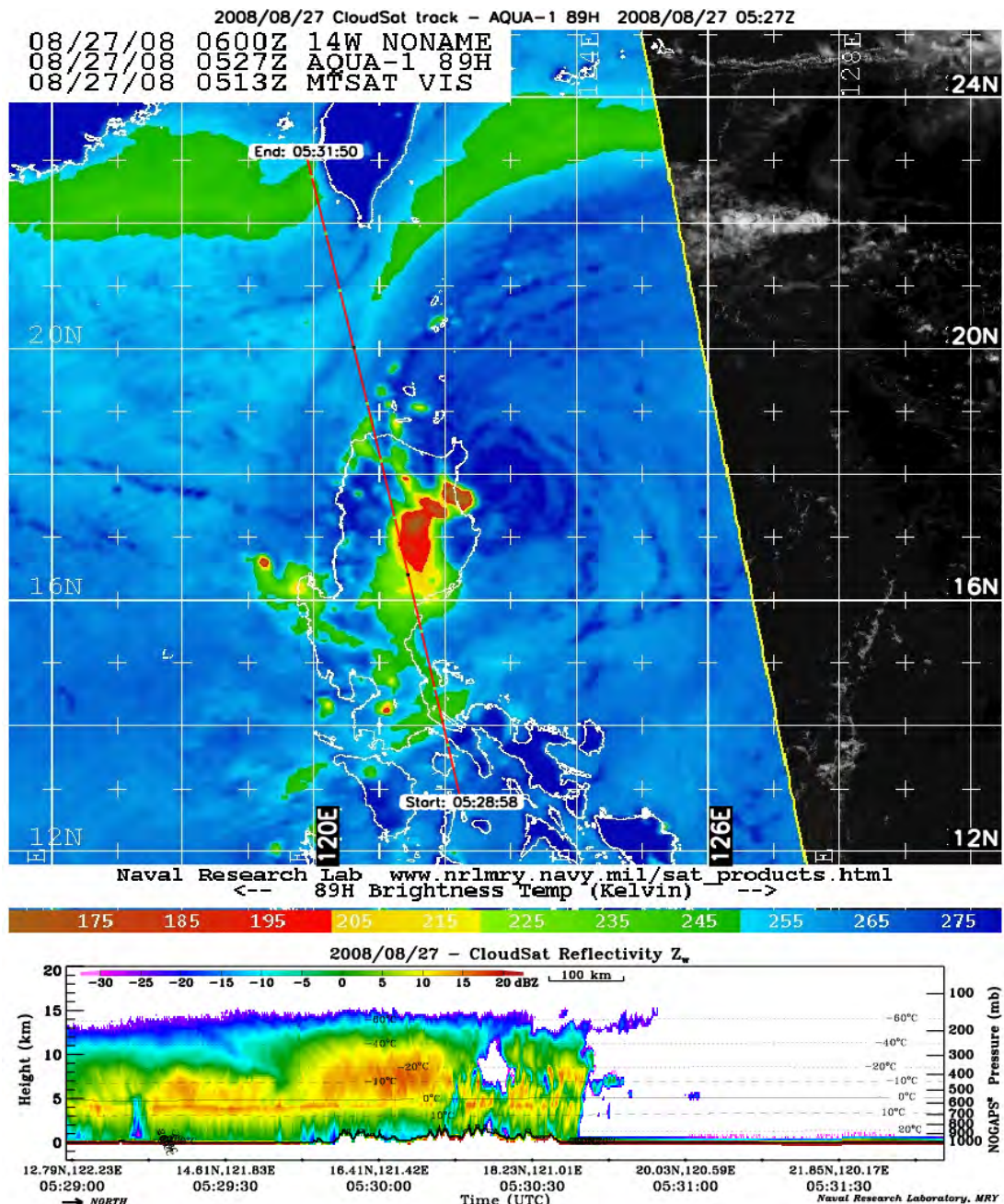


Figure 45. CloudSat satellite pass over 14W at 0527 UTC 27 August 2008.
 Maximum TCC was 12.5 km during this satellite pass. Intensity for 14W at
 time of pass was 50 kt (from Colorado State University.
 URL: <http://reef.atmos.colostate.edu>)

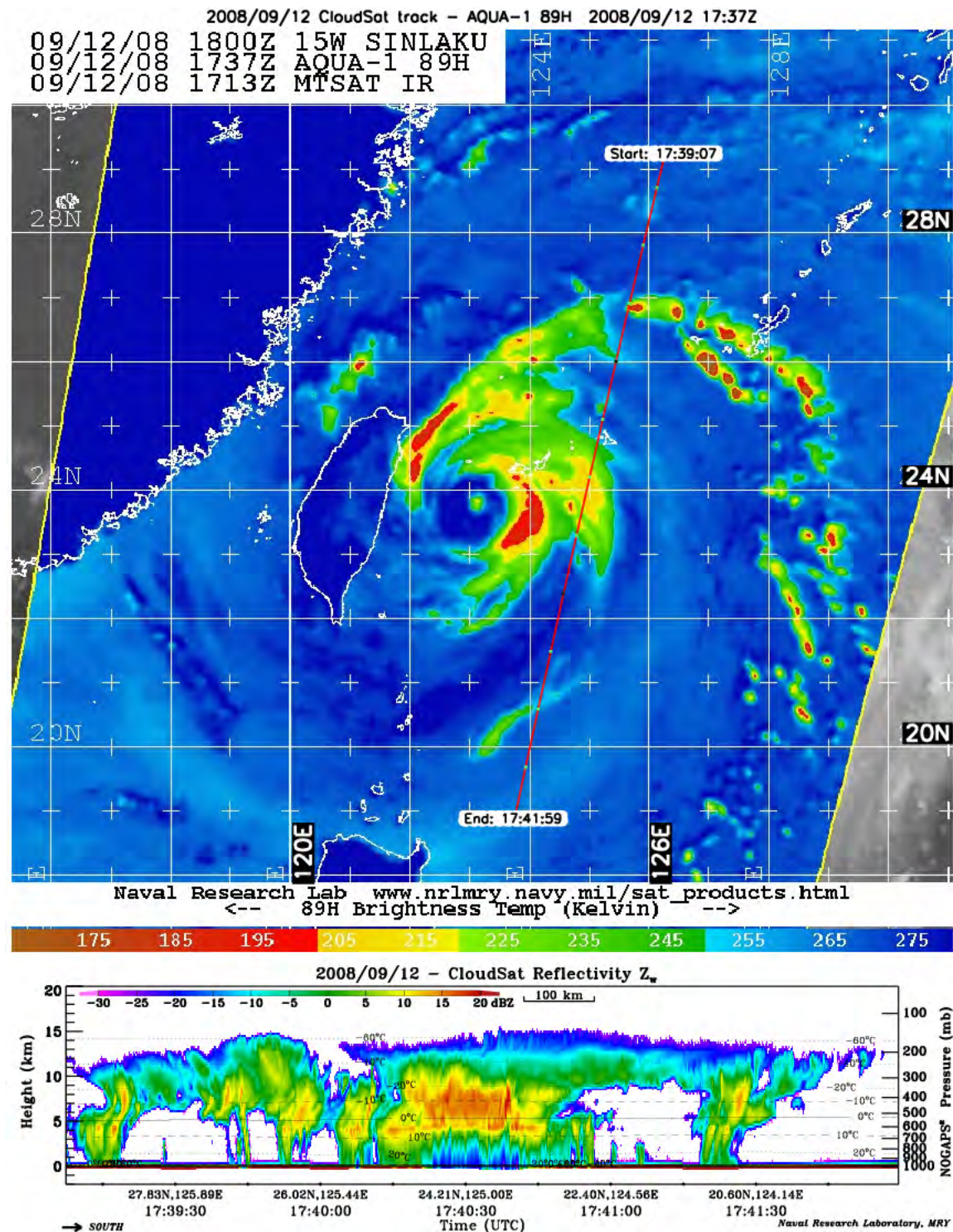


Figure 46. CloudSat satellite pass over 15W at 1737 UTC 12 September 2008. Maximum TCC was 13 km during this satellite pass. Intensity for 15W at time of pass was 100 kt (from Colorado State University. URL: <http://reef.atmos.colostate.edu>)

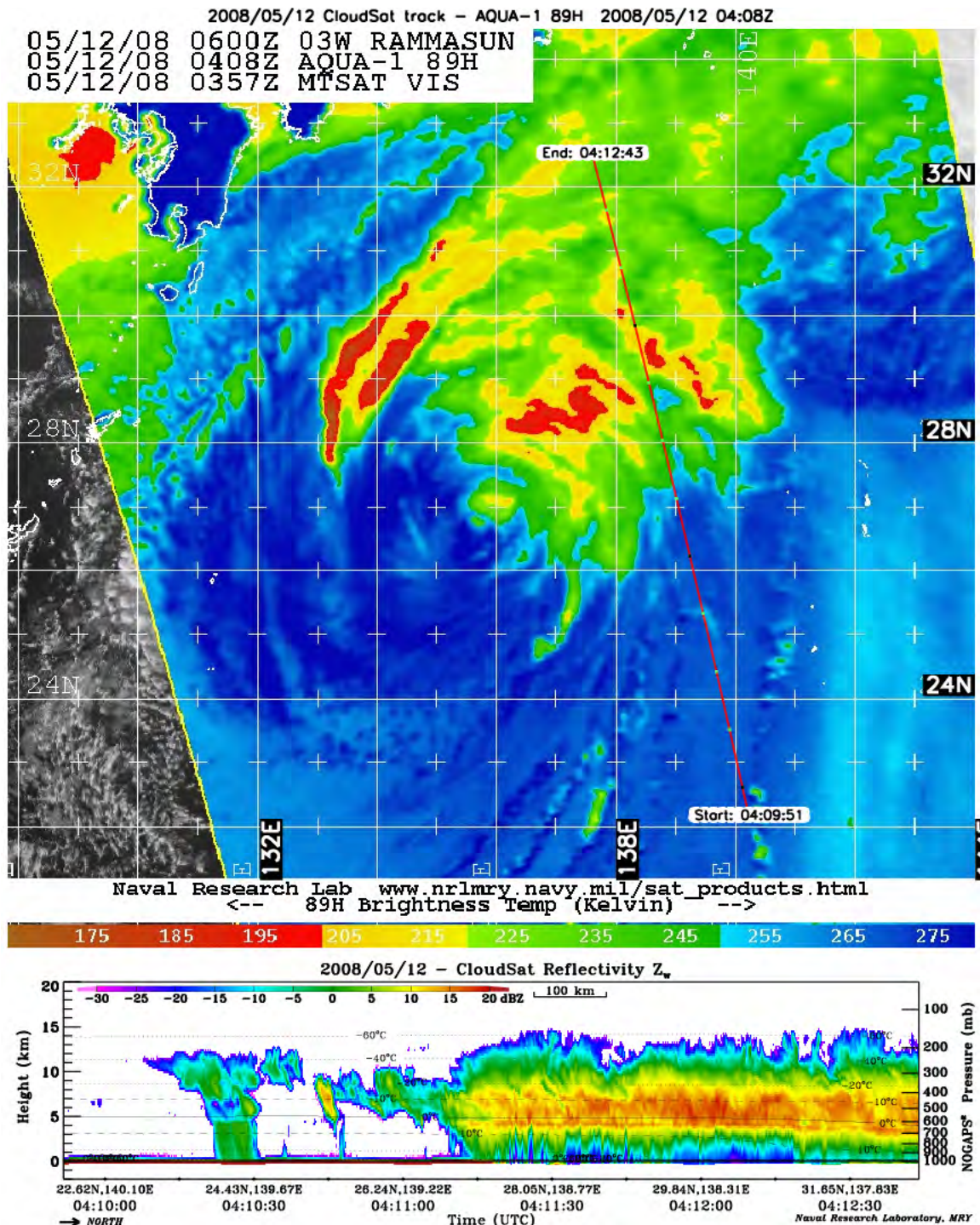


Figure 47. CloudSat satellite pass over 03W at 0408 UTC 12 May 2008.
 Maximum TCC was 10.5 km during this satellite pass. Intensity for 03W at
 time of pass was 75 kt (from Colorado State University. URL:
<http://reef.atmos.colostate.edu>)

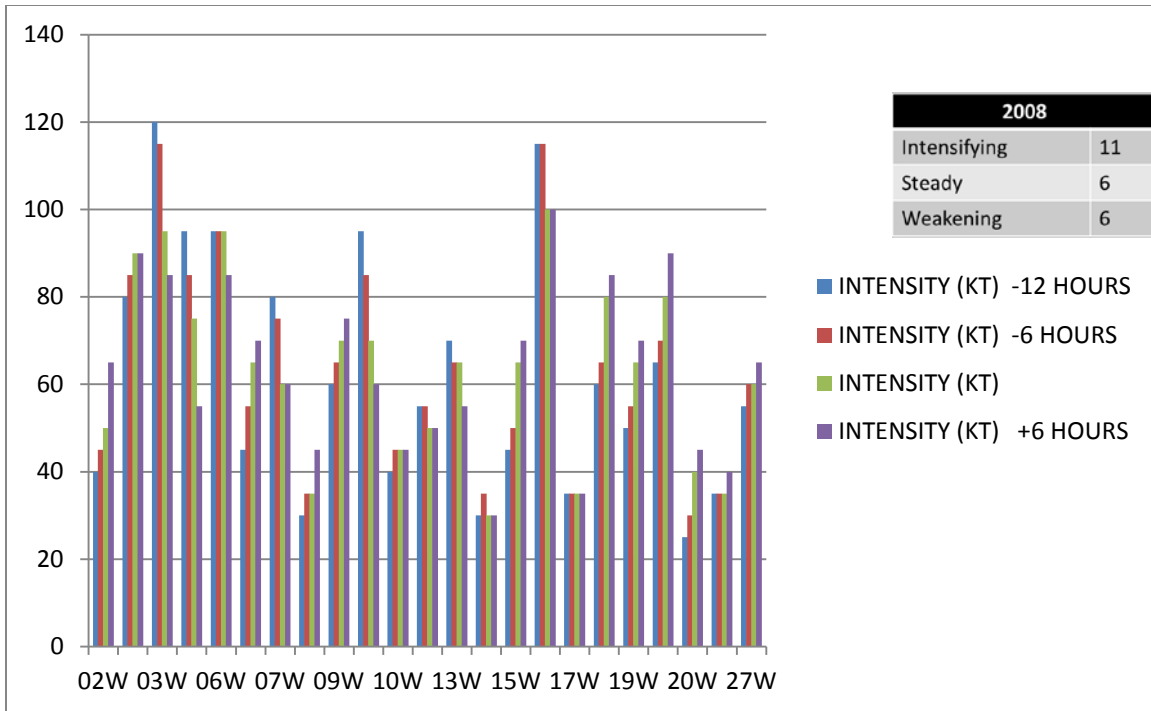


Figure 48. Intensity values (kt) prior to, at, and following the satellite pass over each storm during 2008

4. 2009

In 2009, a total of 28 TCs formed over the WPAC. Of those 27 TCs, CloudSat-based vertical cross-sections were available for 13 TCs. A total of 19 cross-sections are available for 2009 (Figure 49).

2009							
NAME	INTENSITY (KT) -12 HOURS	INTENSITY (KT) -6 HOURS	INTENSITY (KT)	INTENSITY (KT) -6 HOURS	PASS	TOP OF CLOUD (KM)	TOP OF CONVECTIVE CLOUD (KM)
02W	60	65	75	75	1	17	16
07W	60	60	65	65	2	16	15
09W	35	45	50	55	1	17.5	15
09W	80	80	80	80	1	17.5	16
11W	105	110	110	115	2	15.5	14.5
11W	120	115	110	105	1.2	15	14.5
13W	45	45	45	45	1	17	16.5
14W	25	30	30	30	1	15	13
15W	130	130	130	135	1	17	15
15W	120	115	110	100	3	16	12
16W	20	30	35	35	1	17	14
17W	45	50	55	55	1.3	17	15.5
19W	55	70	85	90	2	16.5	14
19W	85	90	105	135	1	17	15.5
22W	65	75	80	85	1	17	16.5
22W	85	85	75	75	1	15.5	13.5
23W	55	50	55	50	1	15	13
26W	135	130	125	125	1	17	14
26W	105	100	100	90	1	16	13.5
MEAN					19	16.4	14.6

Figure 49. Composite of CloudSat data for the year 2009.
Highlighted values mark the maximum for each category

The intensity values for 2009 range from 30 kt (14W) to 130 kt (15W). The ToC for 14W (Figure 50) was 15 km (49.2 kft) with the TCC maximum at 13 km (42.7 kft). The ToC for 15W (Figure 51) was 17 km (55.8 kft) while the maximum TCC was at 15 km (49.2 kft). The difference in intensity for these 2 storms was 100 kt but the difference in cloud heights was unlike 2006–2008 in that there was a 2 km difference between the ToCs and TCCs of the two storms. The minimum TCC values occurred during the second pass of 15W (Figure 52). This minimum value was 12 km (39.4 kft) and was associated with a category 3 storm (110 kt). For each storm over which a CloudSat pass exists (Figure 53), eight were intensifying, six were steady, and five were weakening. The mean ToC value was 16.4 km (53.8 kft) and the mean TCC was 14.6 km (47.9 kft).

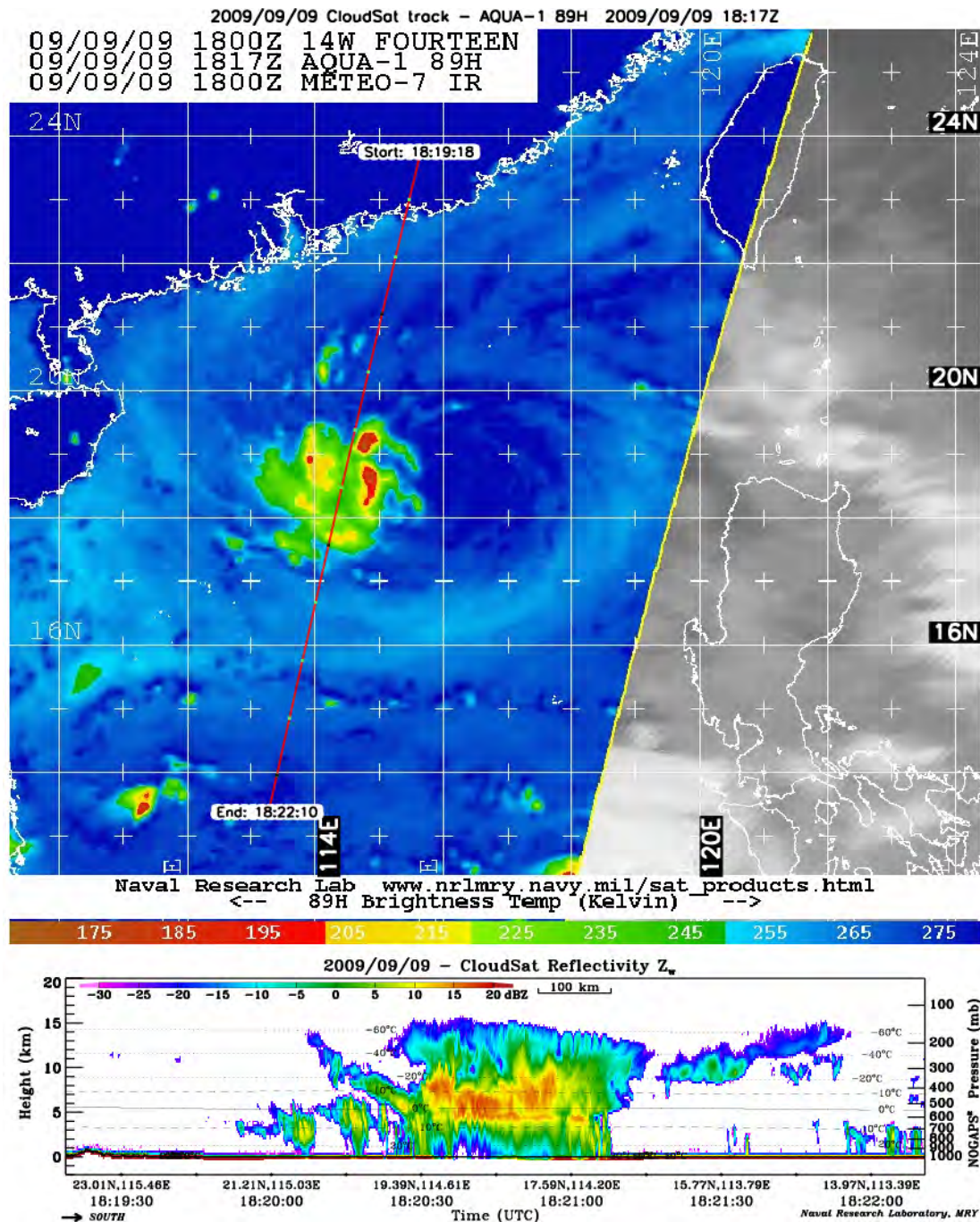


Figure 50. CloudSat satellite pass over 14W at 1817 UTC 09 September 2009. Maximum TCC was 13 km during this satellite pass. Intensity for 14W at time of pass was 30 kt (from Colorado State University.
 URL: <http://reef.atmos.colostate.edu>)

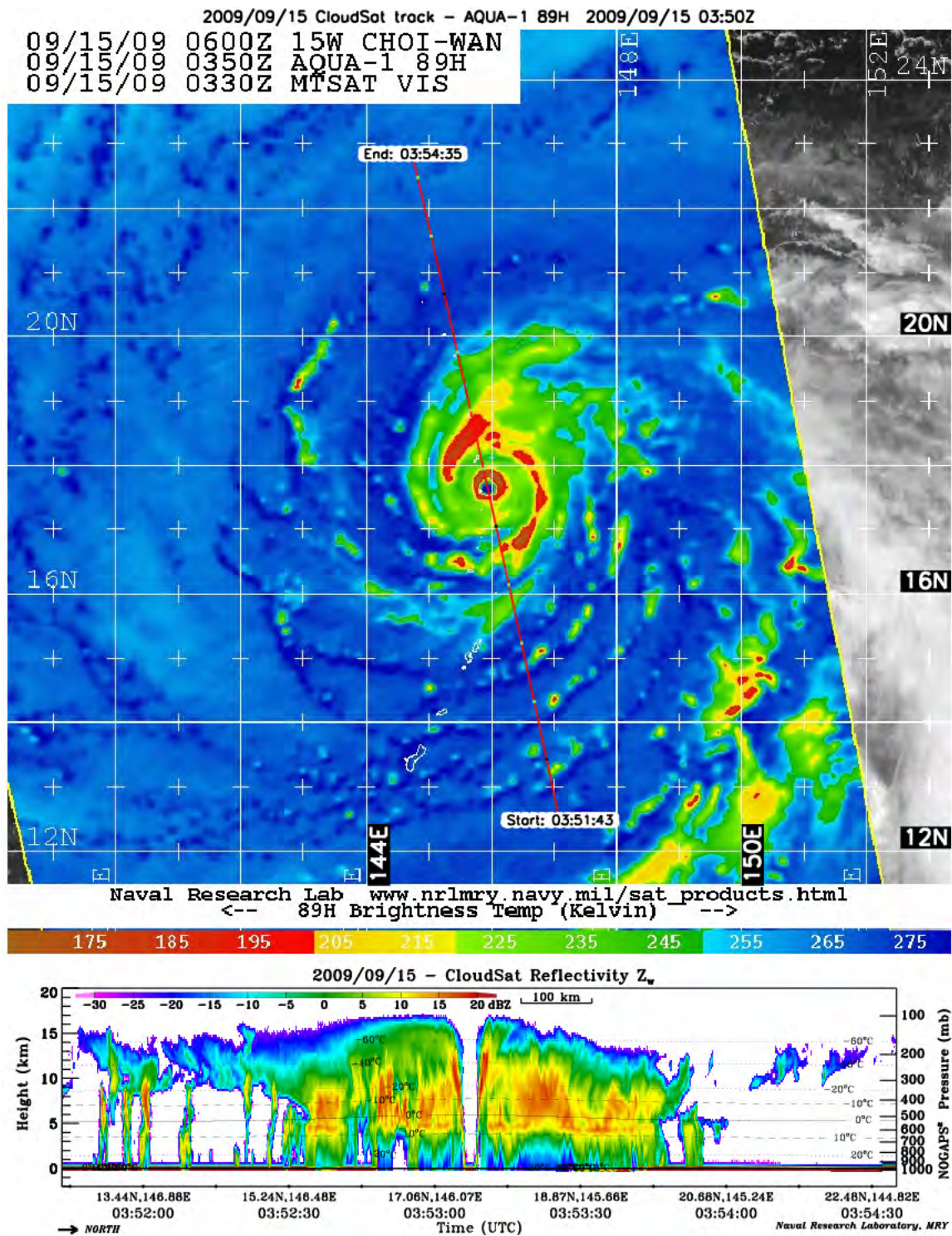


Figure 51. CloudSat satellite pass over 15W at 0350 UTC 15 September 2009. Maximum TCC was 15 km during this satellite pass. Intensity for 15W at time of pass was 130 kt (from Colorado State University. URL: <http://reef.atmos.colostate.edu>)

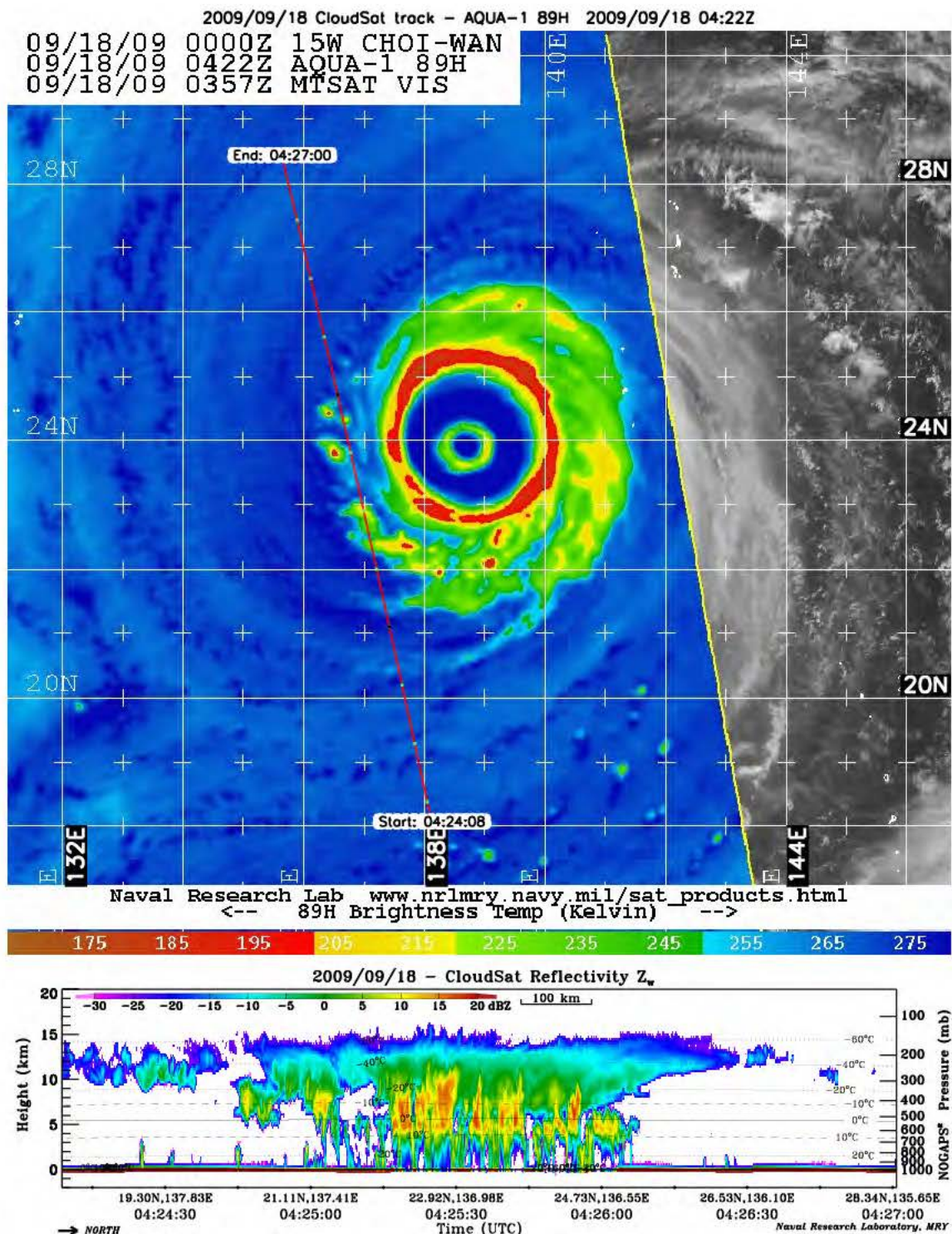


Figure 52. Second CloudSat satellite pass over 15W at 0422 UTC
 18 September 2009. Maximum TCC was 12 km during this satellite pass.
 Intensity for 15W at time of pass was 110 kt (from Colorado State
 University. URL: <http://reef.atmos.colostate.edu>)

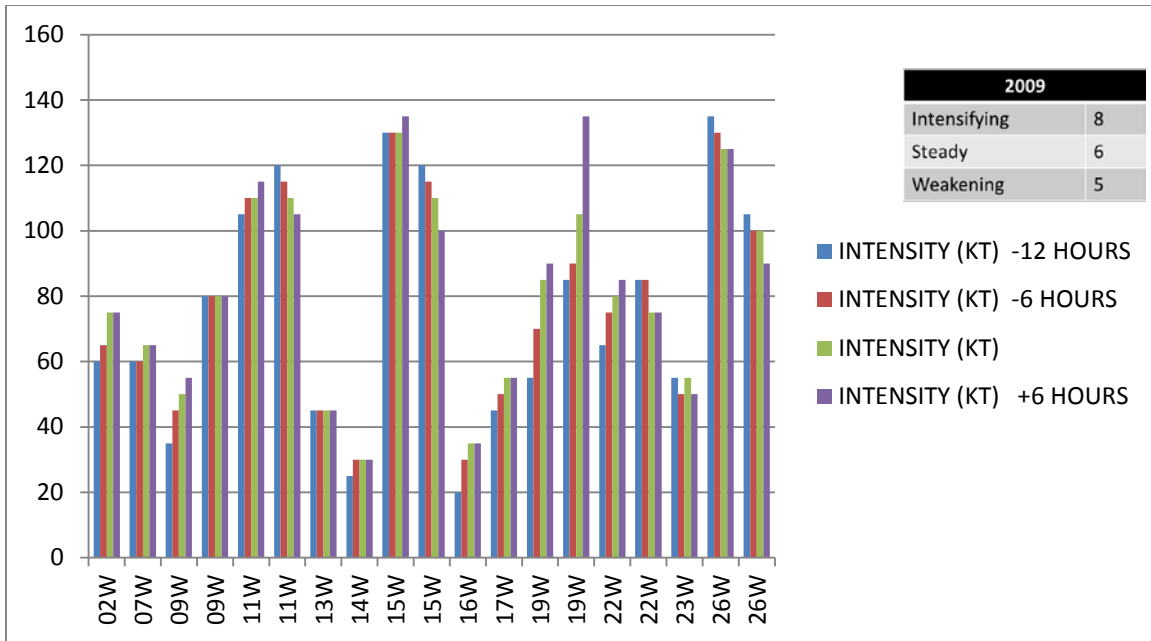


Figure 53. Graph depicting intensity values (kt) leading up to and after the satellite made the pass over the storm (2009)

5. 2010

During 2010 only a total of 19 TCs formed over the WPAC. Of those 19 TCs, CloudSat-based vertical cross-sections were available for 8 TCs. A total of 12 cross-sections are available for 2010 (Figure 54).

2010							
NAME	INTENSITY (KT) -12 HOURS	INTENSITY (KT) -6 HOURS	INTENSITY (KT)	INTENSITY (KT) +6 HOURS	PASS	TOP OF CLOUD (KM)	TOP OF CONVECTIVE CLOUD (KM)
02W	30	30	30	35	1	18	17
02W	50	50	45	35	1	16	12.5
04W	25	25	30	35	3	16	15.5
06W	50	55	60	65	1	17	16
07W	55	60	55	50	1	16	13.5
12W	70	75	80	85	3	15	12.5
12W	105	105	105	105	3	15.5	14
15W	60	70	80	90	1	17	16.5
15W	125	140	145	160	3	15.5	14
15W	120	90	95	95	1	17	16
16W	65	70	70	80	2	15	13
17W	30	30	30	30	1	15.5	15
MEAN					12	16.1	14.6

Figure 54. Composite of CloudSat data for the year 2010. Highlighted values mark the maximum for each category

The intensity values for 2010 range from 30 kt (02W, 04W, and 17W) to 145 kt (15W). The ToC for 02W (Figure 55) was 18 km (59.1 kft) with the maximum TCC at 17 km (55.8 kft). The ToC for 04W (Figure 56) was 16 km (52.5 kft) while the TCC maximum was 15.5 km (50.9 kft). The ToC for 17W (Figure 57) was 15.5 km (50.9 kft) and the TCC maximum was 15 km (49.2 kft). The ToC for 15W (Figure 58) was 15.5 km (50.9 kft) and the TCC reached to 14 km (45.9 kft). The difference in intensity for these storms was 115 kt with 02W having the highest ToC reading for the 5 year study. The minimum TCC values came from the second pass of 02W (Figure 59) and the first pass of 12W. The minimum value for these storms was 12.5 km (41.0 kft) and was associated with a Tropical Storm (02W–45 kt) and a category 1 storm (12W–80 kt). For each storm over which a CloudSat pass exists (Figure 60), six were intensifying, four were steady, and two were weakening. The mean ToC value was 16.1 km (52.8 kft) and the mean TCC was 14.6 km (47.9 kft).

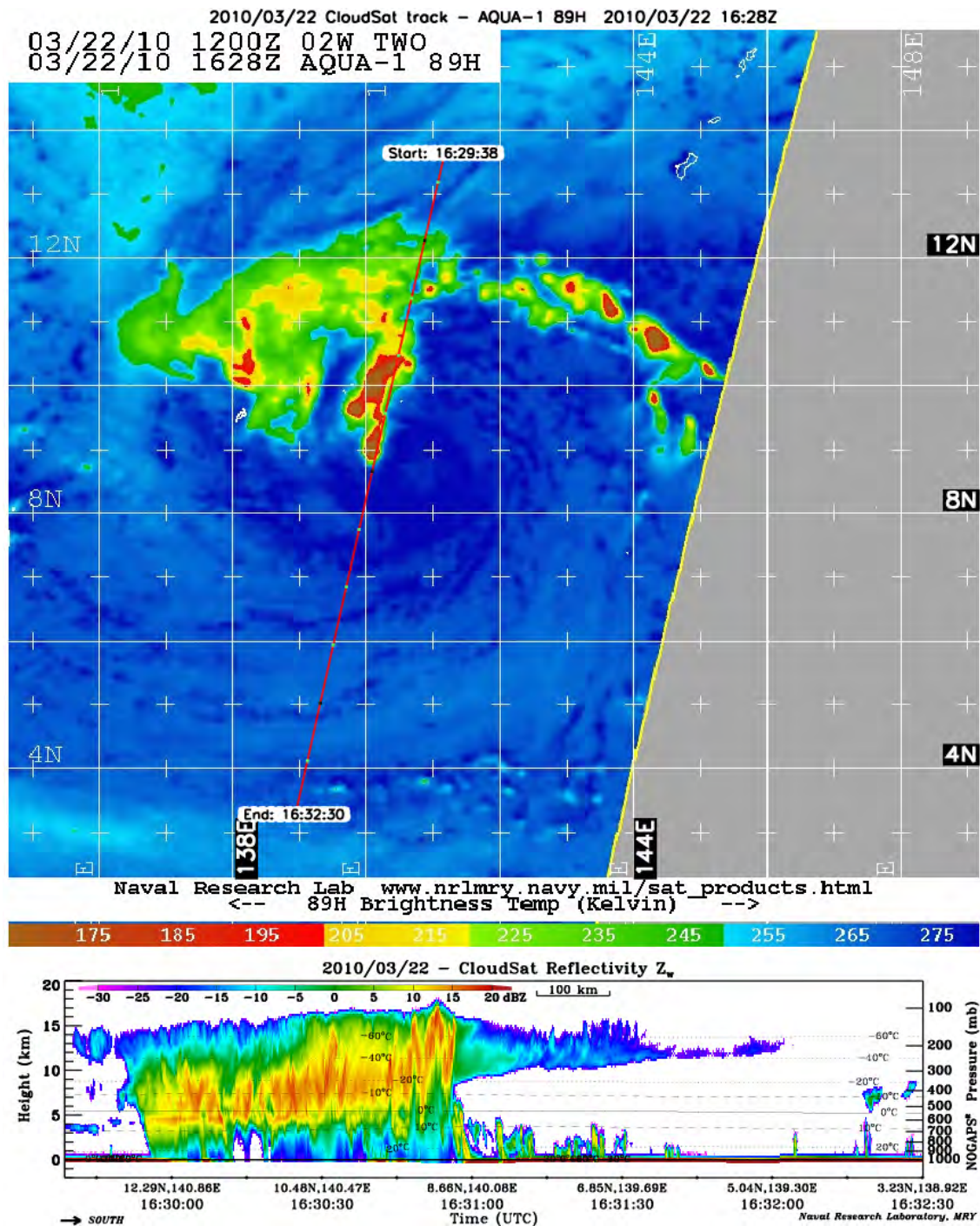


Figure 55. First CloudSat satellite pass over 02W at 1628 UTC 22 March 2010. Maximum TCC was 17 km during this satellite pass. Intensity for 02W at time of pass was 30 kt (from Colorado State University. URL: <http://reef.atmos.colostate.edu>)

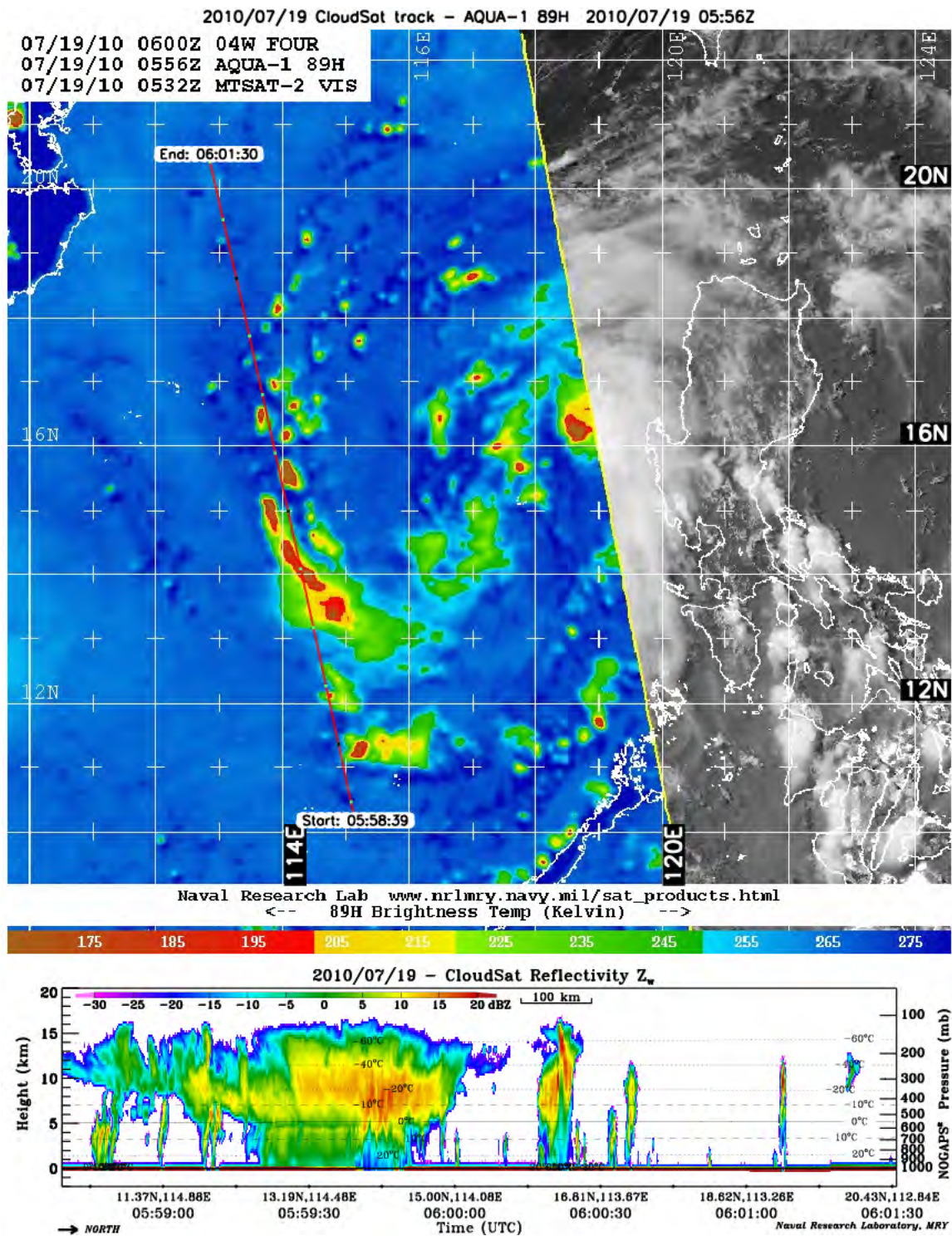


Figure 56. CloudSat satellite pass over 04W at 0556 UTC 19 July 2010.
 Maximum TCC was 15.5 km during this satellite pass. Intensity for 04W
 at time of pass was 30 kt (from Colorado State University.
 URL: <http://reef.atmos.colostate.edu>)

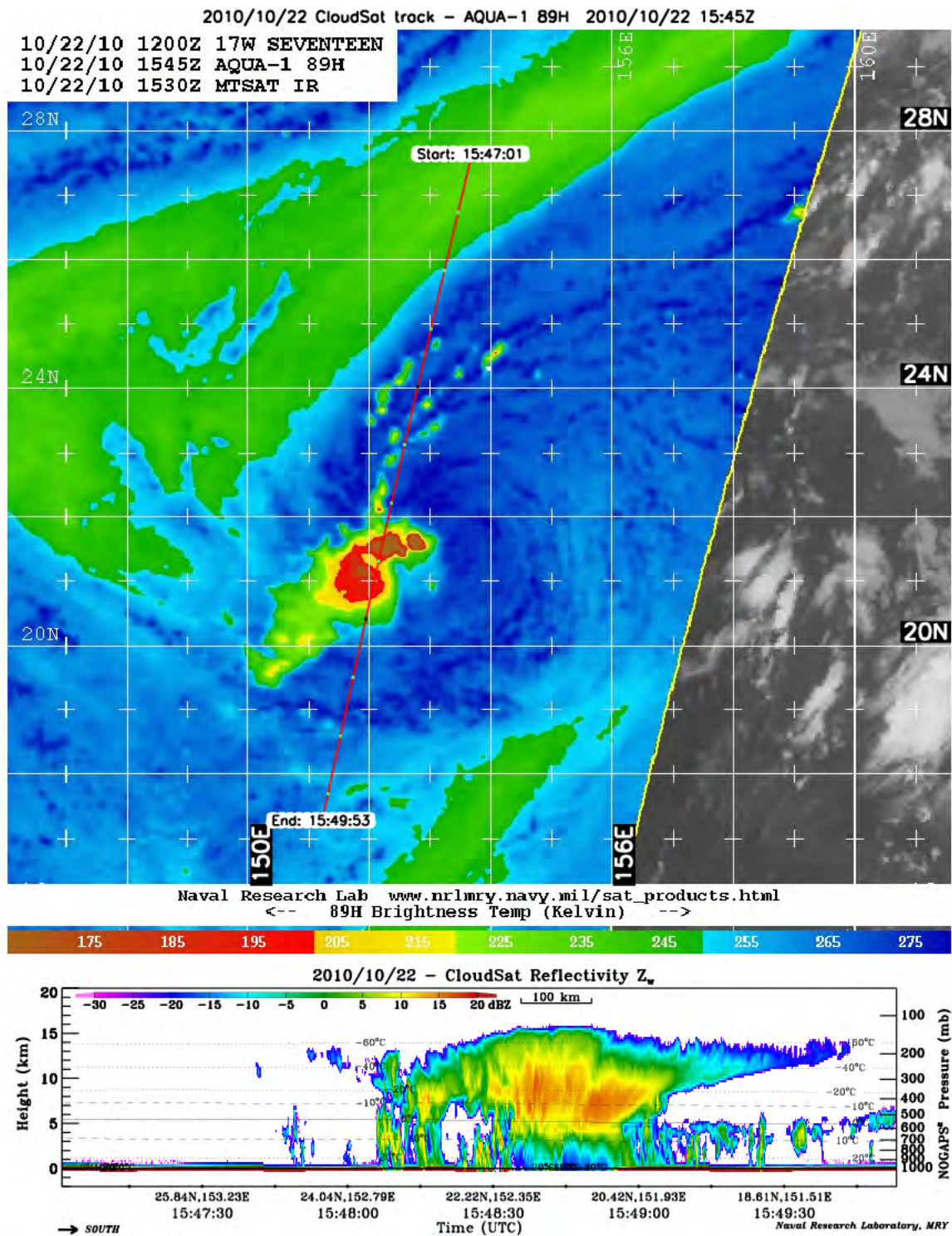


Figure 57. CloudSat satellite pass over 17W at 1545 UTC 22 October 2010. Maximum TCC was 15 km during this satellite pass. Intensity for 17W at time of pass was 30 kt (from Colorado State University. URL: <http://reef.atmos.colostate.edu>)

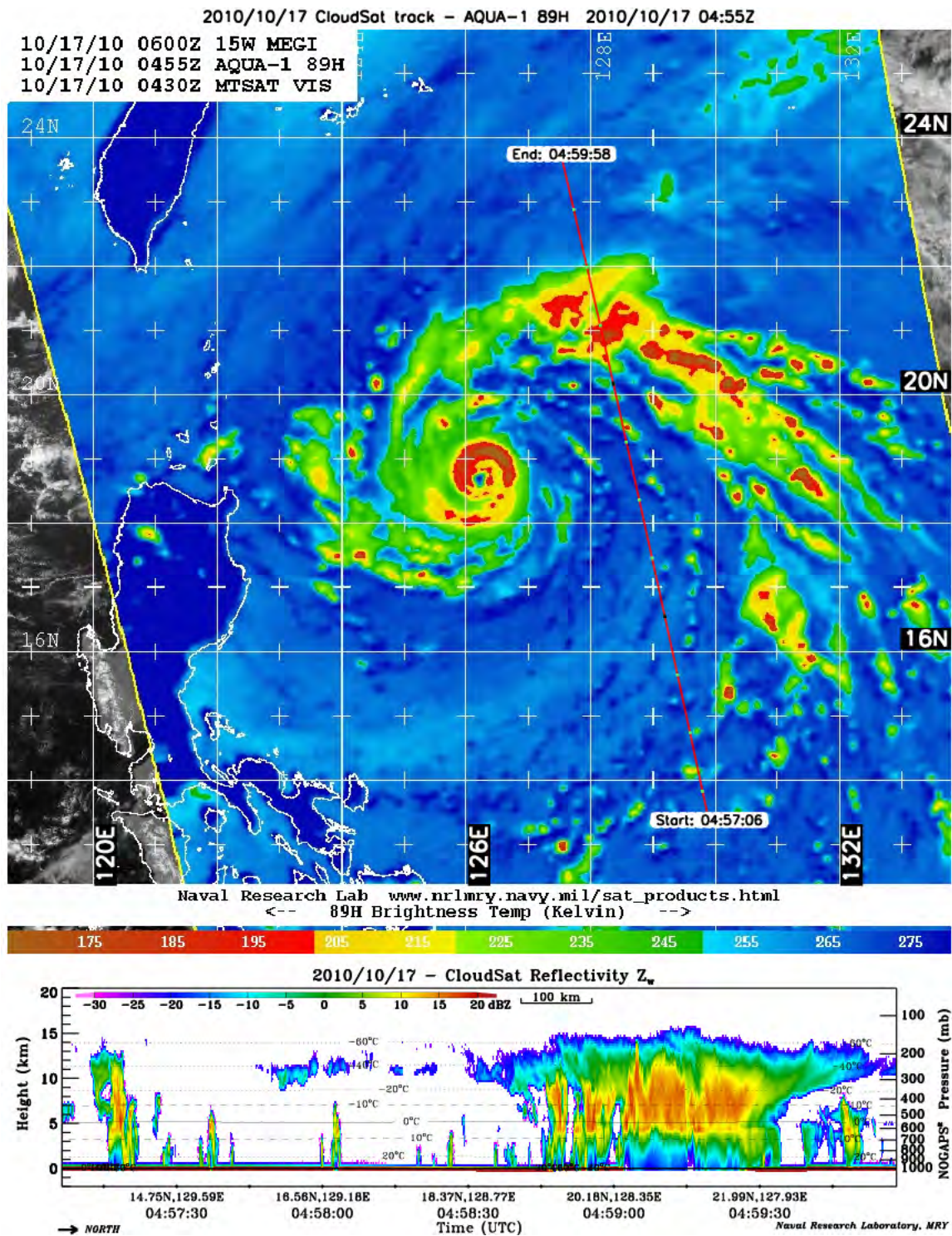


Figure 58. Second CloudSat satellite pass over 15W at 0455 UTC
 17 October 2010. Maximum TCC was 14 km during this satellite pass.
 Intensity for 15W at time of pass was 140 kt (from Colorado State
 University. URL: <http://reef.atmos.colostate.edu>)

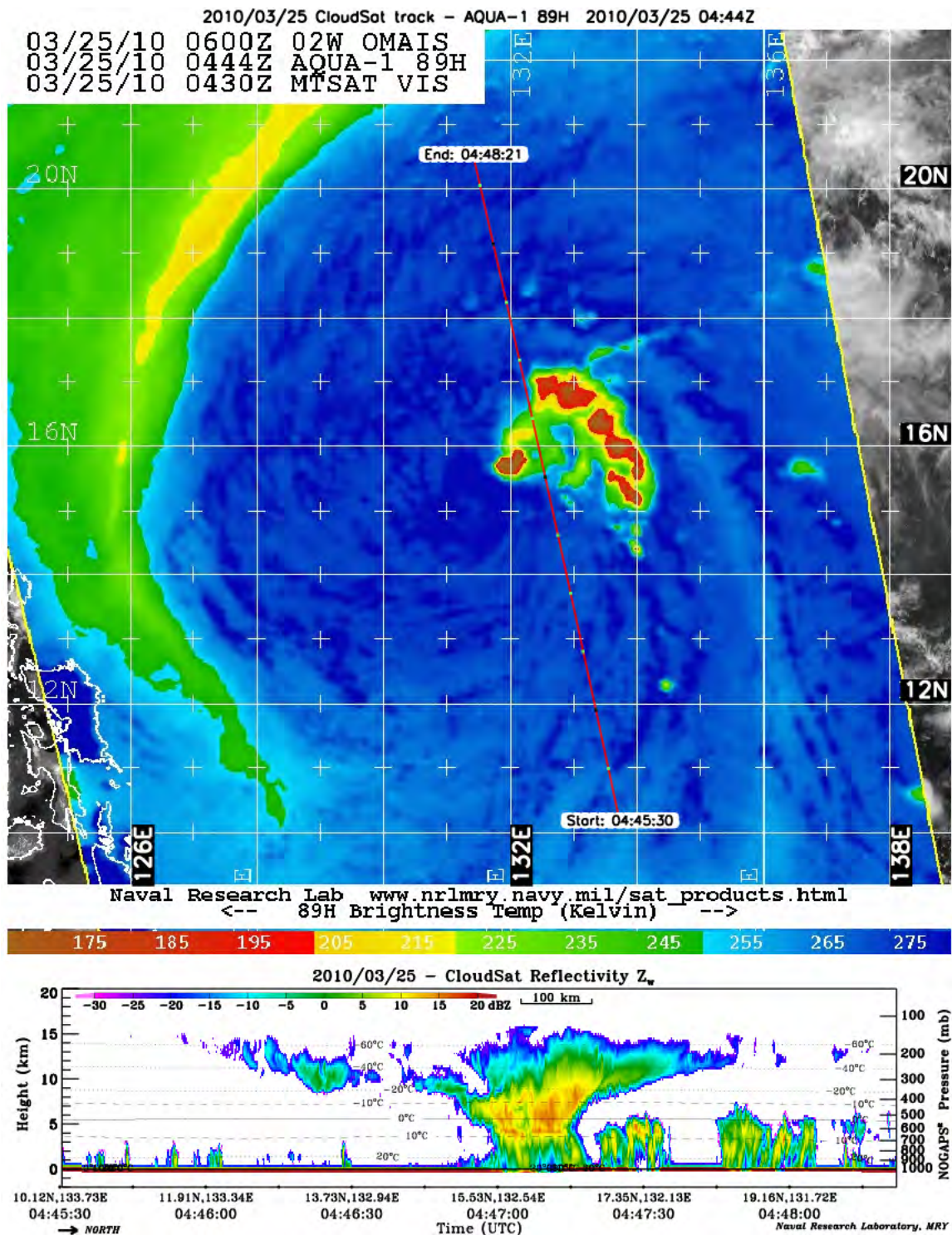


Figure 59. Second CloudSat satellite pass over 02W at 0444 UTC 25 March 2010. Maximum TCC was 12.5 km during this satellite pass. Intensity for 02W at time of pass was 45 kt (from Colorado State University. URL: <http://reef.atmos.colostate.edu>)

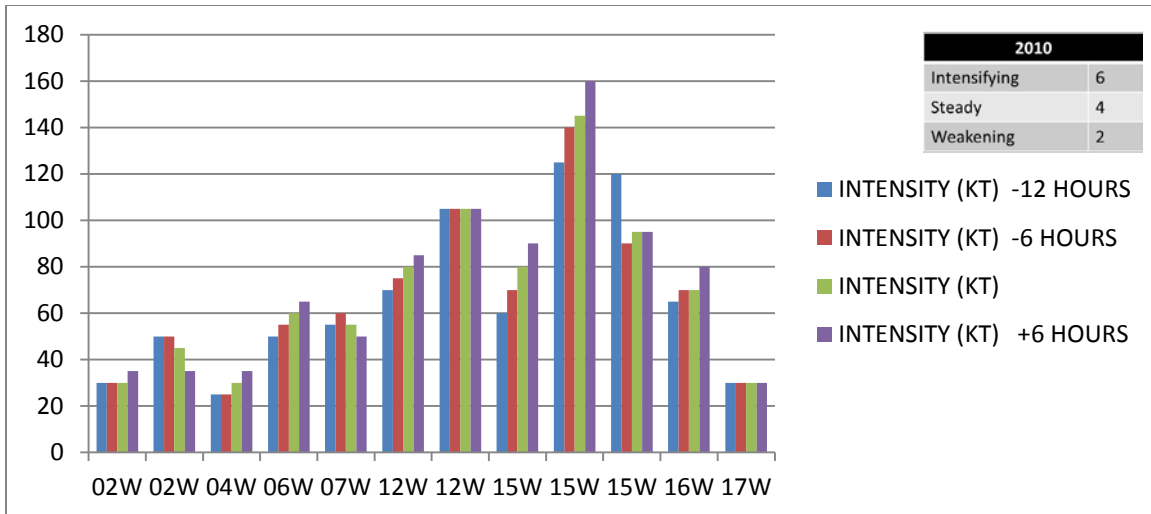


Figure 60. Graph depicting intensity values (kt) leading up to and after the satellite made the pass over the storm (2010)

C. SUMMARY

To compare TC characteristics to cloud heights, the analysis is constrained to only the passes that occurred over the center of each TC (i.e., pass 1). A comparison of the intensity at the time of each CloudSat overpass to both ToC and TCC is conducted (Figure 61). Based on a linear regression, the intensity of the storm at the time of all pass 1's is not directly related to either the ToC (Figure 61a) or TCC (Figure 61b) height. There is, however, a statistically significant relationship between the change in intensity over the 6 h prior to TC CloudSat pass and the ToC height (Figure 62a), but not the TCC height (Figure 62b).

A value, Tdiff, is defined as the height difference between the ToC and the TCC. There is a statistically significant relationship between Tdiff and ToC (Figure 63a) and TCC (Figure 63b). For a very high TCC, the values of Tdiff decrease. Because the ToC height is limited by the presence of the tropical tropopause, for very high TCC heights the ToC height cannot be much greater than the TCC height.

All Years – Pass 1

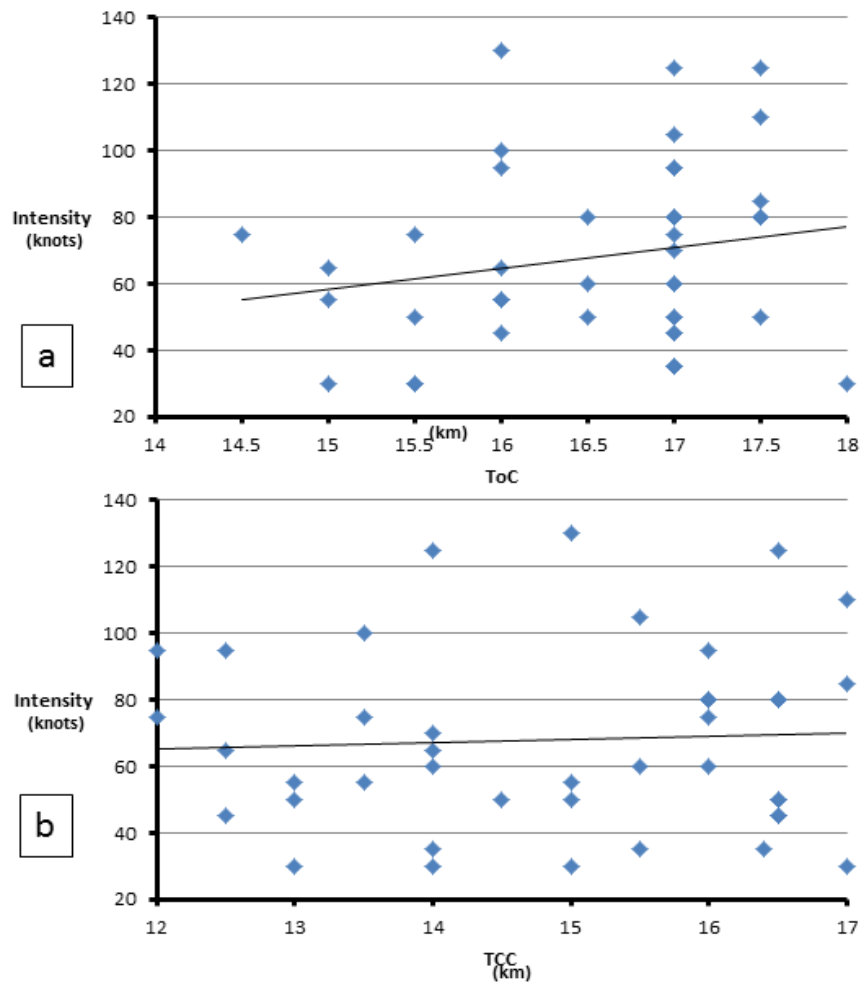


Figure 61. Scatter plot of TC intensity at the time of the CloudSat pass versus the (a) ToC and (b) TCC. The solid black line defines the linear regression between intensity and each height value.

All Years – Pass 1

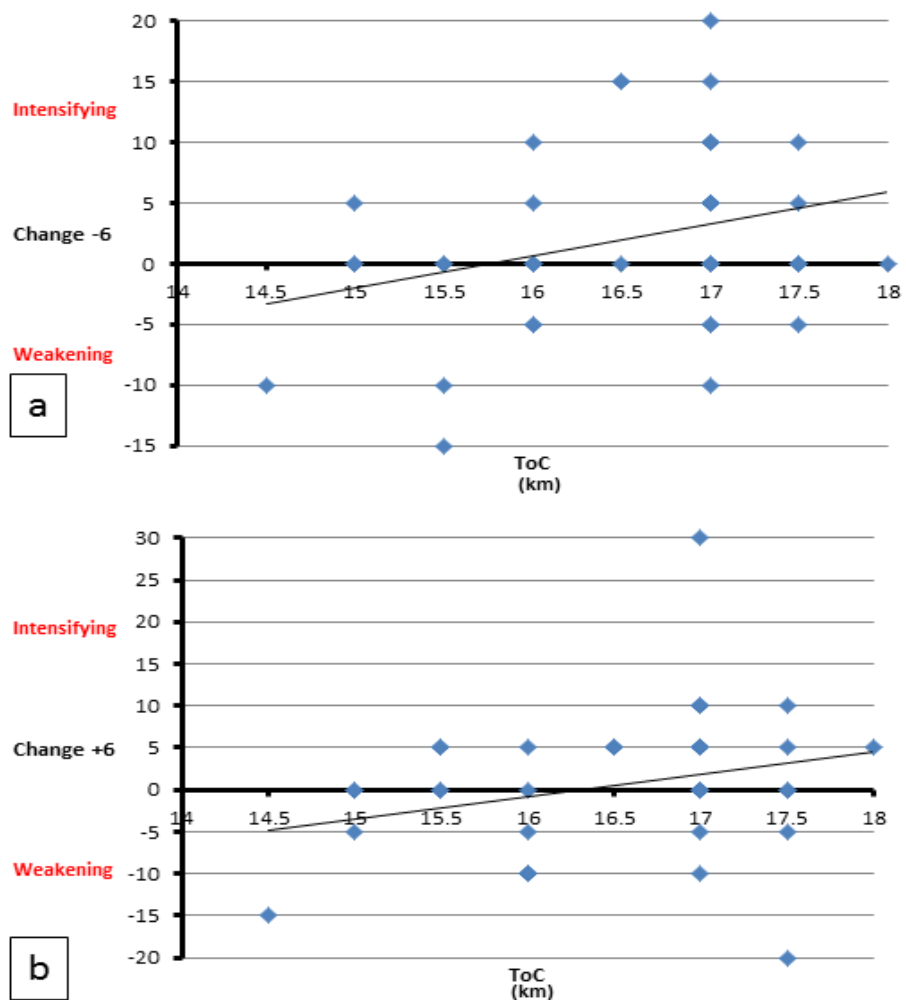


Figure 62. Scatter plot of TC intensity change versus ToC for (a) change in intensity for -6-h versus ToC; (b) change in intensity for +6-h versus ToC. The solid black line defines the linear regression between intensity change and each height value.

All Years – Pass 1

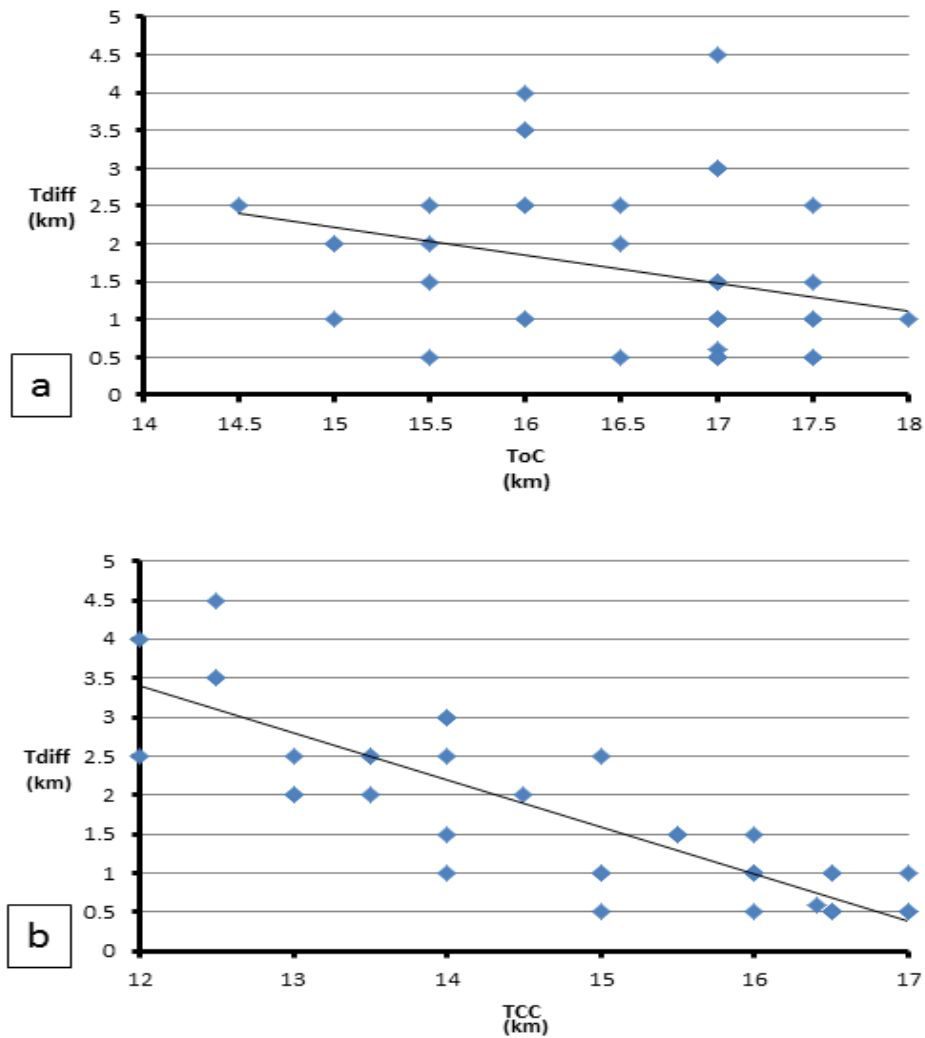


Figure 63. Scatter plot of TC Tdiff versus (a) ToC and (b) TCC. The solid black line defines the linear regression between Tdiff and each height value.

V. CASE STUDIES

While the analysis in Chapter IV used CloudSat data to define ToC and TCC heights, often methods can be used to provide similar values using geostationary imagery (Figure 64). Therefore, the presence of a CloudSat pass is not required. For this study, these geostationary-based analyses were made available for a limited number of cases for the 2013 TC season over the WPAC.

A. TOP OF CONVECTIVE CLOUD (TCC) HEIGHT AND TEMPERATURE

To gain a better perspective on TCC maximum heights and minimum temperatures for the WPAC, three TCs, 19W (Pabuk), 22W (Fitow), and 23W (Danas) that occurred in September and October of 2013 were examined. Based on the CALIPSO analysis methodology (Heidinger 2011), cloud top height and temperature data were obtained for each storm (Figure 64). Each image was analyzed to record the height and temperature values as well as position of the storm center at the time of each satellite-based analysis.

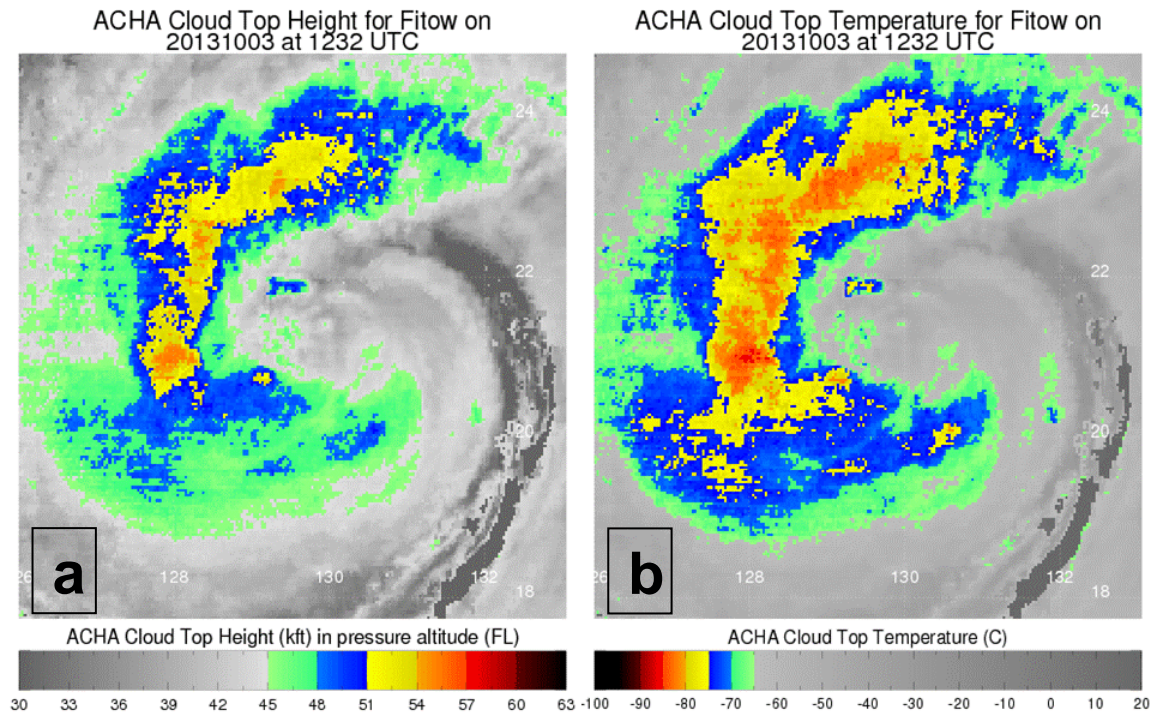


Figure 64. Cloud-top height (a) and cloud-top temperature (b) for Typhoon Fitow at 1232 UTC 30 October 2013

1. 19W (Pabuk)

On 18 September 2013, an area of convection occurred northwest of Guam. It was given the designation 19W (Figure 65) by the JTWC as it moved north very slowly on 21 September. It was upgraded to Tropical Storm Pabuk on 22 September. Tropical Storm Pabuk maintained its strength as a weak eye formed on 23 September. Pabuk was upgraded to a category 2 typhoon by the JTWC on 24 September. After reaching a peak intensity of 90 kt at 0000 UTC 25 September, it gradually weakened before transitioning into an extratropical cyclone on 27 September.

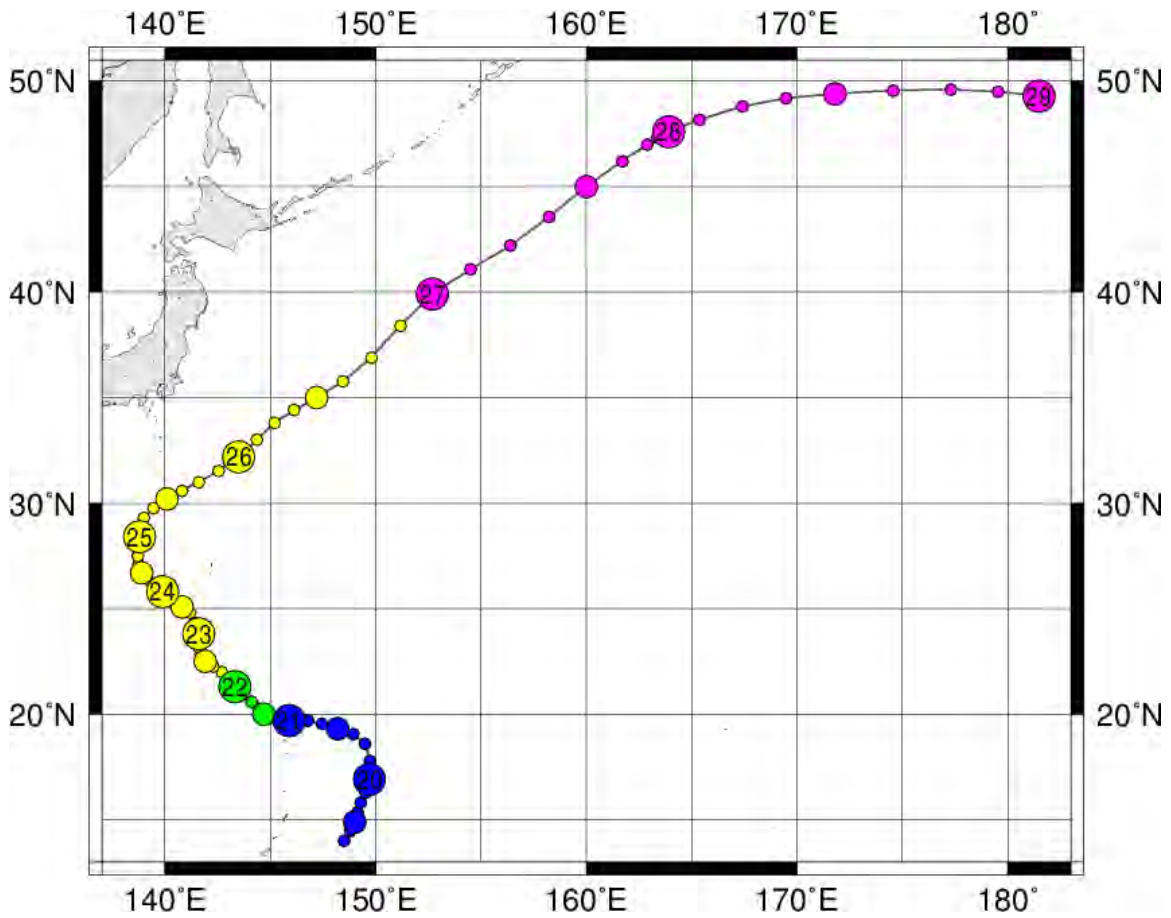


Figure 65. Track of Pabuk during September 2013.

The coldest cloud-top temperature of -90°C occurred during formation at low latitude near 20°N (Figure 66). This is most likely associated with the intensifying storm (see Chapter IV results) and the elevated height of the tropopause at that latitude. As Tropical Storm Pabuk began to move northwestward and intensify, the cloud-top temperatures warmed slightly to range from -80°C to -70°C . Temperatures increased to be above -60°C as the storm moved north of 32°N (Figure 67). The mean TCC temperature throughout the life cycle of 19W was -77.8°C .

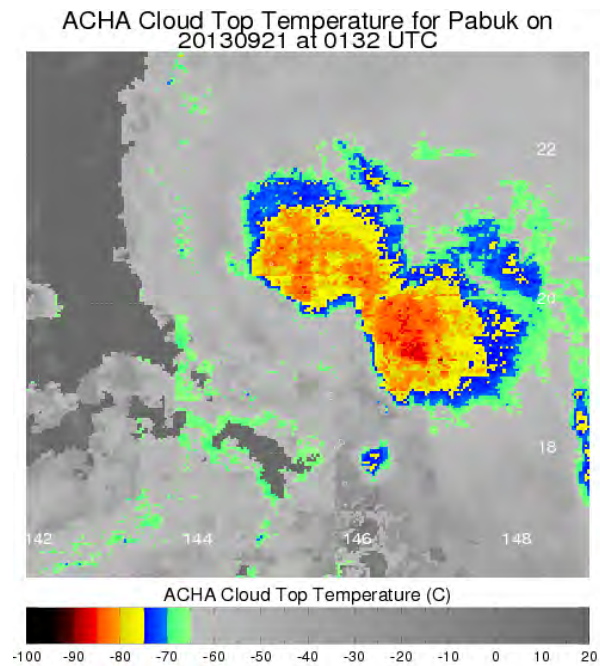


Figure 66. TCC temperature depiction for 19W on 21 Sept at 0132 UTC

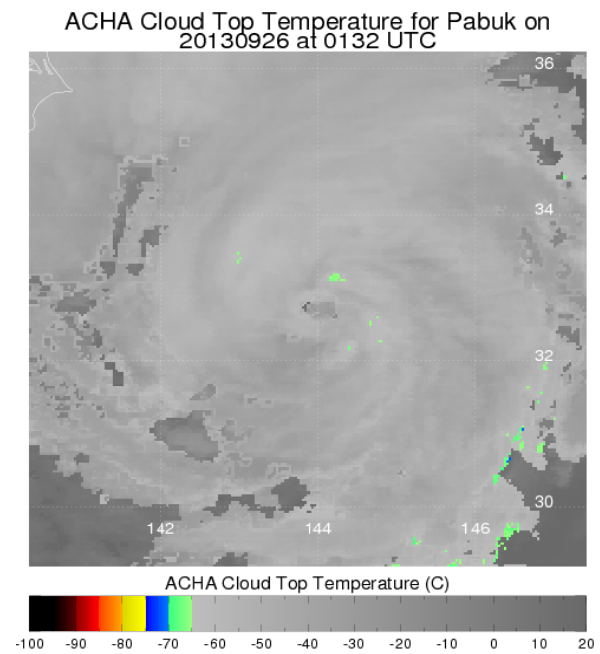


Figure 67. TCC temperature depiction for 19W on 26 Sept at 0132 UTC
when Pabuk was near 33N

The maximum TCC height of 60 kft occurred at 0732 UTC 21 September (Figure 68) which was at the time of formation at 19.6°N. A height of 60 kft was

also recorded at 0732 UTC on 24 September (Figure 69). Temperatures at these times were -90°C and -82°C respectively. The lowest TCC height was 46 kft with a storm intensity of 80 kt at 0132 UTC 26 September (Figure 70) and the temperature was -66°C. The mean TCC height throughout the life cycle of Typhoon Pabuk was 54.8 Kft.

As defined in Chapter IV, there is a statistically significant relationship between the -6-h intensity change and cloud-top height. Using the ACHA data for Pabuk, there is a similar relationship between cloud-top temperature and -6-h intensity change (Figure 71). As intensity change increases, cloud-top temperatures become colder.

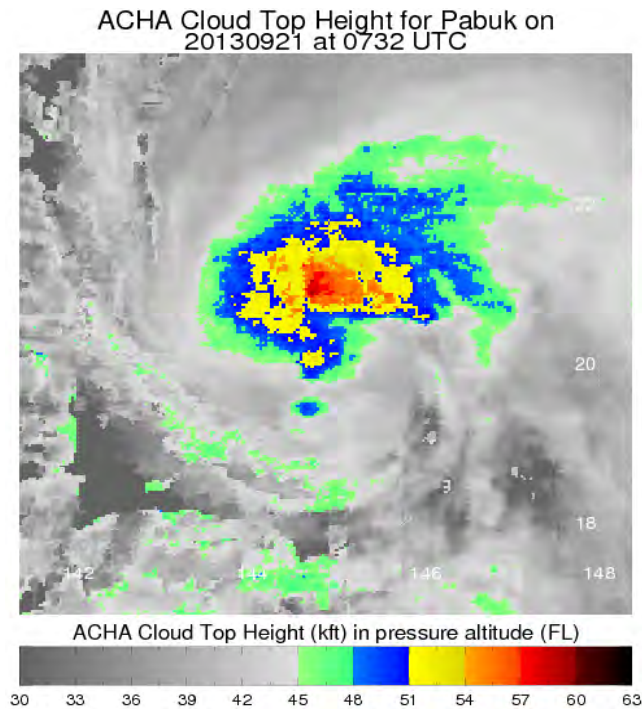


Figure 68. TCC height depiction for 19W on 21 Sept at 0732 UTC

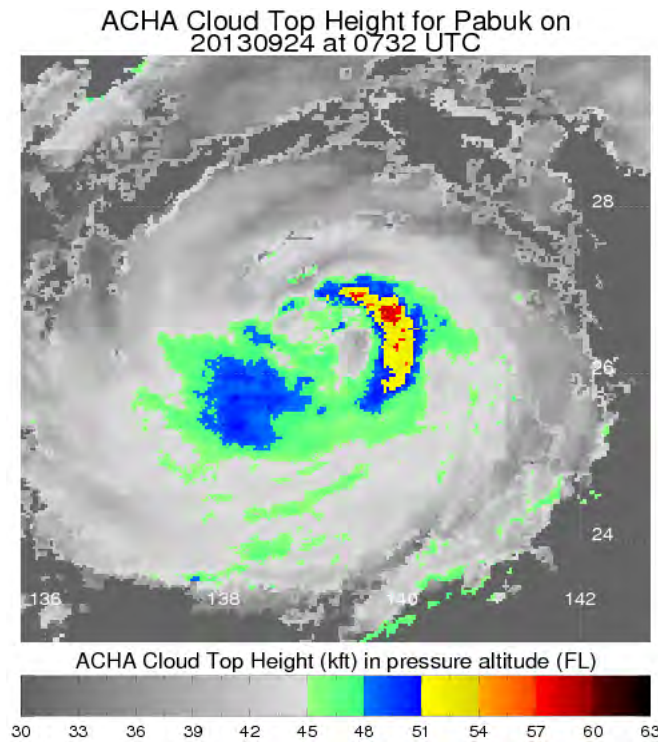


Figure 69. TCC height depiction for 19W on 24 Sept at 0732 UTC

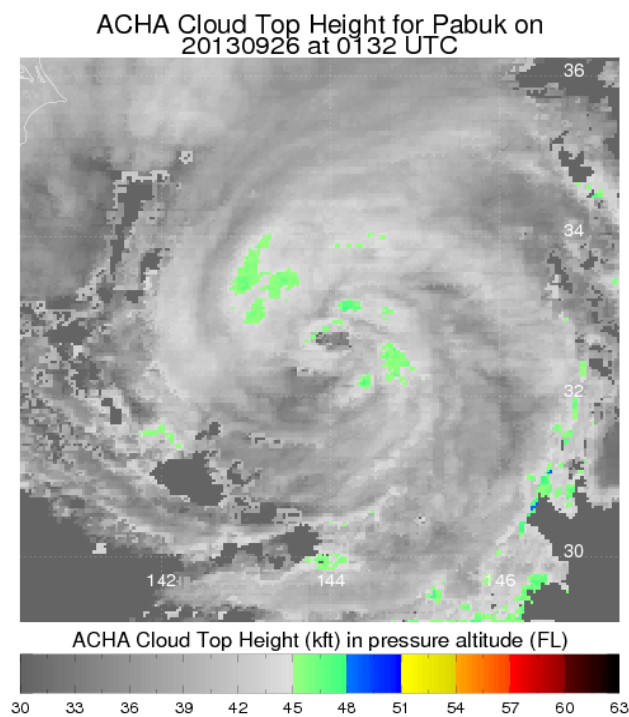


Figure 70. TCC height depiction for 19W on 26 Sept at 0132 UTC

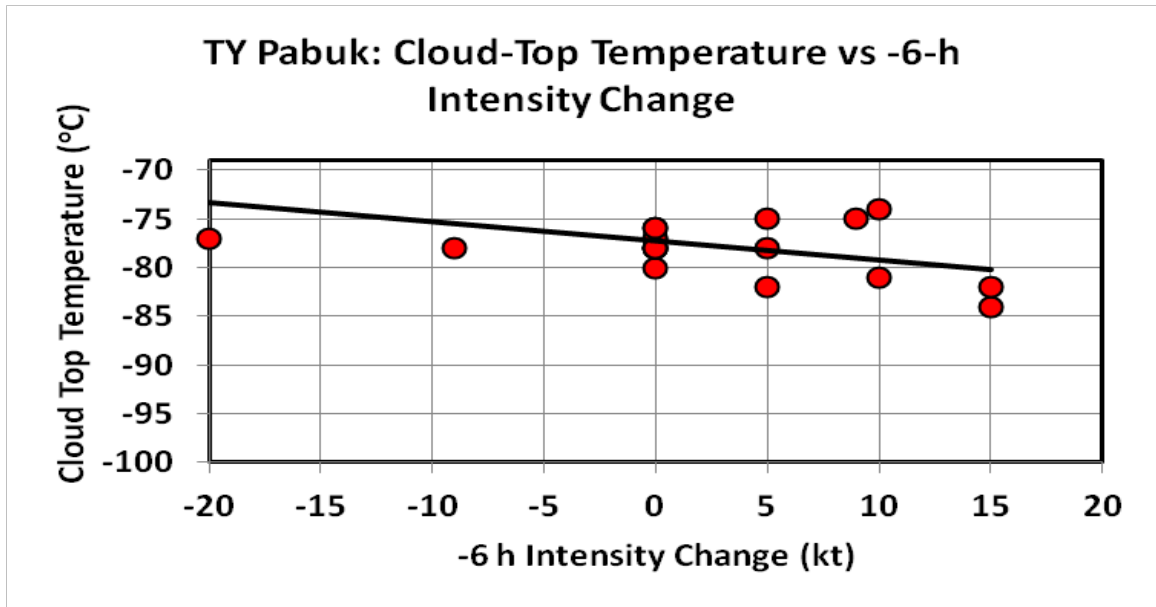


Figure 71. Cloud-top temperature vs -6-h intensity change for TY Pabuk. This image shows a significant linear relationship between decreasing temperatures and TC intensification. The solid black line defines the linear regression between cloud-top temperature and -6-h intensity change

2. 22W (Fitow)

A large tropical disturbance formed east of Palau on 27 September 2013 and intensified to a tropical depression on 29 September (Figure 72). On 30 September, deep convection wrapped around 22W as it became a tropical storm and the Japanese Meteorological Association (JMA) named it Fitow on 01 October. Fitow rapidly intensified into a Category 2 typhoon as it moved north on 03 October. A large eye developed as Typhoon Fitow passed over the southern Japanese Islands late on 04 October. Fitow rapidly weakened to a tropical depression over China late on October 7.

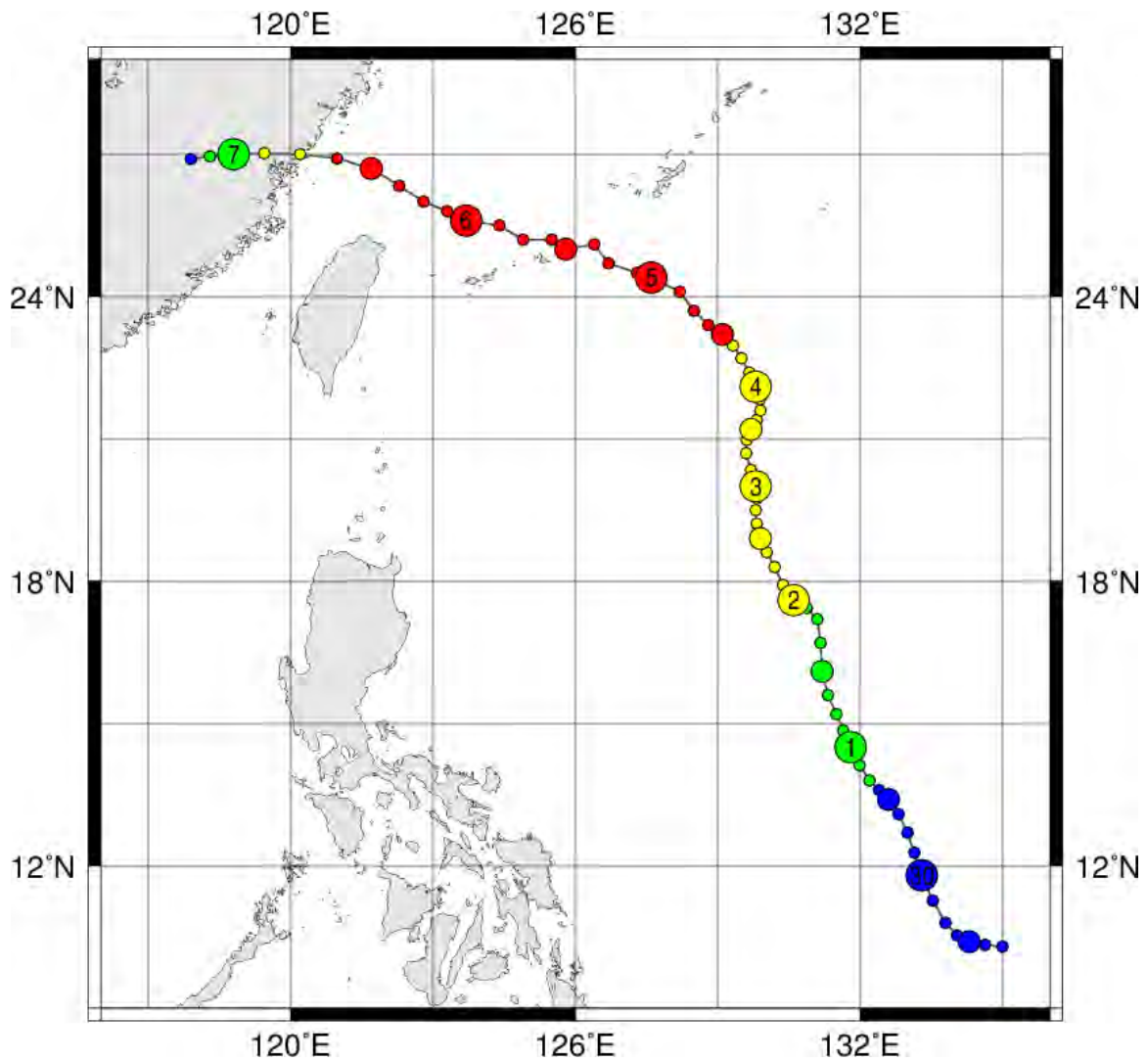


Figure 72. Track of Fitow during September/October 2013

At 0000 UTC 05 October, Typhoon Fitow achieved a maximum intensity of 90 kt. The storm maintained this intensity for 18 hours before slightly decreasing in intensity late on the same day.

As Fitow formed near 20°N, the coldest temperature of -91°C occurred (Figure 73). As with Pabuk, this is most likely associated with the increased height of the tropopause at this low latitude and the fact that the intensity was increasing. As Fitow began to move north-northwest and intensify, the cloud-top temperatures increased slightly to be between -75°C to -80°C. The warmest TCC temperature that was recorded was -71°C. This occurred twice with one at approximately 25.8°N (Figure 74) and the second at approximately 26.8°N. The mean TCC temperature throughout the life cycle of Typhoon Fitow was -81.5°C.

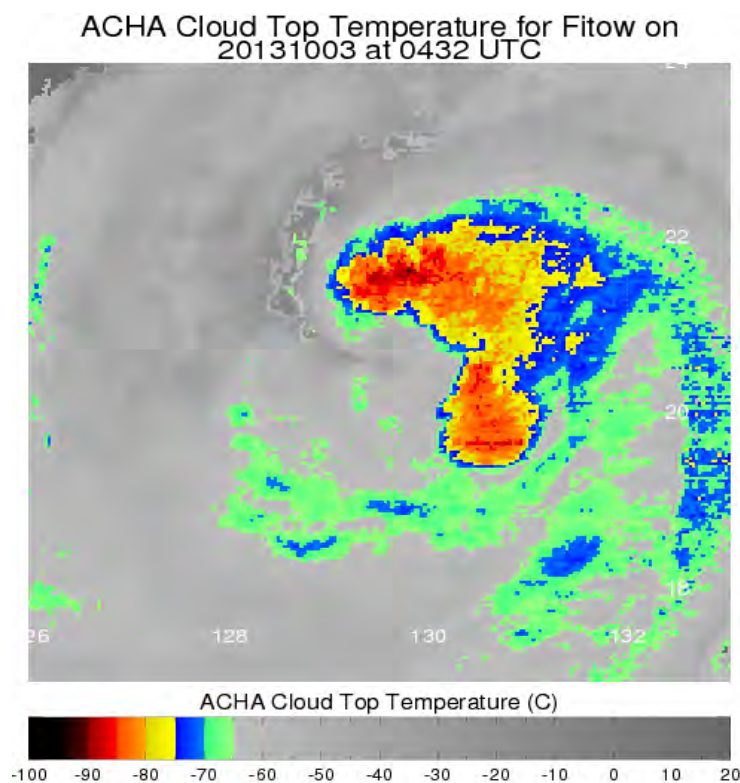


Figure 73. TCC temperature depiction for 22W on 03 Oct at 0432 UTC

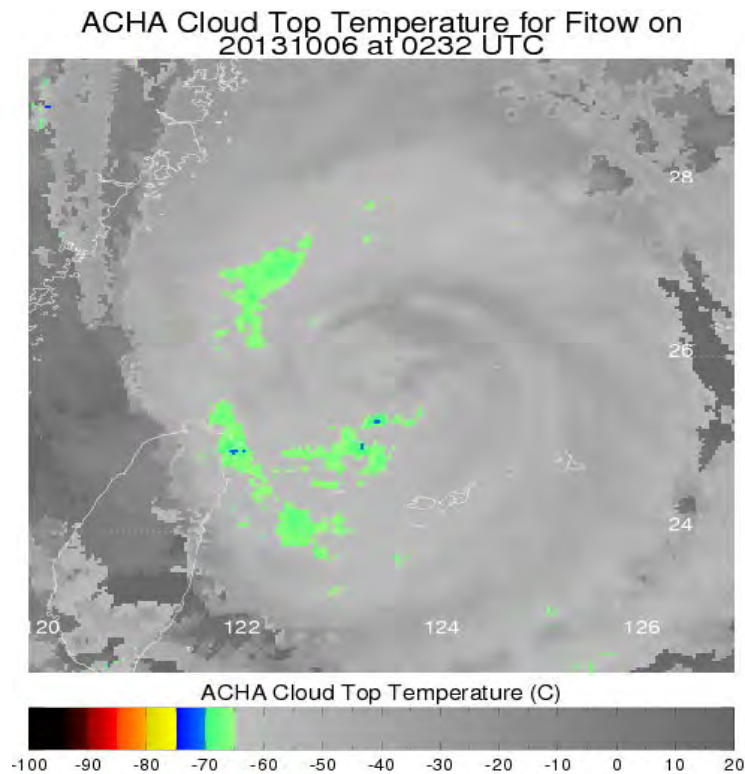


Figure 74. TCC temperature depiction for 22W on 06 Oct at 0232 UTC.

Typhoon Fitow achieved a maximum TCC height of 60 kft occurring at 0632 UTC 03 October (Figure 75). The cloud-top temperature at this time was -91°C . The lowest TCC height recorded was at 48 kft with a storm intensity of 75 kt. This happened at 0232 UTC 06 October (Figure 76) and the cloud-top temperature was -71°C . The mean TCC height throughout the life cycle of Typhoon Fitow was 53.6 kft.

The inverse linear relationship between -6-h intensity change and cloud-top temperature, exhibited in the data for TY Pabuk was more significant in TY Fitow (Figure 77). As intensity change increases, cloud-top temperature becomes colder.

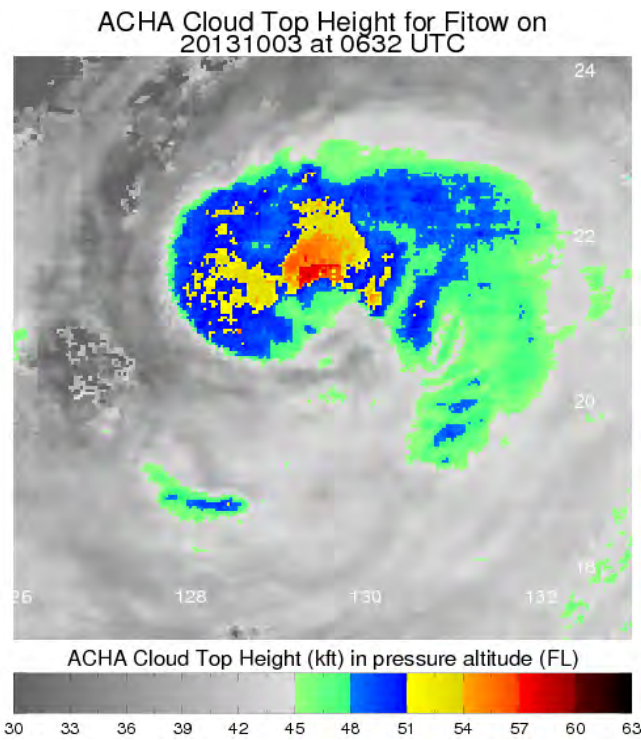


Figure 75. TCC height depiction for 22W on 03 Oct at 0632 UTC

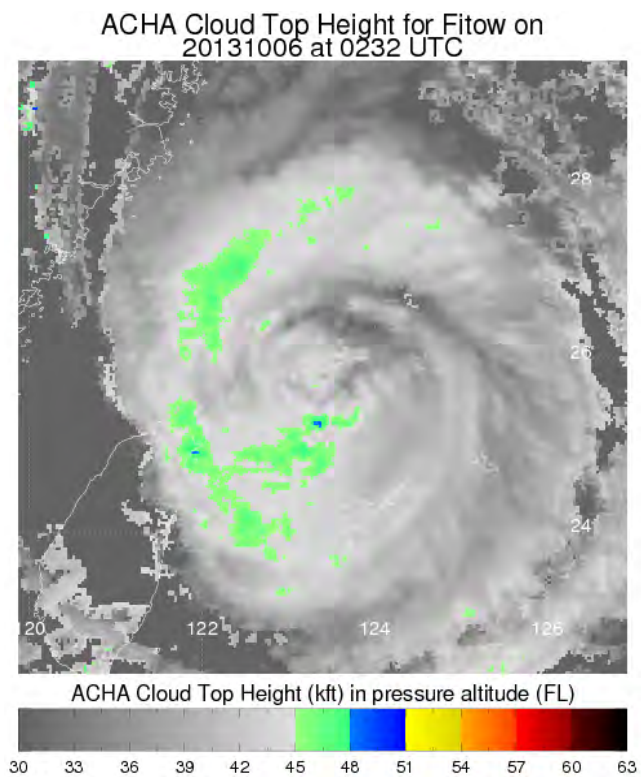


Figure 76. TCC height depiction for 22W on 06 Oct at 0232 UTC

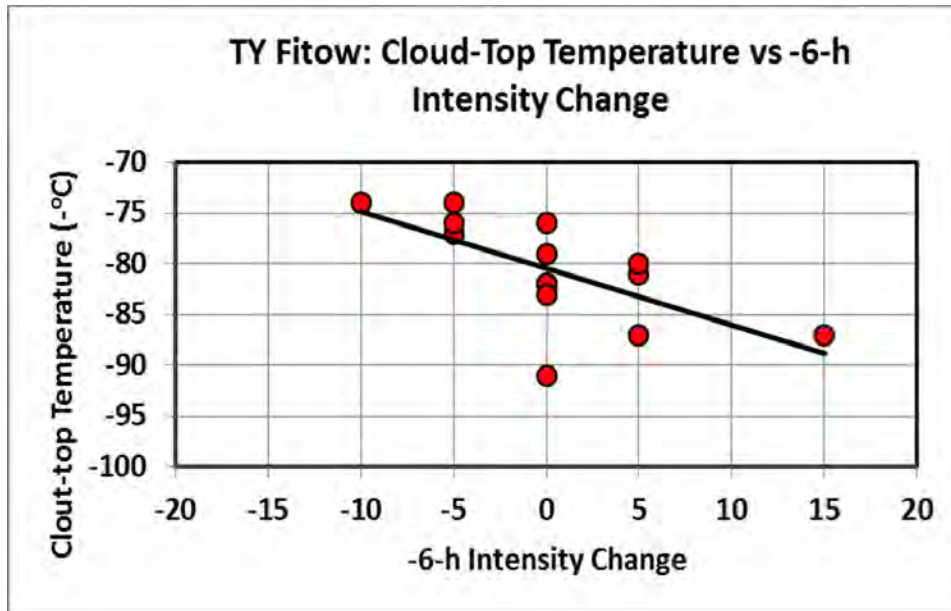


Figure 77. Cloud-top temperature vs -6-h intensity change for TY Fitow. This image shows a significant linear relationship between decreasing temperatures and TC intensification. The solid black line defines the linear regression between cloud-top temperature and -6-h intensity change.

3. 23W (Danas)

On 03 October 2013, a large cloud cluster formed northeast of Guam and strengthened into tropical depression 23W (Figure 78). Late on 04 October, the JMA upgraded the depression to Tropical Storm Danas. On 07 October, Typhoon Danas entered warmer waters as it became an annular category 4 typhoon passing the northern part of Okinawa. Typhoon Danas rapidly weakened as it entered cooler waters near Japan on 08 October. On 09 October, Danas became extratropical as it headed to the northern part of Japan.

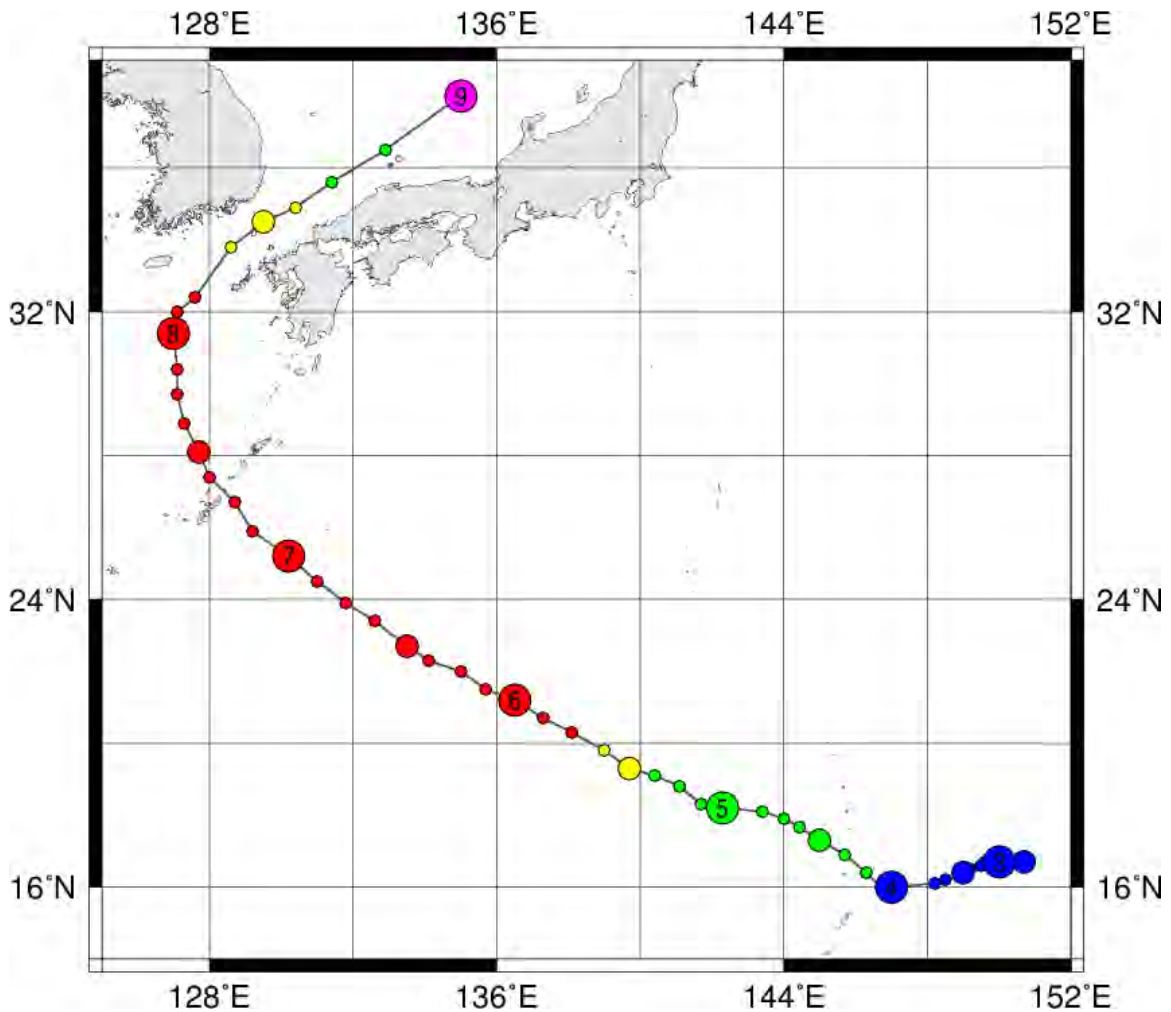


Figure 78. Track of Danas during October 2013

At 0600 UTC 07 October, Typhoon Danas achieved a maximum intensity of 125 kt. The storm maintained this strong intensity for six hours before slightly decreasing to 120 kt at 1200 UTC the same day.

Danas formed near 15.7°N with TCC temperatures fluctuating between -79°C and -85°C. Unlike Pabuk and Fitow, Danas recorded its lowest TCC temperature (-89°C) 44 hours after developing into a tropical depression (Figure 79). The storm at this time was at approximately 19.2°N with an intensity of 60 kt.

Even though Danas was almost two days old, the storm's center was still south of 20°N. As Danas moved northwest of 20°N the storm intensified steadily while the TCC temperatures slowly warmed to the -70s. The warmest TCC temperature during the life cycle of Danas was -68°C. This occurred at approximately 32.8°N (Figure 80) with an intensity of 65 kt. The mean TCC temperature throughout the life cycle of Danas was -80.1°C.

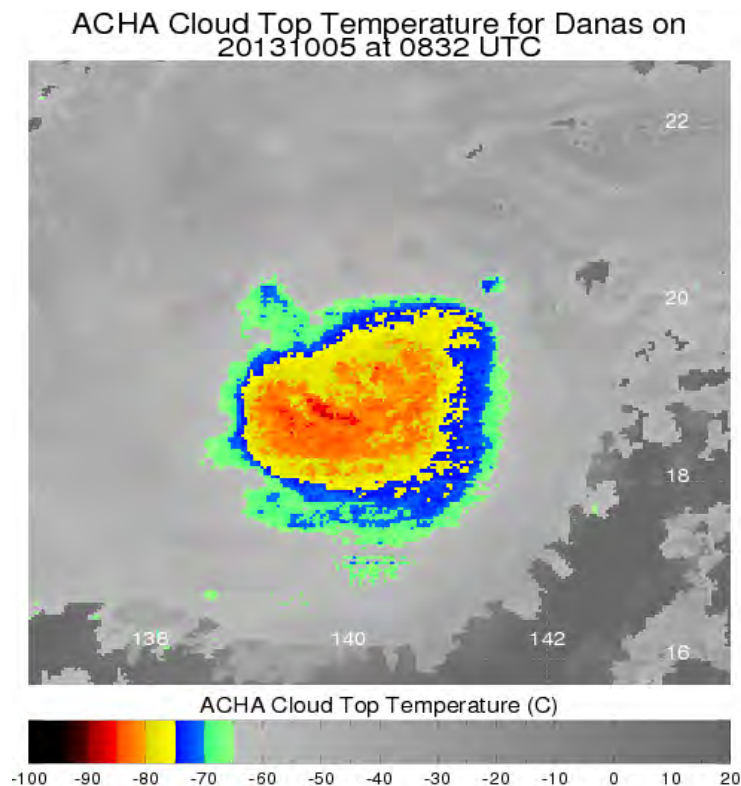


Figure 79. TCC temperature depiction for 23W on 05 Oct at 0832 UTC

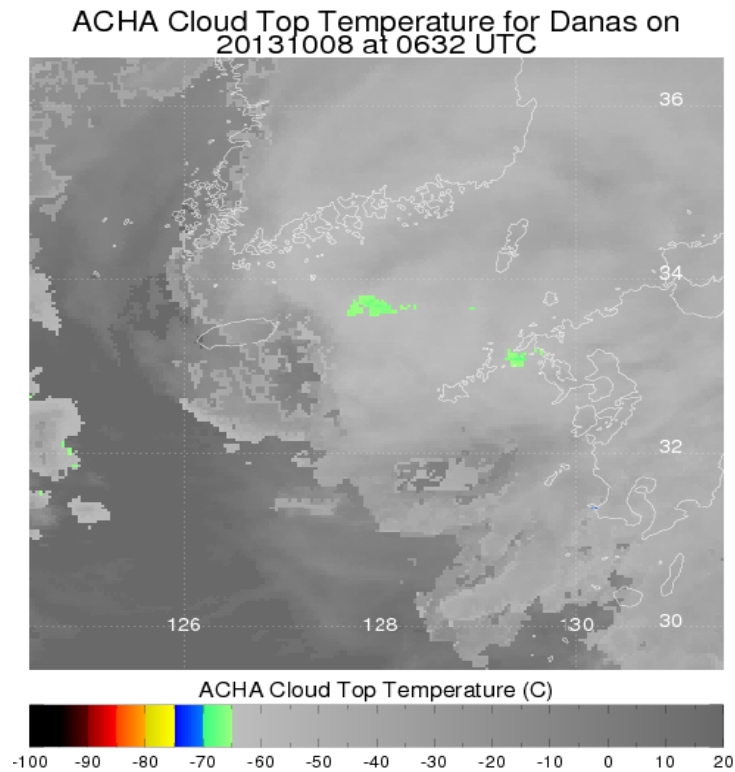


Figure 80. TCC temperature depiction for 23W on 08 Oct at 0632 UTC

Typhoon Danas achieved a maximum TCC height of 59 kft occurring at 2332 UTC 04 October (Figure 81) with a cloud-top temperature at -85°C . The lowest TCC height recorded was at 48 kft when the storm was at a maximum intensity of 125 kt. At 0732 UTC on 07 October (Figure 82) the cloud-top temperature was -71°C . The mean TCC height throughout the life cycle of Typhoon Danas was 52.9 kft.

Contrary to the findings associated with TY Pabuk and TY Fitow, there was no statistical relationship (Figure 83) between -6-h intensity change and cloud-top temperatures for TY Danas. When all three storms are analyzed together (Figure 84), it is clear that the weak relationship between cloud-top

temperature and -6-h intensity change observed during TY Dana reduces the overall significance as the relationships during TY Pabuk (Figure 71) and TY Fitow (Figure 77) were highly significant. Hopefully, as this satellite-based product is used more, the increased data sample will identify a more significant relationship.

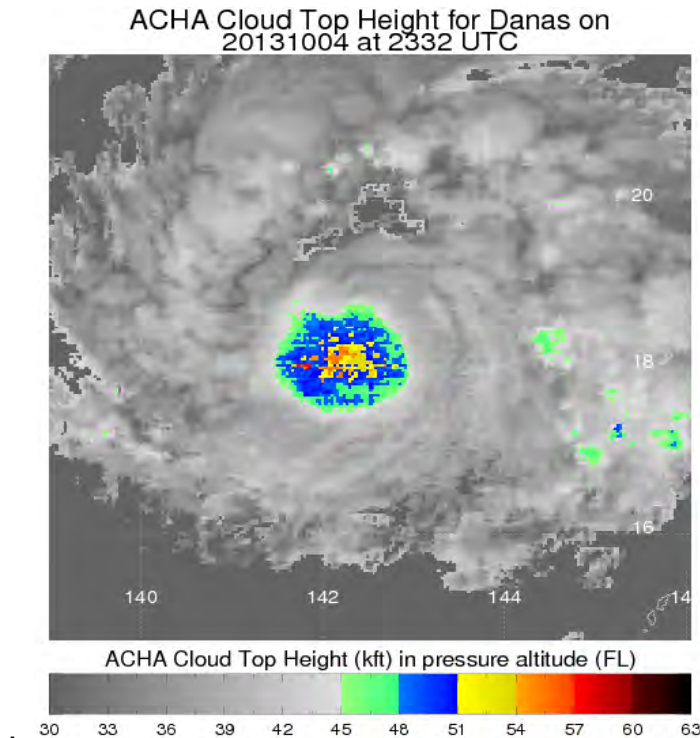


Figure 81. TCC height depiction for 23W on 04 Oct at 2332 UTC

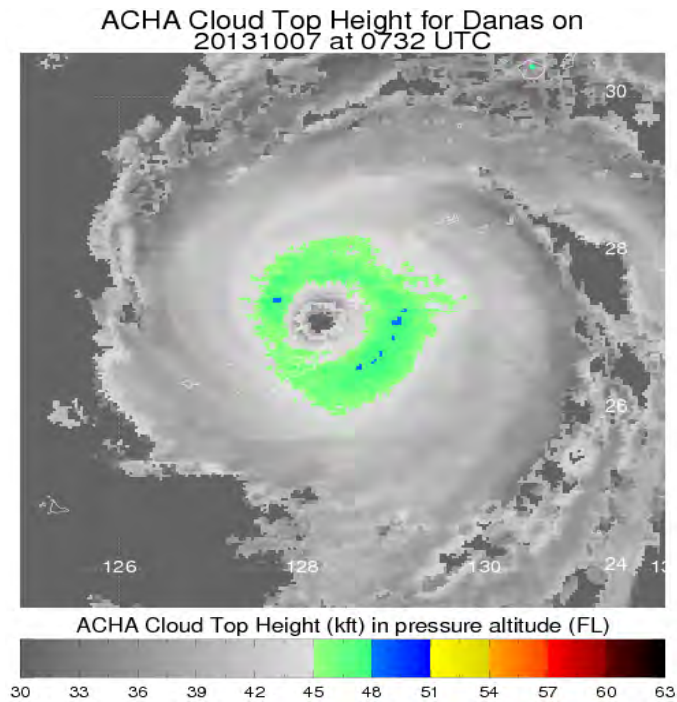


Figure 82. TCC height depiction for 23W on 07 Oct at 0732 UTC

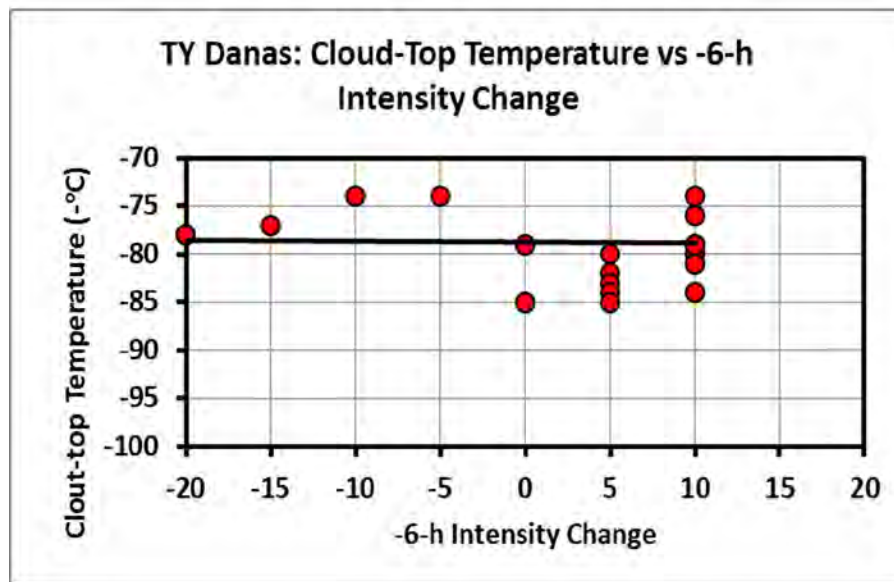


Figure 83. Cloud-top temperature vs -6-h intensity change for TY Danas. This image shows a non-significant linear relationship between decreasing temperatures and TC intensification. The solid black line defines the linear regression between cloud-top temperature and -6-h intensity change

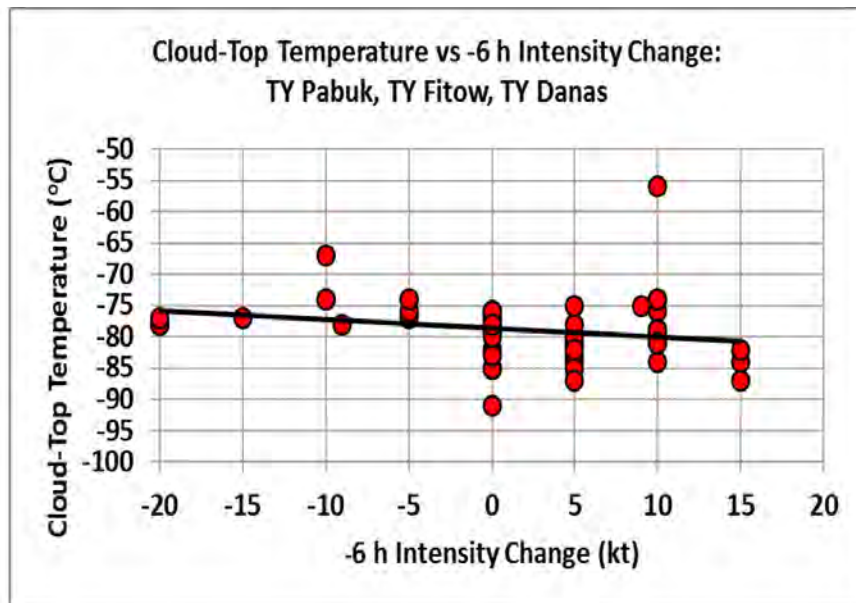


Figure 84. Cloud-top temperature vs -6-h intensity change for all three TCs (TY Pabuk, TY Fitow, TY Danas). This image shows a significant linear relationship between decreasing temperatures and TC intensification. The solid black line defines the linear regression between cloud-top temperature and -6-h intensity change..

VI. CONCLUSION

A. SUMMARY

1. BACKGROUND

The ability to forecast TC formations and intensity is of critical importance to the safety and use of many national assets throughout the WPAC. It has been mandated by the USPACOM to reduce the current uncertainty area by 50% within the next 15 years. To achieve this goal, *in situ* observations throughout the WPAC are necessary. It has been proven that adding these observations would provide improved knowledge of current storm characteristics and improved initial conditions for model-generated forecasts.

A pending data void for viable TC reconnaissance from satellites is projected. Observational capabilities over the WPAC are limited to remotely-sensed data from polar-orbiting and geostationary satellites. Satellite platforms have been reduced through attrition and lack of funding and their future is uncertain. Losing this capability altogether would greatly affect the JTWC and their forecasting ability.

2. REQUIREMENTS AND RESTRICTIONS

During the NASA-led HS3 mission over the Atlantic Ocean, the GH was instrumental in defining the character of the inner TC structure and the large-scale environment in which the tropical cyclone existed. The OUTFLOW program is projected to occur over the WPAC during September and October of 2015–2017. This will provide an excellent opportunity for the GH to prove its value by providing *in situ* data to JTWC forecasters and provide valuable input for proper initialization of the numerical weather prediction models.

3. WPAC TC CLIMATOLOGY

Based on the five years of CloudSat overpasses of WPAC TCs, it is concluded that it is possible for the GH to conduct reconnaissance and avoid

hazardous turbulence and lightning over the majority of WPAC TCs. The overall 5 year mean for the ToC was 16.1 km (52.8 kft) and the mean for the TCC was 14.2 km (46.6 kft). The highest ToC that occurred was in 2010 and that altitude was 18.0 km (59.1 kft) at 9°N. At such low latitudes, the tropical tropopause is very high, which contributes to very high cloud heights and cold temperatures. The highest TCC that occurred was at an altitude of 17.0 km (55.8 kft) and that happened every year but 2009. The highest TCC for 2009 was 16.5 km (54.1 kft). The GH would be able to maintain a 5,000 ft separation (when flying at maximum altitude) above the TCC to avoid possible lightning and severe turbulence. There will be the rare exception in that the top of convection will reach even higher than 17.0 km (55.8 kft).

4. CASE STUDIES

The cloud-top temperatures associated with three storms during 2013 that formed south of 20°N and tracked northwestward were examined. Storms 19W and 22W had maximum intensities of 90 kt that placed them into category 2 status while 23W had a maximum intensity of 125 kt, which is a category 4 storm. All three storms achieved their coldest TCC temperatures when their center was south of 20°N regardless of intensity. Only with 22W did that correspond with the maximum TCC height. The mean TCC height for these three storms was 53.8 kft which is significantly higher than the 46.6 kft mean from the 5 year study in chapter IV. The reason for the difference is that hourly TCC heights during the entire life cycle of these three storms were available as opposed to certain “snapshots” at periodic times of CloudSat overpasses for the storms researched in the 5 year study. Many snapshots were taken when the storm was well north of 20°N limiting the convective extent due to the lower height of the tropopause. The GH can expect to encounter the coldest temperatures when flying south of 20°N as TCC temperatures averaged -84.6°C when the storm had an intensity of at least 35 kt. The three storm overall mean TCC temperature was -79.8°C.

Tropical Cyclone reconnaissance by the Global Hawk can be a temporary but relatively affordable option for all but the most rapidly intensifying tropical cyclones or tropical cyclones at very low latitudes and is highly recommended.

B. RECOMMENDATIONS FOR FUTURE STUDY

Tropical cyclone research is an intense ongoing science that has acquired even greater importance in this era of global climate change. Increased study of TC track forecasting utilizing dropsonde data in the WPAC is recommended to further enhance the forecast ability of numerical models and forecasters. Additional research is needed to enhance TC intensity forecasting for both the WPAC and Atlantic Ocean basins as there has been minimal improvement over the last 20 years.

Expanded climatology research is needed for possible GH staging bases in the WPAC. The rate of flight cancelations and diverts seem to be abundant at the current GH staging base at Anderson AFB in Guam. Other strategic airfields might be more beneficial for future GH flights.

THIS PAGE INTENTIONALLY LEFT BLANK

APPENDIX A. 19W (PABUK) HOURLY DATA

19W (PABUK)

DATE	TIME	TCC (Kft)	INTENSITY (kt)	TEMP (-C)	LAT / LONG
21-Sep	0032Z	58	25 G 35	85	19.6 N / 145.5 E
	0132Z	58		90	
	0232Z				
	0332Z	58		85	
	0432Z	57		87	
	0532Z	58		90	
	0632Z	57	40 G 50	84	20.3 N / 145.0 E
	0732Z	60		90	
	0832Z	59		86	
	0932Z	55		83	
	1032Z	57		82	
	1132Z	57		80	
	1232Z	55	40 G 50	77	20.6 N / 144.4 E
	1332Z	57		80	
	1432Z	54		78	
	1532Z	54		76	
	1632Z	53		75	
	1732Z	53		76	
	1832Z	51	50 G 65	74	20.6 N / 143.7 E
	1932Z	51		74	
	2032Z	52		74	
	2132Z	56		76	
	2232Z	53		75	
	2332Z	50		71	
22-Sep	0032Z	52	50 G 65	75	21.2 N / 143.2 E
	0132Z	52		74	
	0232Z	55		77	
	0332Z	52		75	
	0432Z	54		76	
	0532Z	51		72	
	0632Z	56	50 G 65	78	22.2 N / 142.7 E
	0732Z	55		78	
	0832Z	56		80	
	0932Z	57		80	
	1032Z	57		80	
	1132Z	57		80	
	1232Z	56	50 G 65	80	22.7 N / 142.1 E
	1332Z	57		82	
	1432Z	56		80	
	1532Z	58		84	

23-Sep	1632Z	59	50 G 65	85	23.1 N / 141.7 E
	1732Z	57		82	
	1832Z	54		78	
	1932Z	54		77	
	2032Z	57		83	
	2132Z	57	60 G 75	80	23.8 N / 141.2 E
	2232Z	56		80	
	2332Z	56		80	
	0032Z	57		81	
	0132Z	55		81	
	0232Z	55	60 G 75	79	24.7 N / 140.9 E
	0332Z	54		79	
	0432Z	55		79	
	0532Z	55		78	
	0632Z	53		76	
	0732Z	53	65 G 80	75	25.2 N / 140.7 E
	0832Z	52		75	
	0932Z	56		78	
	1032Z	55		78	
	1132Z	54		77	
24-Sep	1232Z	55	65 G 80	78	25.7 N / 140.0 E
	1332Z	56		78	
	1432Z	56		80	
	1532Z	56		80	
	1632Z	56		80	
	1732Z	56	65 G 80	79	25.9 N / 139.6 E
	1832Z	55		78	
	1932Z	58		80	
	2032Z	57		81	
	2132Z	55		79	
	2232Z	57	65 G 80	81	26.1 N / 139.3 E
	2332Z	59		80	
	0032Z	57		78	
	0132Z	55		80	
	0232Z	53		77	
	0332Z	52	65 G 80	75	26.4 N / 139.0 E
	0432Z	54		77	
	0532Z	52		75	
	0632Z	57		78	
	0732Z	60		82	
	0832Z	58	70 G 85	80	
	0932Z	58		83	
	1032Z	54		78	
	1132Z	52		75	
	1232Z	57		82	
	1332Z	52		76	
	1432Z	55		79	

25-Sep	1532Z	54	85 G 105	79	27.7 N / 138.5 E
	1632Z	54		78	
	1732Z	55		80	
	1832Z	58		82	
	1932Z	58		80	
	2032Z	59	90 G 110	81	28.5 N / 138.6 E
	2132Z	59		81	
	2232Z	57		80	
	2332Z	53		79	
	0032Z	52		75	
	0132Z	51	90 G 110	75	29.3 N / 139.1 E
	0232Z	51		74	
	0332Z	54		79	
	0432Z	58		77	
	0532Z	58		77	
	0632Z	58	90 G 110	77	30.2 N / 140.1 E
	0732Z	58		77	
	0832Z	58		76	
	0932Z	58		76	
	1032Z	59		78	
	1132Z	58	90 G 110	77	
	1232Z	58		76	
	1332Z	58		76	
	1432Z	58		76	
	1532Z	58		76	
	1632Z	56	90 G 110	77	31.2 N / 141.4 E
	1732Z	56		80	
	1832Z	57		78	
	1932Z	54		77	
	2032Z	54		77	
26-Sep	2132Z	52	80 G 100	74	32.2 N / 143.3 E
	2232Z	50		72	
	2332Z	50		71	
	0032Z	47		67	
	0132Z	46		66	
	0232Z	50	60 G 75	72	33.9 N / 145.5 E
	0332Z	50		73	
	0432Z	50		73	
	0532Z	47		67	
	0632Z	55		77	
	0732Z	55		76	
	0832Z	52		75	
	0932Z	49		74	
	1032Z	48		69	
	1132Z	47		66	
	1232Z	50		70	
	1332Z	52		75	

	1432Z	53		77	
	1532Z	53		76	
	1632Z	55		78	
	1732Z	51		75	
MEAN		54.8		77.8	
		16.7 km			

APPENDIX B. 22W (FITOW) HOURLY DATA

22W (FITOW)

DATE	TIME	ToC (Kft)	INTENSITY (kt)	TEMP (-C)	LAT / LONG
3-Oct	0032Z	56	60 G 75	89	20.0 N / 129.5 E
	0132Z	55		89	
	0232Z	54		87	
	0332Z	56		90	
	0432Z	58		91	
	0532Z	59		90	
	0632Z	60	60 G 75	91	20.6 N / 129.5 E
	0732Z	59		91	
	0832Z	57		90	
	0932Z	58		90	
	1032Z	58		91	
	1132Z	56		90	
	1232Z	56	65 G 80	87	21.1 N / 129.5 E
	1332Z	55		87	
	1432Z	54		84	
	1532Z	56		88	
	1632Z	55		87	
	1732Z	55		89	
	1832Z	54	80 G 100	87	22.0 N / 129.7 E
	1932Z	56		86	
	2032Z	56		85	
	2132Z	55		84	
	2232Z	58		89	
	2332Z	53		81	
4-Oct	0032Z	53	80 G 100	82	22.2 N / 129.8 E
	0132Z	49		76	
	0232Z	52		81	
	0332Z	52		79	
	0432Z	53		83	
	0532Z	57		84	
	0632Z	56	85 G 105	81	22.7 N / 129.7 E
	0732Z	55		84	
	0832Z	58		88	
	0932Z	58		89	
	1032Z	58		87	
	1132Z	56		85	

5-Oct	1232Z	53	85 G 105	82	23.2 N / 129.2 E
	1332Z	54		84	
	1432Z	54		83	
	1532Z	55		84	
	1632Z	54		86	
	1732Z	53		83	
	1832Z	53	85 G 105	83	23.7 N / 128.5 E
	1932Z	54		83	
	2032Z	54		81	
	2132Z	53		79	
	2232Z	56		84	
	2332Z	52		79	
	0032Z	54	90 G 110	80	24.4 N / 127.6 E
	0132Z	53		80	
	0232Z	52		79	
	0332Z	53		79	
	0432Z	52		77	
	0532Z	53		80	
	0632Z	50	90 G 110	76	24.6 N / 127.0 E
	0732Z	50		75	
	0832Z	52		77	
	0932Z	53		84	
	1032Z	55		85	
	1132Z	54		81	
	1232Z	53	90 G 110	79	25.0 N / 125.9 E
	1332Z	53		80	
	1432Z	53		78	
	1532Z	51		76	
	1632Z	50		74	
	1732Z	52		78	
6-Oct	1832Z	52	85 G 105	77	25.4 N / 124.6 E
	1932Z	52		75	
	2032Z	50		76	
	2132Z	54		84	
	2232Z	54		80	
	2332Z	53		76	
	0032Z	50	75 G 90	74	25.7 N / 123.6 E
	0132Z	49		73	
	0232Z	48		71	
	0332Z	54		80	
	0432Z	51		75	
	0532Z	51		75	

	0632Z	51	70 G 85	76	26.0 N / 123.1 E
	0732Z	52		75	
	0832Z	51		75	
	0932Z	52		77	
	1032Z	51		75	
	1132Z	49		71	
	1232Z	50	65 G 80	74	27.0 N / 121.7 E
	1332Z	50		73	
	1432Z	50		75	
	1532Z	50		75	
	1632Z	50		76	
	1732Z	53		78	
MEAN		53.6		81.5	
		16.3 km			

THIS PAGE INTENTIONALLY LEFT BLANK

APPENDIX C. 23W (DANAS) HOURLY DATA

23W (DANAS)

DATE	TIME	ToC (Kft)	INTENSITY (kt)	TEMP (-C)	LAT / LONG
3-Oct	0032Z	53	TCFA	82	
	0132Z	52		85	
	0232Z	52		80	
	0332Z	52		80	
	0432Z	51		79	
	0532Z	51		80	
	0632Z	52	TCFA	85	
	0732Z	52		83	
	0832Z	52		85	
	0932Z	51		80	
	1032Z	52		80	
	1132Z	51		78	
	1232Z	51	20 G 30	79	15.8 N / 148.4 E
	1332Z	52		80	
	1432Z	50		77	
	1532Z	50		77	
	1632Z				
	1732Z	54		85	
	1832Z		30 G 40		15.9 N / 147.4 E
	1932Z	50		76	
	2032Z	50		76	
	2132Z				
	2232Z	49		74	
	2332Z				
4-Oct	0032Z	51	30 G 40	85	16.1 N / 146.5 E
	0132Z	54		83	
	0232Z	53		79	
	0332Z	53		77	
	0432Z	53		80	
	0532Z	56		85	
	0632Z	53	30 G 40	79	16.6 N / 145.6 E
	0732Z	55		82	
	0832Z	54		82	
	0932Z	55		84	
	1032Z	55		84	
	1132Z	56		84	

5-Oct	1232Z	54	35 G 45	82	17.2 N / 144.8 E
	1332Z	54		85	
	1432Z	53		80	
	1532Z	52		79	
	1632Z	54		84	
	1732Z	54		82	
	1832Z	56	45 G 55	84	17.8 N / 143.9 E
	1932Z	53		82	
	2032Z	52		80	
	2132Z	52		80	
	2232Z	57		85	
	2332Z	59		85	
	0032Z	56	50 G 65	83	18.2 N / 142.4 E
	0132Z	54		83	
	0232Z	53		80	
	0332Z	57		87	
	0432Z	54		87	
	0532Z	55		86	
	0632Z	54	55 G 70	84	18.9 N / 140.9 E
	0732Z	57		88	
	0832Z	56		89	
	0932Z	56		89	
	1032Z	55		85	
	1132Z	56		88	
	1232Z	56	65 G 80	86	19.5 N / 139.5 E
	1332Z	56		86	
	1432Z	53		82	
	1532Z	52		83	
	1632Z	52		84	
	1732Z	52		82	
6-Oct	1832Z	54	70 G 85	85	20.3 N / 138.1 E
	1932Z	56		84	
	2032Z	54		81	
	2132Z	54		81	
	2232Z	54		83	
	2332Z	54		81	
	0032Z	53	80 G 100	79	21.2 N / 136.3 E
	0132Z	53		80	
	0232Z	53		80	
	0332Z	53		81	
	0432Z	54		83	
	0532Z	52		80	

7-Oct	0632Z	52	85 G 105	80	22.0 N / 135.0 E
	0732Z	54		83	
	0832Z	54		83	
	0932Z	52		81	
	1032Z	53		81	
	1132Z	53		81	
	1232Z	53	95 G 115	80	22.7 N / 133.4 E
	1332Z	54		80	
	1432Z	53		78	
	1532Z	53		78	
	1632Z	56		81	
	1732Z	53		79	
	1832Z	52	105 G 130	81	24.0 N / 131.6 E
	1932Z	52		81	
	2032Z	52		80	
	2132Z	52		81	
	2232Z	56		85	
	2332Z	52		79	
	0032Z	51	115 G 140	79	25.3 N / 130.0 E
	0132Z	50		74	
	0232Z	49		74	
	0332Z	49		74	
	0432Z	49		73	
	0532Z	50		74	
	0632Z	50	125 G 150	74	26.6 N / 128.7 E
	0732Z	48		71	
	0832Z	48		71	
	0932Z	49		73	
	1032Z	50		74	
	1132Z	49		74	
	1232Z	50	120 G 145	74	28.0 N / 127.7 E
	1332Z	51		75	
	1432Z	52		77	
	1532Z	54		78	
	1632Z	54		78	
	1732Z	53		78	
	1832Z	53	100 G 125	78	29.7 N / 127.1 E
	1932Z	55		82	
	2032Z	53		79	
	2132Z	53		78	
	2232Z	54		78	
	2332Z	55		77	

8-Oct	0032Z	55	85 G 105	77	31.3 N / 126.9 E
	0132Z	55		76	
	0232Z	54		80	
	0332Z	53		77	
	0432Z	51		76	
	0532Z	47	65 G 80	71	32.8 N / 127.8 E
	0632Z	56		68	
	0732Z	58		72	
	0832Z	50		74	
	0932Z	51		76	
	1032Z	52		75	
	1132Z	52		74	
	1232Z		55 G 70		34.5 N / 129.6 E
MEAN		52.9		80.1	

16.1 km

LIST OF REFERENCES

- Bedka, K.M., Brunner, J., Dworak, R., Feltz, W., Otkin, J., and Greenwalk, T., 2010: Objective satellite-based overshooting cloud-top detection using infrared window channel brightness temperature gradient. *J. Appl. Meteor. and Clim.*, **49**, 181–202.
- Boain, Ronald, J., 2003: The CloudSat mission: A virtual platform advances in the astronautical sciences (0065–3438), *Iss. Suppl.*, **114**, 2121–2138
- Bowditch, N., American Practical Navigator Volume 1 1977. [Available online at <ftp://ftp.flaterco.com/xtide/Bowditch.pdf>.]
- Cecil, D.J., Quinlan, K.R., Mach, D.M. 2010: Intense Convection Observed by NASA ER-2 in Hurricane Emily (2005). *Mon. Wea. Rev.*, **138**, 765–780.
- Colorado State University: 2006–2010 CloudSat tropical cyclone images. [Available online at <http://reef.atmos.colostate.edu>.]
- Cox, T., Ivan Somers, David J. Fratello, 2006: Earth observations and the role of UAVs: A capabilities assessment. v. 1.1, 29–33.
- Darack, E/Weatherwise, 2012 (Mar-Apr): UAVs: the new frontier for weather research and prediction. [Available online at [http://www.weatherwise.org/Archives/Back Issues/2012/March-April 2012/UAVs-full.html](http://www.weatherwise.org/Archives/Back%20Issues/2012/March-April%202012/UAVs-full.html).]
- Dave Fratello, Dee Porter, “NASA Global Hawk Project Description and Status,” April 7, 2009. [Available online at http://hsrp.nsstc.nasa.gov/documents/fratello_globalhawk.pdf.]
- Elsberry, R. L., and P. A. Harr, 2008: Tropical cyclone structure (TCS2008) field experiment: science basis, observational platforms, and strategy. *Asia-Pacific J. Atmos. Sci.*, **44**, 122–143.
- Emanuel, K. (2007), Comment on ‘Sea-surface temperatures and tropical cyclones in the Atlantic basin by Patrick J. Michaels, Paul C. Knappenberger, and Robert E. Davis, *Geophys. Res. Lett.*, **34**, L06702.
- Gentry, B., and Coauthors, 2007: Development of an airborne molecular direct detection Doppler lidar for tropospheric wind profiling. *Proc. Lidar Remote Sensing for Environmental Monitoring*, San Diego, CA, International Society for Optics and Photonics, U63–U68.

- Goerss, J. S., C. R. Sampson, J. M. Gross, 2004: A history of western north pacific tropical cyclone track forecast skill. *Wea. Forecasting*, **19**, 633–638.
- Goerss, James S., 2009: Impact of satellite observations on the tropical cyclone track forecasts of the navy operational global atmospheric prediction system. *Mon. Wea. Rev.*, **137**, 41–50.
- Gray, W.M., 1979: Hurricanes: Their formation, structure and likely role in the tropical circulation. *Meteorology over the Tropical Oceans*, 155–218.
- Halverson, J. B., J. Simpson, G. Heymsfield, H. Pierce, T. Hock, L. Ritchie, 2006: Warm core structure of hurricane erin diagnosed from high altitude dropwindsondes during camex-4. *J. Atmos. Sci.*, **63**, 309–324.
- Harnisch, F., and M. Weissmann, 2010: Sensitivity of typhoon forecasts to different subsets of targeted dropsonde observations. *Mon. Wea. Rev.*, **138**, 2664–2680.
- Harr, P. A., D. Anwender, S. C. Jones, 2008: Predictability associated with the downstream impacts of the extratropical transition of tropical cyclones: Methodology and a case study of Typhoon Nabi (2005). *Mon. Wea. Rev.*, **136**, 3205–3225.
- Heidinger, A., 2011: ABI Cloud Height. URL: http://www.goes-r.gov/products/ATBDs/baseline/Cloud_CldHeight_v2.0_no_color.pdf
- Heymsfield et al., 2008: Status of the High-Altitude Imaging Wind and Rain Airborne Profiler (HIWRAP). [Available online at http://esto.nasa.gov/conferences/estc2008/papers/Heymsfield_Gerald_B5P2.pdf.]
- Hock, T. F., and J. L. Franklin, 1999: The NCAR GPS dropwindsonde. *Bull. Amer. Meteor. Soc.*, **80**, 407–420.
- J. Chris Naftel, “NASA Global Hawk: A New Tool for Earth Science Research,” NASA/TM-2009–214647, May 2009. [Available online at http://ntrs.nasa.gov/archive/nasa/casi.ntrs.nasa.gov/20090019745_2009018152.pdf.]
- JTWC, 2006: Annual Tropical Cyclone Report. [Available online at <http://jtwccdn.appspot.com/NOOC/nmfc-ph/RSS/jtwc/atcr/2006atcr.pdf>.]
- JTWC, 2007: Annual Tropical Cyclone Report. [Available online at <http://jtwccdn.appspot.com/NOOC/nmfc-ph/RSS/jtwc/atcr/2007atcr.pdf>.]

- JTWC, 2008: Annual Tropical Cyclone Report. [Available online at <http://jtwccdn.appspot.com/NOOC/nmfc-ph/RSS/jtwc/atcr/2008atcr.pdf>.]
- JTWC, 2009: Annual Tropical Cyclone Report. [Available online at <http://jtwccdn.appspot.com/NOOC/nmfc-ph/RSS/jtwc/atcr/2009atcr.pdf>.]
- JTWC, 2010: Annual Tropical Cyclone Report. [Available online at <http://jtwccdn.appspot.com/NOOC/nmfc-ph/RSS/jtwc/atcr/2010atcr.pdf>.]
- JTWC, 2011: Annual Tropical Cyclone Report. [Available online at <http://jtwccdn.appspot.com/NOOC/nmfc-ph/RSS/jtwc/atcr/2011atcr.pdf>.]
- Jones et al., 2008: Improved Microwave Remote Sensing of Hurricane Wind Speed and Rain Rates Using the Hurricane Imaging Radiometer (HIRAD). [Available online at http://ktb.engin.umich.edu/RSG/pubs_files/AMS-2008_EI-Nimri_et al_HIRAD_Sims.pdf.]
- Jones, S. C., and Co-authors, 2003: The extratropical transition of tropical cyclones: Forecast challenges, current understanding, and future directions. *Wea. Forecasting*, **18**, 1052–1092.
- Justice, E., 2012: HS3 hurricane intensity change and internal processes [Available online at http://espo.nasa.gov/missions/hs3/content/HS3_Hurricane_Intensity_Change_and_Internal_Processes.]
- Lin, Po-Hsiung, 2006: OBSERVATIONS: The first successful typhoon eyewall-penetration reconnaissance flight mission conducted by the unmanned aerial vehicle, aerosonde. *Bull. Amer. Meteor. Soc.*, **87**, 1481–1483.
- Lin, Po-Hsiung, Cheng-Shang Lee, 2008: The Eyewall-Penetration Reconnaissance Observation of Typhoon Longwang (2005) with Unmanned Aerial Vehicle, Aerosonde. *J. Atmos. Oceanic Technol.*, **25**, 15–25.
- Merrill, R. T., 1988: Environmental influences on hurricane intensification. *J. Atmos. Sci.*, **45**, 1678–1687.
- Monette, S. A., Velden, C.S., Rozoff, C.M., 2012: Examining trends in satellite-detected overshooting tops as a potential predictor of tropical cyclone rapid intensification. [Available online at http://www.goes-r.gov/downloads/ScienceWeek/2013/posters/03-18/Sarah_Monette.pdf.]
- Naftel, Chris, NASA Global Hawk Project, Update and Future, A New Tool for Earth Science Research, Nov. 16, 2009. [Available online at http://ntrs.nasa.gov/archive/nasa/casi.ntrs.nasa.gov/20090040628_2009041381.pdf.]

- NASA News Fact Sheet: Global Hawk: High-altitude, long-endurance science aircraft, March 22, 2012. [Available online at <http://www.nasa.gov/centers/dryden/news/FactSheets/FS-098-DFRC.html>.]
- P. A. Harr, 2011: Tropical cyclone reconnaissance with the Global Hawk: operational requirements, benefits, and feasibility. *CRUSER Newsletter*, October 2011. [Available at <http://www.nps.edu/CRUSER>.]
- Parry, D., NRL researchers use unmanned aircraft to probe hurricane outflow jets. [Available online at <http://www.nrl.navy.mil/media/news-releases/2012/nrl-researchers-use-unmanned-aircraft-to-probe-hurricane-outflow-jets>.]
- Reynolds, C. A., M. S. Peng, and J.-H. Chen, 2009: Recurving tropical cyclones: singular vector sensitivity and downstream impacts. *Mon. Wea. Rev.*, **137**, 1320–1337.
- Schultz, B, 2009: Tropical Cyclone Conference. [Available online at <http://www.docstoc.com/docs/52191999/TROPICAL-CYCLONE-CONFERENCE-29-APR-2009>.]
- Stephen Cole, Beth Hagenauer, NASA debuts Global Hawk autonomous aircraft for Earth Science, Jan. 15, 2009. [Available online at http://www.nasa.gov/home/hqnews/2009/jan/HQ_09-008_Global_Hawk.html.]
- Tourville, N. D., 2011: Level 3 tropical cyclone product process description and interface control document. CloudSat Project. [Available online at http://reef.atmos.colostate.edu/~natalie/tc/CSTC_README.pdf.]
- Uhlhorn, E. W., and P. G. Black, 2003: Verification of remotely sensed sea surface winds in hurricanes. *J. Atmos. Oceanic Technol.*, **20**, 99–116.
- Uhle, W.W., 2009: Goals for tropical cyclone forecasting. Ser: **J33**/#002, 3pp.
- University of Wisconsin: ACHA cloud top height and cloud top temperature images. [Available online at <http://cimss.ssec.wisc.edu>.]
- Weissmann, M., F. Harnisch, C.-C. Wu, P.-H. Lin, Y. Ohta, K. Yamashita, Y.-H. Kim, E.-H. Jeon, T. Nakazawa, and S. Aberson, 2011: The influence of assimilating dropwindsonde data on typhoon track and midlatitude forecasts. *Mon. Wea. Rev.*, **139**, 908–920.
- Wu, C.-C., and Co-authors, 2005: Dropwindsonde observations for typhoon surveillance near the Taiwan Region (DOTSTAR): An overview. *Bull. Amer. Meteor. Soc.*, **86**, 787–790.

Zipser, E., and Coauthors, 2013: HS3 Global Hawk flight rules for storm avoidance. Discussion Paper.

Zipser, E., G. Heymsfield, 2011: NASA GRIP 2010 overview of research flights. GRIP Science Meeting June 6–8, 2001. Los Angeles, CA

THIS PAGE INTENTIONALLY LEFT BLANK

INITIAL DISTRIBUTION LIST

1. Defense Technical Information Center
Ft. Belvoir, Virginia
2. Dudley Knox Library
Naval Postgraduate School
Monterey, California